Paleoseismological Investigations of the Eastern Part of the Khlong Marui Fault Zone in Surat Thani Province, Southern Thailand

Prakrit Noppradit

A Thesis Submitted in Partial Fulfillment of the Requirements
for the Degree of Master of Science in Geophysics
Prince of Songkla University
2013

Thesis Title	Paleoseismological Investigations of the Eastern Part of the Khlong Marui Fault Zone in Surat Thani Province, Southern Thailand
Author	Mr.Prakrit Noppradit
Major Program	Geophysics

Major Advisor:

……

(Dr.Helmut Dürrast)

Co-advisor:

……

(Dr.Sommai Changkian)

Examing Commitee:

……Chairperson

(Dr.Tidarut Vichaidid)

……

(Dr.Christoph Schmidt)

……

(Prof.Dr.Ludwig Zöller)

……

(Dr.Sommai Changkian)

……

(Dr.Helmut Dürrast)

The Graduate School, Prince of Songkla University, has approved this thesis as partial fulfillment of the requirements for the Master of Science Degree in Geophysics.

……..……..

(Assoc.Prof.Dr.Teerapol Srichana)

Dean of Graduate School

This is to certify that the work here submitted is the result of the candidate's own investigations. Due acknowledgement has been made of any assistance received.

……. Signature
(Dr.Helmut Dürrast)
Major Advisor

……. Signature
(Mr.Prakrit Noppradit)
Candidate

I hereby certify that this work has not been accepted in substance for any degree, and is not being currently submitted in candidature for any degree.

……. Signature
(Mr.Prakrit Noppradit)
Candidate

ชื่อวิทยานิพนธ์ การสำรวจเหตุการณ์แผ่นดินไหวยุคโบราณบริเวณกลุ่มรอยเลื่อนคลองมะรุ่ยด้านตะวันออกจังหวัดสุราษฎร์ธานีประเทศไทย

ผู้เขียน ว่าที่ร้อยตรีประกฤษฎ์ นพประดิษฐ์

สาขาวิชา ธรณีฟิสิกส์

ปีการศึกษา 2556

บทคัดย่อ

ภาคใต้ของประเทศไทยตั้งอยู่บนแหลมมลายูมีกลุ่มรอยเลื่อนมีพลังสองกลุ่มพาดผ่าน ได้แก่ กลุ่มรอยเลื่อนคลองมะรุ่ย และกลุ่มรอยเลื่อนระนอง โดยกลุ่มรอยเลื่อนทั้งสองวางตัวในแนวตะวันตกเฉียงใต้-ตะวันออกเฉียงเหนือในปี พ.ศ. 2548 ได้มีการศึกษาแผ่นดินไหวขนาดเล็กที่มีขนาดน้อยกว่า 4.5 ในบริเวณภาคใต้ นอกจากนี้ในปี พ.ศ.2550 ยังได้มีการศึกษาเหตุการณ์แผ่นดินไหวในอดีตในบริเวณกลุ่มรอยเลื่อนคลองมะรุ่ยฝั่งตะวันตกโดยกรมทรัพยากรธรณีพบว่ามีเหตุการณ์แผ่นดินไหวขนาดใหญ่เกิดขึ้นเมื่อไม่กี่พันปีที่ผ่านมา สำหรับการศึกษาเหตุการณ์แผ่นดินไหวในอดีตบริเวณกลุ่มรอยเลื่อนคลองมะรุ่ยทางด้านตะวันออกในครั้งนี้ ได้เลือกพื้นที่ศึกษาในบริเวณจังหวัดสุราษฎร์ธานีโดยใช้วิธีเทอร์โมลูมิเนสเซนส์ (TL) และออพติคอลลีสติมูเลตเตดลูมิเนสเซนส์ (OSL)ในการศึกษาระยะเวลาการเกิดเหตุการณ์แผ่นดินไหว และใช้การเรียงลำดับของชั้นตะกอนรวมไปถึงหลักฐานทางธรณีวิทยาในการศึกษาระดับความรุนแรงของแผ่นดินไหวในหน่วยโมเมนแมกนิจูด จากผลการศึกษาในครั้งนี้พบว่าได้มีเหตุการณ์แผ่นดินไหวอย่างน้อยสามช่วงเวลา ได้แก่ ช่วง 33,000-112,000 ปี, 2,500-10,000 ปี และ น้อยกว่า 2,500 ปี นั่นหมายความว่ากลุ่มรอยเลื่อนคลองมะรุ่ยสามารถจัดเป็นรอยเลื่อนมีพลังจริง นอกจากนี้ยังพบว่าเหตุการณ์แผ่นดินไหวที่เคยเกิดขึ้นเหล่านี้มีขนาดมากกว่า 6.6และมากที่สุดที่ 7.8 ซึ่งยังไม่เคยบันทึกได้โดยเครื่องวัดแผ่นดินไหว (seismogram) จากข้อมูลนี้อาจจะใช้ในการเตรียมรับมือกับเหตุการณ์แผ่นดินไหวที่จะเกิดขึ้นในอนาคตได้

Thesis Title	Paleoseismological investigations of the eastern part of the Khlong Marui Fault Zone in Surat Thani Province, Southern Thailand
Author	Prakrit Noppradit
Major Program	Geophysics
Academic year	2013

Abstract

In Southern Thailand two major strike slip faults are crossing the Malay Peninsula, the Khlong Marui (KMFZ) and the Ranong Fault Zone from SW to NE, which were identified as inactive before 2004 by the Department of Mineral Resources (DMR), Thailand. Seismological observations in 2005 have confirmed seismicity with low magnitudes (M<4.5) along the faults and in southern Thailand. Paleoseismological investigations of the clearly exposed western part of the KMFZ by the DMR in 2007 have shown that paleoearthquakes occurred in the last few thousand years. For the eastern part, mainly in Surat Thani Province, where the fault is less exposed, this study could identify several locations with evidences of paleoearthquakes. Both thermoluminescence and optically-stimulated luminescence method were applied in this study to determine the occurrence time of the paleoseismological events. The paleoearthquake magnitude was determined by detailed investigations in changes and displacements of the stratigraphy and geologic setting. From the results it can be concluded that there has been at least three periods of paleoearthquakes at the eastern part of the KMFZ, at 33-112 ka, 2.5–10 ka, and younger than 2.5 ka. The KMFZ can be classified as an active fault. The paleoseismological results also have shown that the KMFZ can generate higher magnitude earthquakes than any seismogram has ever recorded for this area with Mw more than 6.6 and maximal 7.8 and by this indicate that these magnitudes can be also expected in the future along this fault. Any seismic hazard analysis for this area has to take this into account.

ACKNOWLEDGEMENTS

This thesis could be finished smoothly only because many people gave me their supervision, support, and advice. Firstly, I would deeply thank Dr. Helmut Dürrast, my advisor. He supervised me closely since I started to plan this work until it was finished. Moreover, he provided me with opportunities so that I got excellent experiences. He gave me not only knowledge, but also the understanding and philosophy for the real life. He could be a guide.

I would like to thank Dr. Sommai Chankian, my co-advisor for his knowledge and experiences in thermoluminescence (TL) dating. Moreover, I could use his knowledge for my work on optically-stimulated luminescence (OSL) dating.

I would like to thank Prof. Dr. Ludwig Zöller and his staff, Mr. Manfred Fischer, from the University Bayreuth, Germany. They gave me valuable experience in OSL dating both in experimental work and theoretical background. They also supported me during my stay in Germany; places and a social life I have never experienced before.

I would like to thank the Development and Promotion of Science and Technology (DPST) talent project for financial support, which included the research visit at the University Bayreuth that was of high value for me. Part of the fieldwork was supported by the Electricity Generating Authority of Thailand (EGAT) and the Geophysics Research Center (GRC), as well as the Graduate School, and the Department of Physics, both at the Prince of Songkla University.

Many of my friends, geophysics students at PSU Hatyai, Physics students at PSU Pattani, and geomorphology students at the University Bayreuth, helped me to make my work a success, especially Ms. Usa Nilsuwan, Ms. Samareeya Padu, and Mr. Thomas Kolb. Finally, I would like to thank my family who gave me the encouragement and motivation to finish my studies successfully.

Prakrit Noppradit

TABLE OF CONTENTS

TABLE OF CONTENTS (CONTINUED)

TABLE OF CONTENTS (CONTINUED)

LIST OF TABLE

LIST OF FIGURE

LIST OF FIGURE (CONTINUED)

LIST OF FIGURE (CONTINUED)

LIST OF FIGURE (CONTINUED)

LIST OF FIGURE (CONTINUED)

LIST OF FIGURE (CONTINUED)

CHAPTER 1
INTRODUCTION

1.1 Introduction

1.1.1 Role of paleoseismological research for seismic risk assessment

Earthquakes are defined as a trembling of the earth caused by a sudden release of energy stored in subsurface rock units (e.g. Kurniawan et al. 2009). The effect of earthquake activities can pose a significant hazard to the lives of people and the infrastructure because the ground acceleration associated with the seismic waves can result in the collapse of buildings and other structures. Moreover, there are secondary effects, like landslides and tsunamis, which also result in loss of lives and destruction of infrastructure. In order to understand and estimate the existing hazard for an area, the study of earthquakes in this area is necessary, the present earthquakes as well as the past ones.

For the study of the present or modern earthquakes instrumental data from seismometers are used, so called seismograms. Seismogram data give information about the seismic waves propagated from the earthquake hypocenter (origin point of an earthquake) to the seismometer station. From the analysis of seismograms from different stations the earthquake parameters can be determined, like location, occurrence time, and magnitude.

A magnitude of an earthquake provides a unit of how "big" an earthquake is. Spence et al. (1989) presented a summary of several earthquake magnitudes, like local magnitude (M_L), calculated from maximum amplitude of wave train measured assuming the parameter of a Wood–Anderson seismometer, surface wave magnitude (M_S), calculated from the maximal amplitude with a certain period of the surface waves, body-wave magnitude (m_b), calculated from the amplitude and period of the ground motion (velocity), and moment magnitude (M_w), calculated from the seismic moment that is related to fault geometry and the low frequency part of the

amplitude–frequency diagram. The earthquake magnitude is in logarithm scale of the related factors (amplitude of recorded wave, seismic moment).

The effect of earthquake activities can pose a significant hazard to the lives of people and the infrastructure. Although the sources of the earthquakes are often known, for example active faults, it is often not known due to limitations in available seismological data what earthquake with what magnitude a fault has been generated in the past. Such information is an important base for a seismic hazard analysis as seismological observations worldwide started in the 1912 (DMR, 2013) and in Thailand in 1963 (TMD, 2013). Paleoseismological methods provide a tool to investigate earthquakes in the past before any instrumental records where available as an earthquake leaves evidence in the geological record.

1.1.2 Aim of the study

In Southern Thailand two major strike slip faults are crossing the Malay Peninsula from SW to NE, the Khlong Marui (KMFZ) and the Ranong Fault Zone (RFZ), which were identified as inactive before 2004 by the Department of Mineral Resources (DMR), Thailand, however no seismicity studies have been carried out at that time. Seismological observations by Dürrast et al. (2007) in early 2005 have confirmed seismicity with low magnitudes ($M<4.5$) along the faults and in southern Thailand. As earthquakes can have an effect on local people in this area the seismicity needs to be known so that a seismic hazard analysis can be carried out as a base for preparedness and mitigation efforts.

This study is applying both thermoluminescence (TL) and optically-stimulated luminescence (OSL) method to determine the occurrence time of the geological events identified as possible past earthquakes along the eastern part of the active Khlong Marui Fault Zone where less reliable data were available so far. Moreover, the earthquake magnitude is determined by detailed investigations in changes of the stratigraphy and geologic setting. These data will then be part of a seismic hazard analysis of the area.

1.2 Paleoseismology research

For earthquakes in the past there are no instrumental records available. However, usually an earthquake leaves evidence in the geological record, like faults, landslides, or stream changes, which can be used to study past earthquakes. Paleoseismology is a tool for investigating geological evidence in order to determine the occurrence of earthquakes in historical and geological time. Three parameters have to be resolved, comparable to the earthquake determination with instrumental data using seismograms: 1) the location of an earthquake, 2) its occurrence time, and 3) its size, generally known as magnitude (McCalpin 2008).

The geological record and the geomorphology of a fault zone can be used to identify and evaluate the location of a paleoearthquake (Fattahi 2009). Geochronological analysis of sediments related to the paleoearthquake is required for evaluating occurrence time of the past earthquake. There are many techniques available to date sediments such as radioactive carbon, electron spin resonance (ESR), thermoluminescence (TL), or optically-stimulated luminescence (OSL). The use of one of these methods depends on what kind of material was found in the sediment and the limitations of each technique. For the magnitude determination, several techniques can be used as presented by McCalpin (2008), like the logarithm of rupture length and/or the displacement of a fault.

1.2.1 Geological record of earthquakes

A fault movement is evidence for the occurrence of an earthquake. The geological environment of a fault zone where earthquakes happened provides information about the past movements. In generally, a fault is a crack in the earth's crust resulting from the displacement of one side with respect to the other. After the fault moves in vertical direction, one side of it moves in higher level that called fault scarp. There are three main fault types that consisting of normal, reverse, and strike-slip fault as shown in Figure 1.1. For a normal fault, a footwall (the block of rock lying under an inclined geologic fault plane) moves in upward direction that is

opposite to a reverse fault in Figure 1.2. For a strike-slip fault, the surfaces on the opposite sides of a fault plane have moved horizontally and parallel to the strike of the fault. The strike-slip fault is defined by the movement in horizontal direction from a top view: the counter-clockwise movement called sinestral, and the clockwise movement called dextral.

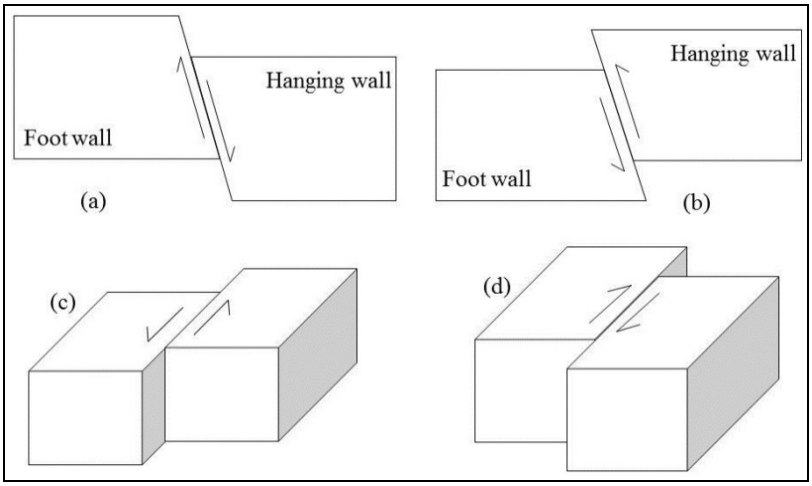

Figure 1.1 Fault types: (a) normal, (b) reverse, (c) sinestral strike-slip, and (d) dextral strike-slip.

McCalpin (2008) described the tectonic environments that are related to the three major fault types: (1) the normal fault accommodates typically in a crustal extensional environment. Extensional tectonic forces result from three sources: crustal-scale extension related to plate motion, mid-to-upper-crustal extension where extensional secondary faults form related to the major reverse or strike-slip faults or upper-crustal extension due to gravitational collapse of very elevated terrain. (2) The second is the compressional environment that accommodates reverse faults. The reverse fault is shown in Figure 1.2. (3) The last one is the strike-slip environment that typically accommodates strike-slip faults. The normal component in the strike-slip environment is called a negative flower structure as shown in Figure 1.3(a), and the reverse fault component is called a positive flower structure as shown in Figure 1.3(b).

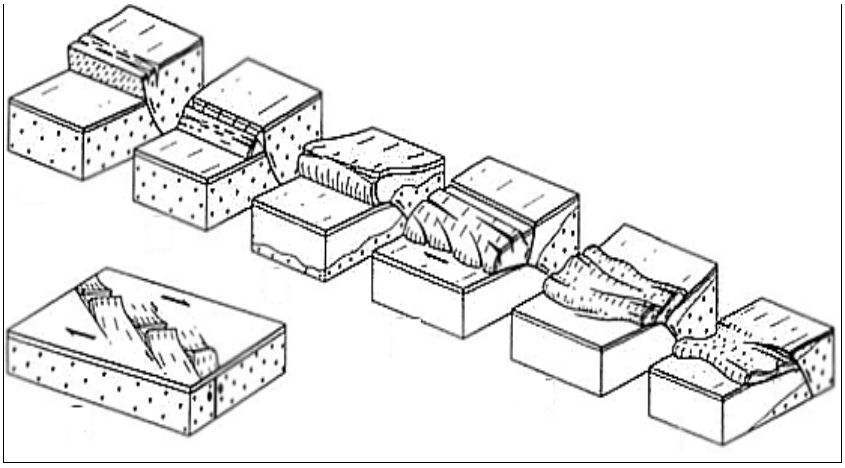

Figure 1.2 Reverse fault environments and it development over time, top from left to right. The left-below is a reverse fault in a strike-slip environment (McCalpin 2008).

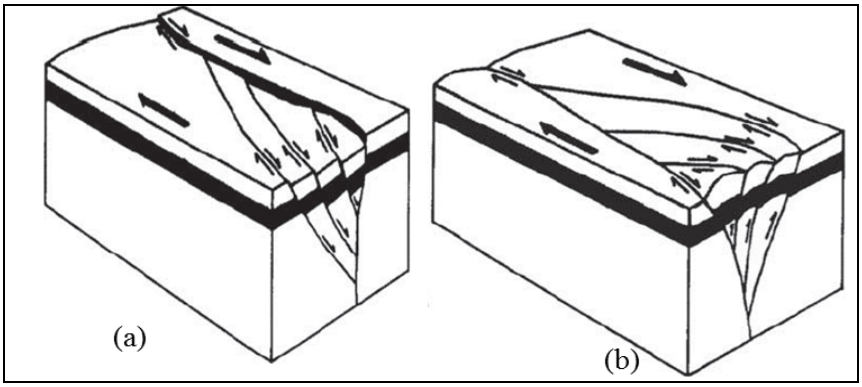

Figure 1.3 Strike-slip environment: (a) right lateral extensional duplex, and (b) right lateral contractional duplex (McCalpin 2008).

Fattahi (2009) described that after an earthquake event two sides of a fault will have a difference in elevation or offset, and sediments, colluvium, alluvium, or aeolian, will laid or progressively fill the lower side. These sediments can be used to apply dating techniques to evaluate their ages. Nichols (2009) described the alluvium sediment occurring process: differences in the velocity of the water can result in sediments that have different particle size either to erode, transport or to deposit. The so called Hjülstrom diagram as shown in Figure 1.4 is presenting this as a relationship between grain size and flow speed. Similarly, the factor that affects the colluvium is the gravitational force, e.g. hill slope deposit. Aeolian sediments are transported by wind, so those deposits are made up mainly of wind-blown material (Nichols 2009), which is fine grained sediments up to sand size.

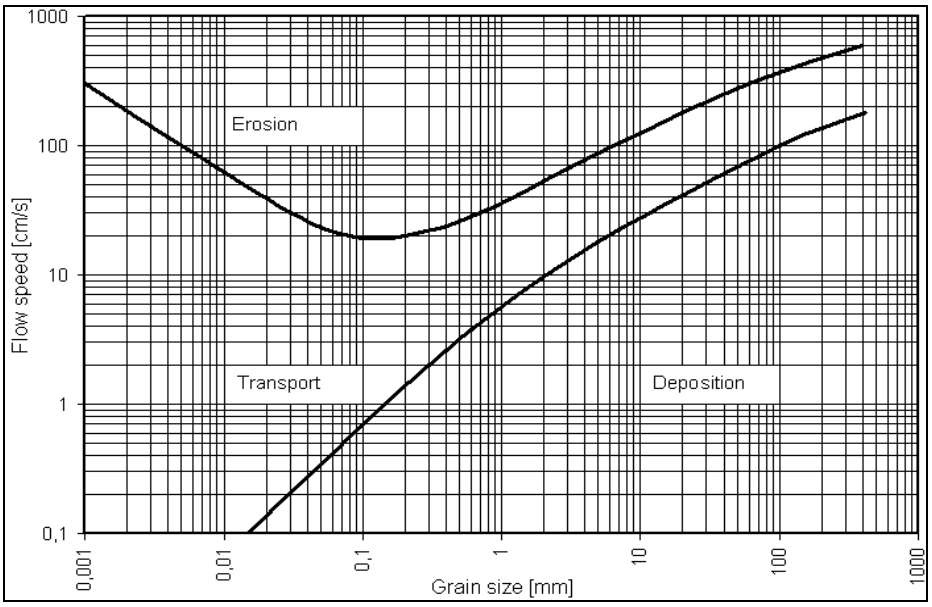

Figure 1.4 Hjülstrom diagram described water transport and size of particle; the erosional upper, transportational middle, and depositional lower part (Nichols 2009).

1.2.2 Paleoseismological studies in strike slip tectonic regimes

Rodríguez-Pascua et al. (2009) studied the tectonic slip-rate of Pozohondo Fault in Albacete Province, Spain, from Quaternary sediments. The Pozohondo Fault is a NW-SE right lateral oblique-fault. It is approximately 55 km in length. The Uranium-Thorium dating method was applied to date sediments related to paleoearthquakes. Field GPS, aerial orthophoto, and Ortho-Landsat 7 were used to determine the surface rupture length. Fault displacement was measured directly to scarp. The result gave three stage of tectonic. Stage 1 was between 400–700 ka that has 0.09 mm/y slip rate. Stage 2 was between 100–400 ka that has 0.05 mm/y slip rate. Stage 3 was between 100 ka to present that has two paleoearthquake events. From stage 1 to 3, there were magnitudes calculated from Wells and Coppersmith (1994) with values of 6.0–7.0.

The Department of Mineral Resources (DMR 2011) has assigned the Department of Earth Science, Kasetsart University to study the recurrence interval in Utaradit and Pua fault in Northern of Thailand. The digital elevation model (DEM)

was preliminarily used before fieldwork, mainly geophysics using ground penetrating radar (GPR), trenching, and sampling. The thermoluminescence dating and radioactive carbon age dating were used to date sediments related to past earthquakes. The oblique normal fault was found at Ban Rai Teentok site. Its stratigraphy, dating results and evolution are shown in Figure 1.5. The sediment unit A was formed before 12,000 years ago before an earthquake occurred between 12,000–10,300 years ago (see the discontinuity of unit A). Then unit B, C, D, E, F, and G, respectively, occurred. From these results, it can be concluded that this fault was moved around 11,200 years ago. The surface rupture length was used to determine the possible maximum magnitude around 5.8.

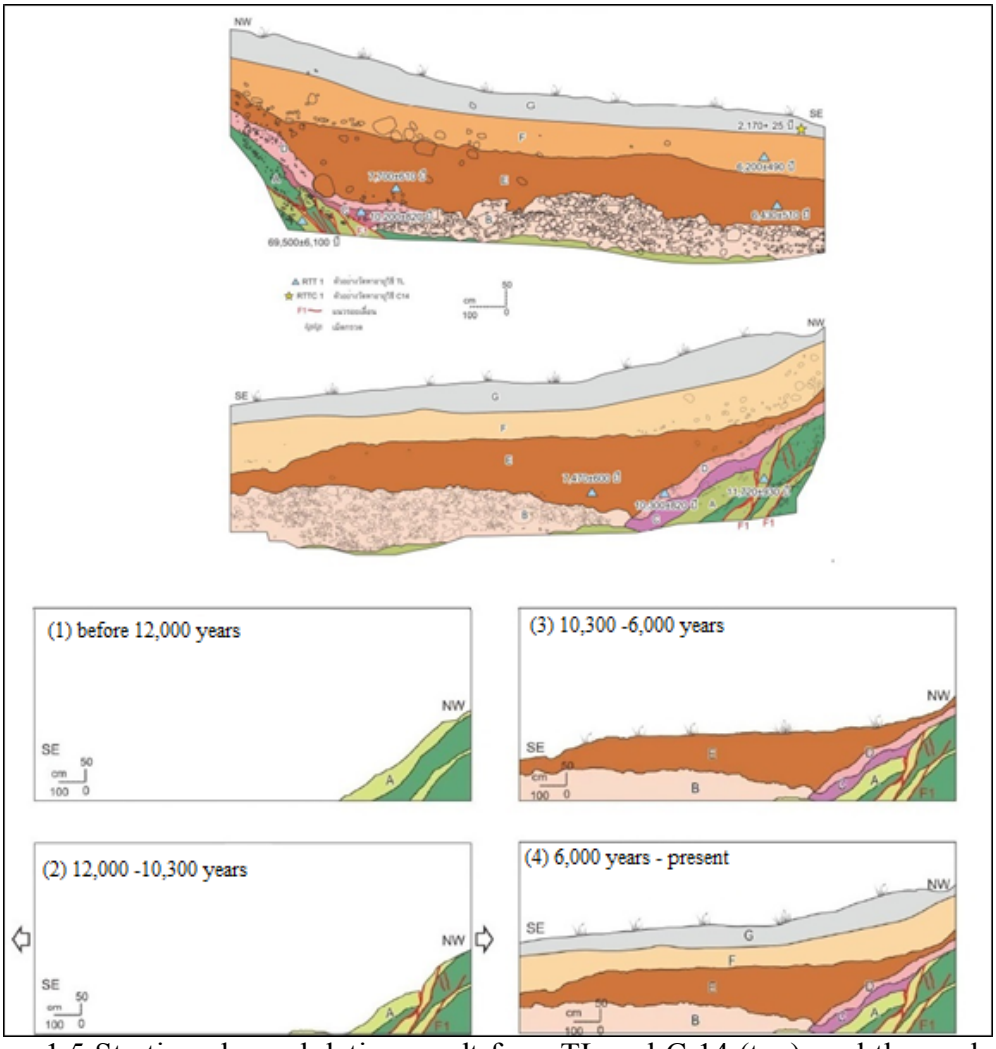

Figure 1.5 Stratigraphy and dating result from TL and C-14 (top), and the evolution of the fault with the earthquake occurrence shown in frame (2) before the other sediments settled (3 and 4) (bottom) (after DMR 2011).

1.2.3 Paleoseismological studies in Southern Thailand

Sutiwanich et al. (2008) carried out paleoseismic investigations at the KMFZ for the Khlang Tham Dam seismic analysis. The south-western segment of the Khlong Marui fault zone in Pang Nga Province gave paleoearthquakes results with ages from TL dating of less than 10,000 years (in average 3,000 years), which can be seen as the last movement. Moreover, they found that a return period of 5,300 years in this area with a maximum 5.5 paleoearthquake magnitude.

The Department of Mineral Resources (DMR 2007) assigned the Department of Geology, Chulalongkorn University, to carry out a preliminarily study on the recurrence interval of the RFZ and the southwestern and middle part of the KMFZ. Remote sensing, topographic surveys, and geophysical investigations were applied to study tectonic geomorphology and locate trenches and sampling location. The TL, C-14, and ESR dating were applied to determine the last fault movement. Trenching and outcrops were used to define sediment stratigraphy related to paleoearthquake. Their study concluded that the last movement of the KMFZ was 1,200 years ago and that of the RFZ 2,000 years. Moreover, the recurrence interval of the KMFZ and RFZ is 1,000 years and 2,000 years, respectively.

A location in Vibhavadi District in Surat Thani Province was presented in DMR (2007). The surface rupture length was determined from remote sensing data at 330 m length. Additionally, a stream offset was found. Three sedimentary units were found: 0.1-1.7 m thick light brown sand as top layer (Unit C in Figure 1.6), about 0.3 m thick brown sandy gravel in the middle (Unit B in Figure 1.6), and white to light brown sandstone at the base (Unit A in Figure 1.6). The TL and C-14 dating were applied for dating the sediments at the bottom of Unit C, which gave 220-584 ka of TL ages and 1,240-5,570 years of C-14 ages. Moreover, the age of Unit A was determined by TL with 787 ka. The TL results were not used in the further interpretation because of assumed uncertainties. Therefore, only the C-14 ages were used for the interpretation of past earthquakes. The surface rupture length by remote sensing was 17 km giving a 6.5 maximum paleoearthquake magnitude.

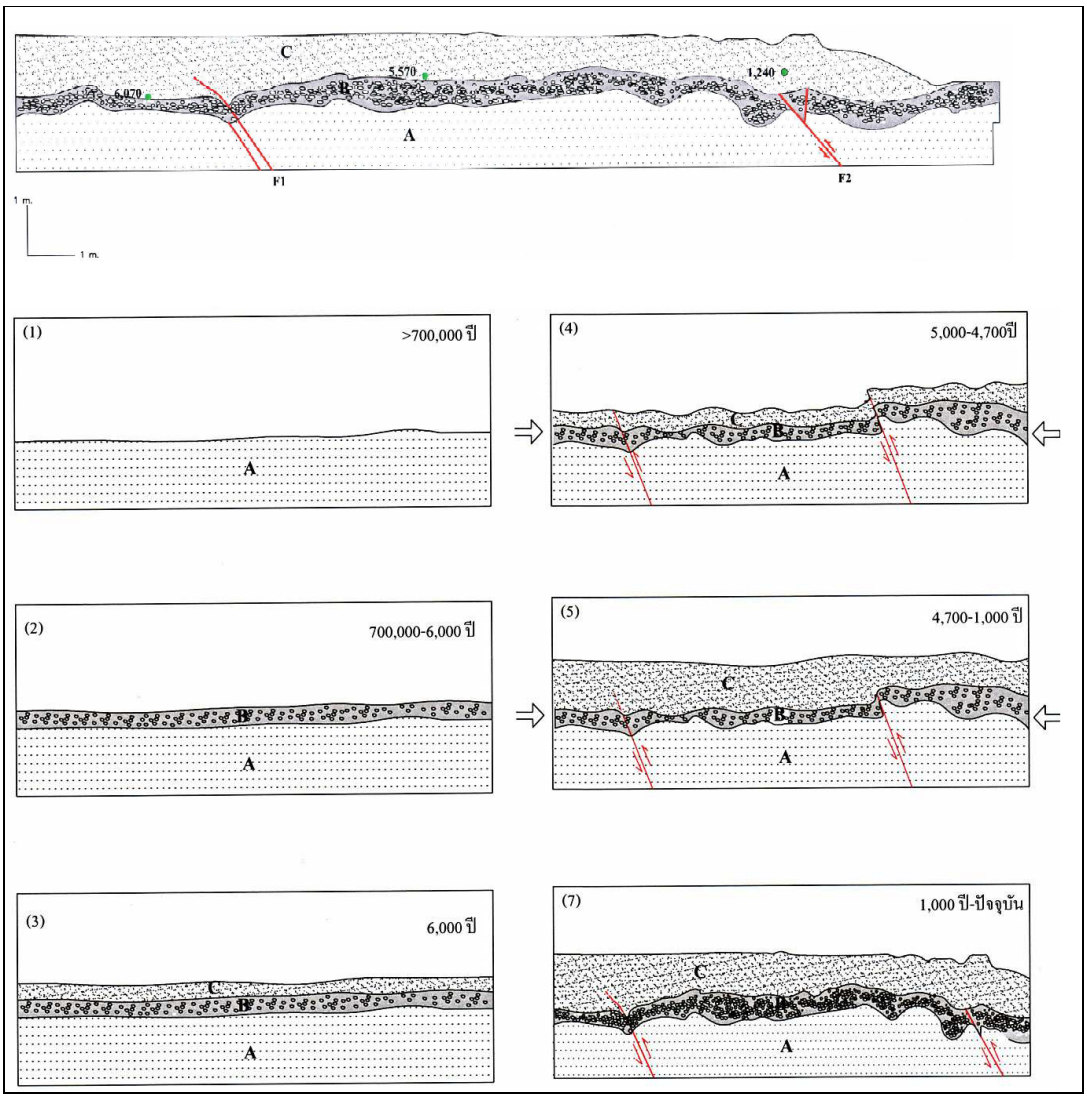

Figure 1.6 Sediment stratigraphy at Vibhavadi area (top), and the evolution of the sediments in the stratigraphy which earthquakes occurred between 1,000 and 4,700 years ago (bottom) (DMR 2007).

1.3 Study area

Southern of Thailand is located on the Malaysian Peninsular between latitude 5 and 11 degree north, and it is situated between the Gulf of Thailand in the East and the Andaman Sea in the West. In the upper part is the Tanawasri mountain range, which is located at the border between Thailand and Myanmar. The middle part has two mountain ranges, Nakhon Sri Thammarat range and Phuket range, located in NS direction. In the lowest part, there is Sankalakiri mountain range as a

border between Thailand and Malaysia. Southern Thailand is affected from both the SE monsoon and NW monsoon that brings rainfall from mid of May until mid of February. The rainfall can be as much as 4,000 mm per year (TMD 2007).

Quaternary sediments in the upper eastern coast of Southern Thailand are classified by Chotikasathien and Kohpina (1993) as shown in Figure 1.7, based on the environment of deposition: A). non-marine lithofacies, and B). coastal lithofacies. These two lithofacies can be further classified as following. Non-marine lithofacies: A1. Regolith: Layer of loose, heterogeneous material covering solid rock. A2. Colluvium: Loose deposits of rock debris accumulated through the action of gravity at the base of a cliff or slope. A3. Alluvium: Loose, unconsolidated (not cemented together into a solid rock) soil or sediments, which has been eroded, reshaped by water in some form, and re–deposited in a non-marine setting. Coastal lithofacies: B1. Deltaic sediments: Sediments that were formed at the mouth of a river, where the river flows into an ocean, sea, estuary, lake, or reservoir. B2. Estuarine and intertidal mud flat: Coastal wetlands that were formed when mud is deposited by tides, rivers, or estuarine activities. B3. Coastal barrier sand.

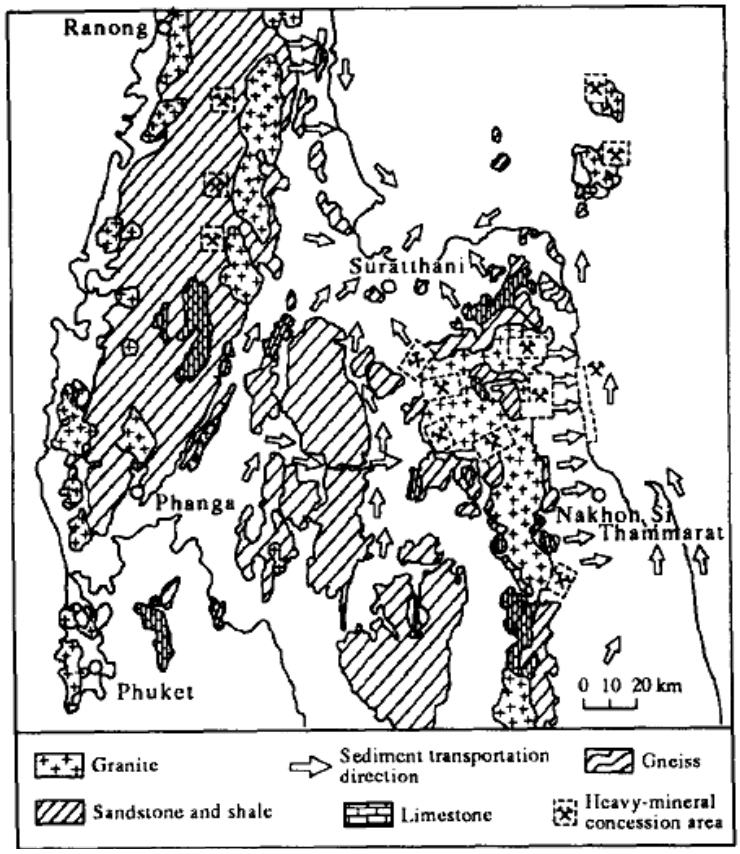

Figure 1.7 Geologic setting and sediment transportation in the upper part of Southern Thailand (Chotikasathien and Kohpina 1993).

Surat Thani Province was selected as the study area for this work. It is located at the upper eastern coast of Southern Thailand. The area comprises various geologic settings (DMR 2007): 1) granites of Triasic and Jurassic age, 2) mudstone, shale, sandstone, and siltstone of Permo-Carboniferous, which are overlain by 3) Permian limestone, 4) Mesozoic sedimentary rocks (major rocks exposed are interbeds of sandstone and shale and locally lenses of limestone), 5) Cenozoic sediment deposits (as shown in Figure 1.8). According to DMR (2007) the KMFZ appears in NE-SW direction from Chaiya coastline via Vibhavadi district until Phang Nga bay at the western coast (Figure 1.8). Note, that all maps presented in this work, which are in the Universal Transverse Mercator (UTM) grid, are using the WGS–84 as base map, and all UTM maps are in Zone 47.

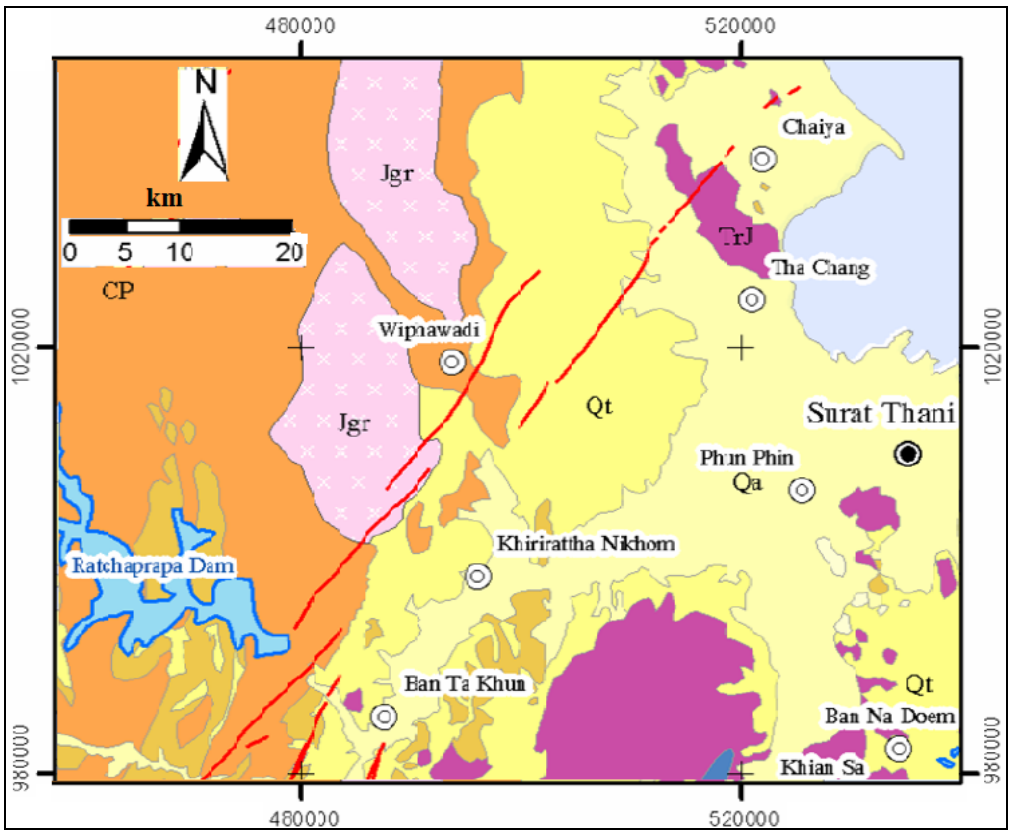

Figure 1.8 Geological map of Surat Thani province in UTM grid (Bureau of Geological Survey 2007); CP = pebbly mudstone, Jgr = Granite, TrJ= Sandstone and siltstone, Qt = Terrace and colluvial deposit, and Qa = alluvial deposit.

Vibhavadi district is located more than 50 m above sea level (up to 1,000 m in the mountains). It is in the hills of the Phuket mountain range. Tha Chang district extends from the coast to the Bandon Bay in the east until the ridge of the Phuket mountain range, which forms the boundary between the provinces of Surat Thani and Ranong.

1.4 Fault zone in southern of Thailand

Kosuwan et al. (2004) defined fifteen active faults in Thailand with two in Southern Thailand, the Ranong Fault Zone (RFZ) and the Khlong Marui Fault Zone (KMFZ) (Figure 1.5). Watkinson et al. (2008) described these as major NNE-trending strike-slip faults, diachronous reversal in shear sense, originated before but active during the India–Eurasia collision. They can be divided into four phases of

movement; D1 low grade ductile dextral strike-slip shear complete before 87 Ma, D2 medium to high grade ductile dextral strike-slip shear after 72 Ma and before 56 Ma, D3 brittle sinistral and sinistral reverse oblique strike-slip shear after 52 Ma, and D4 brittle dextral strike-slip shear at about 23 Ma.

The KMFZ is 130 km long and mainly passes Tertiary granites and Cenozoic sediments (Kosuwan et al. 2004). It cuts across the Phang Nga Bay and Ban Don Bay (see Figure 1.9). The KMFZ can generate a maximum earthquake magnitude of M 6.9 according to Sutiwanich et al. (2008). The RFZ extends from Prachup Khirikhan at the Gulf of Thailand coast southwest towards Ranong at the Andaman Sea. The total fault length is approximately 220 km. The fault zone, which follows the channel of the Kraburi River, has its subsidiary faults cutting Late Cretaceous granites and Cenozoic sediments (Kosuwan et al. 2004). There were three significant instrumental earthquake reports along the RFZ and KMFZ reported by TMD (2013); (1) 16 May 1933 at RFZ with M 6.5, (2) 27 September 2006 at RFZ with M 4.7, and (3) 23 December 2008 at KMF Z with M 4.1 (TMD 2013).

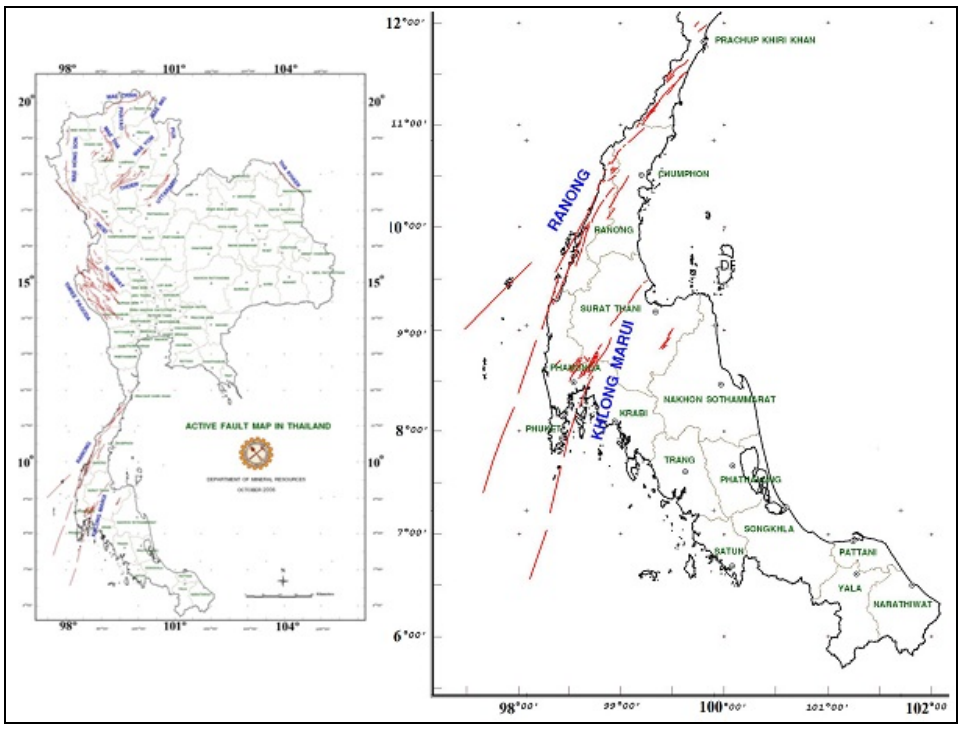

Figure 1.9 Active faults in Thailand (left) and in Southern Thailand (right) (after Kosuwan et al. 2004).

DMR (2007) concluded there several earthquakes occurred in southern Thailand based on instrumental data from the Thai Meteorology Department, Prince of Songkla University, and the United States Geological Survey (USGS). Body wave magnitudes (mb) were observed with mb 4 to 5 about 1,879 times, between mb 5 to 6 about 378 times, and more than 6 for 13 times. An earthquake map based on instrumental data is presented in Figure 1.10.

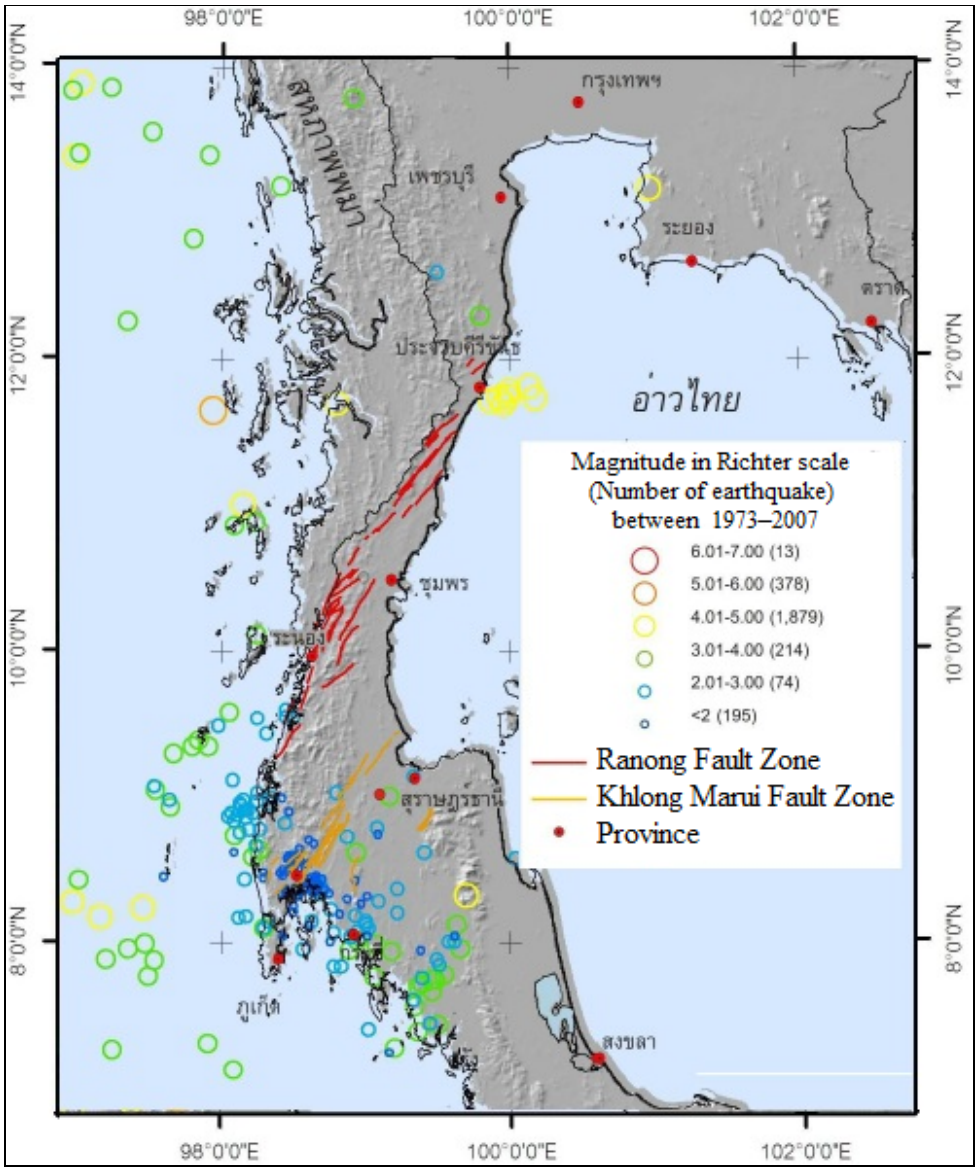

Figure 1.10 Instrumental earthquake map of Southern Thailand 1973–2007, modified from DMR (2007). Different colors mark different magnitude ranges.

1.5 Luminescence dating of sediments

Luminescence is light released from matter responded by some external stimulations. In this study, luminescence as a property of matter, here minerals, stimulated by light or/and heat is applied to determine the ages of sediments related to activities of paleoseismological events. These signals are accumulated by ionizing radiation.

1.5.1 Natural ionizing radiation

Ionizing radiation is defined as the radiation consisting of particles, X-rays, or gamma rays with sufficient energy to cause ionization in the medium through which it passes. In the environment natural radioactive elements are generally found such as uranium, thorium, and potassium as well as their daughter products (Lian and Huntley 2002), emitting ionizing radiation such as alpha, beta, and gamma. These radiations have cause the environmental dose rate, or the rate of radiation to the environment. Preusser et al. (2008) separated the environmental dose rate into three types; cosmic radiation, external radiation, and internal radiation as shown in Figure 1.11.

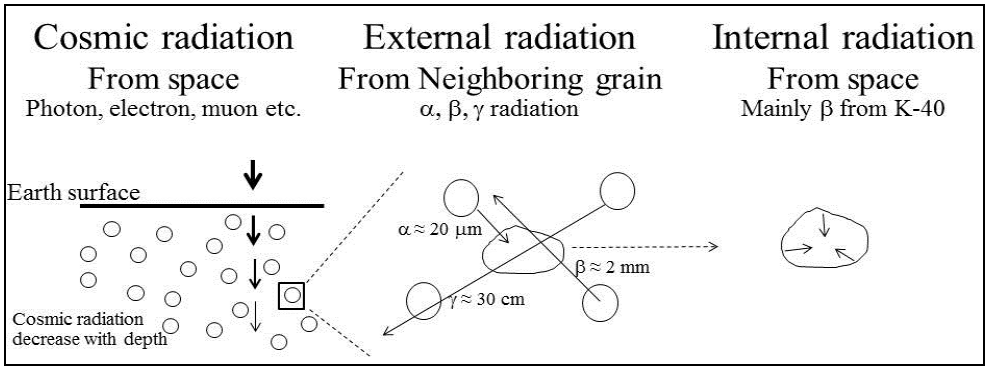

Figure 1.11 Natural ionizing radiation that has an effect on the environmental dose rate (after Preusser et al. 2008).

The internal radiation usually comes from potassium feldspar, which has a component of K-40 (radioactive isotope). The external dose rate is the radiation

of the surrounding grains towards the mineral of interest. Each particle/ray has different abilities to penetrate into the sediment and therefore different penetration depths: approximately 20 μm of alpha, 2 mm for beta, and 20–30 cm for gamma (Aitken 1998). The cosmic radiation is the third factor affecting the dose rate. This radiation is from the cosmogenic particles that result from the interaction between solar radiation, earth magnetic field, and gases in the atmosphere.

1.5.2 Origin of luminescence signal

Usually, all minerals or crystals contain a vast number of point defects. Even when in quartz the concentration of these defects is in the order of ppb, it should be noted that about 10^{13} defects per cm^3 are present (Preusser et al. 2009). These defects, such as O atoms vacancy between Si atoms in quartz minerals, can make Si atoms to have a positive charge. Thus, electrons can be trapped there as shown in Figure 1.12(c). The mechanisms how electrons can be trapped can be described by the band theory.

Aitken (1985), Preusser et al. (2008), and Fattahi (2009) used the band theory in order to describe the occurrence of the luminescence phenomena. When minerals and their valence band electrons are exposed to ionizing radiation, these electrons are exited until they contain sufficient energy to reach the conduction band (CB). Some electrons may become detached from their parent nuclei in the crystal lattice and diffuse in the vicinity of defects in the conduction band and become trapped at the trap (T) level located below the conduction band. The duration and the intensity of the radiation are proportional to the number of trapped electrons as shown in Figure 1.12(a).

In case the accumulated electrons in the minerals are exposed to sunlight or heat, they will receive enough energy to change to the conduction band level again before suddenly decreasing their energy level to the recombination center (R), where the energy level is between T and the valence band. When particles,

electrons, decrease their energy, light is released called the luminescence as shown in Figure 1.12(b).

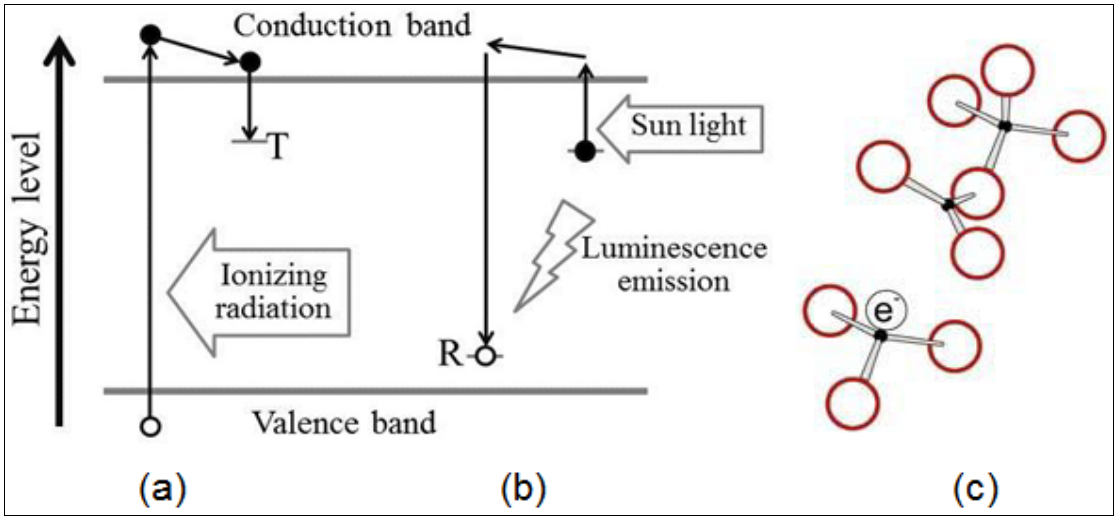

Figure 1.12 Luminescence processes: (a) mineral received ionizing radiation and electrons are trapped (energy level T) and accumulated, (b) after the crystal is exposed to sunlight or heat it decreases the energy level to R and releases luminescence light, (c) quartz defect structure that shows O defects and trapped electrons (circle = O atom, dot = Si atom).

In practice, minerals, which are widely used as dosimeters and for the dating, are quartz and feldspar. Quartz, which is commonly found in sediments, can resist weathering and its properties are relatively good investigated (Preusser et al. 2008), and therefore is a preferred mineral in luminescence dating. However, in some environments, quartz cannot be found. Then feldspar is chosen to be the dosimeter, because feldspar can accumulate electrons in a larger amount than quartz. Feldspar can also be used to date older ages than using quartz.

1.5.3 Luminescence dating in geological study

When studying of geological events that occurred in the past the time when events occurred is necessary to be determined. Many techniques are available

for dating these events, but every technique has its limitation, like gas isotopes were leaked in loose sediments or the ages were over estimated. The luminescence technique, both TL and OSL, has the advantage to date the time when sediment were the last time exposed to sunlight (Fattahi 2009); like in Figure 1.13 indicated by the black dot. When this sediment was not exposed to sunlight, the luminescence signal increased. However, after it received sunlight, the signal was reset until it was covered again. That means that the signal has been being accumulated from that time to present (Figure 1.13). The amount of accumulated electron is used to determine how long that sediment has been disconnected from sunlight (related to the geological events).

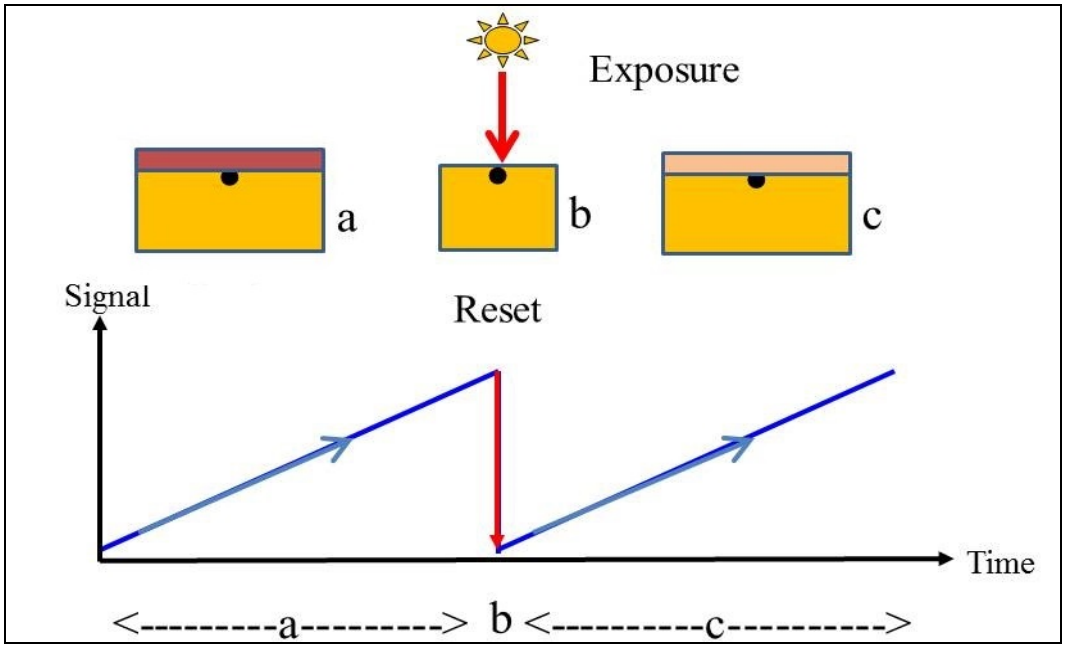

Figure 1.13 Accumulation and releasing of luminescence signal in a sediment (a), (c) upper sediment layer is covering the black dot and luminescence signal started to accumulate in traps, (b) black dot being exposed to sunlight which lead to the luminescence signal reset to zero.

However, there is a weakness of the luminescence technique that is the incomplete bleaching of minerals in sediments like the colluvium. These sediments are eroded and transported along hill slopes by flowing water under gravity, and that usually forms wedge-shaped deposits at the foot-slope (Fuchs and Lang 2009). Fuchs

and Lang (2009) also offered a method to achieve good quality results: (1) study of the equivalent dose distribution of small aliquots and single grains, (2) comparison of luminescence signals with different light sensitivity, (3) stratigraphic consistency of OSL age estimates, and (4) comparison of OSL-ages and independent age control. The remaining percentage of the luminescence signal for each mineral, both for TL and OSL, after bleaching at day light and under water are presented in Figure 1.14.

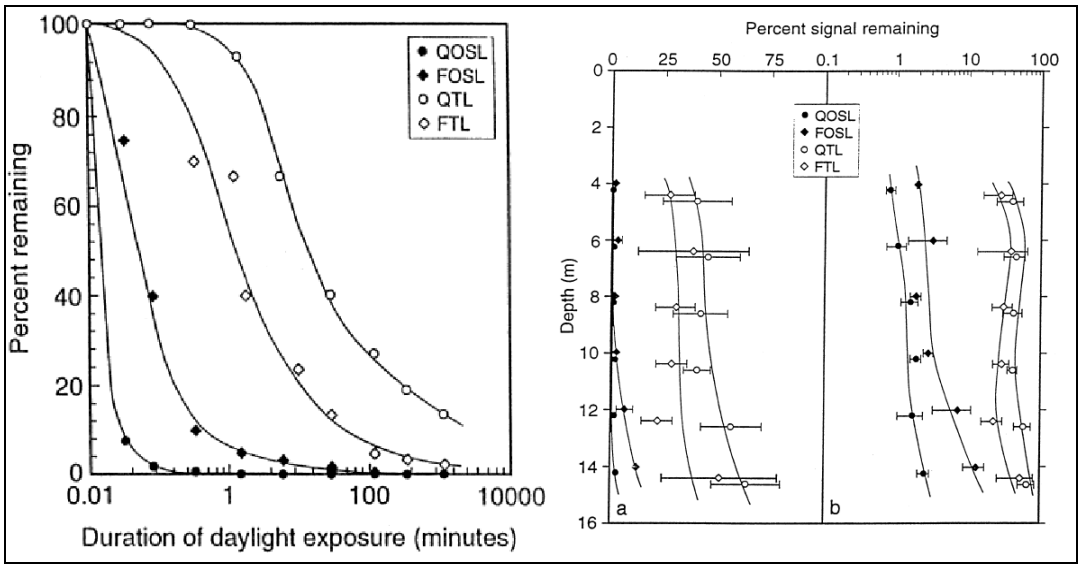

Figure 1.14 TL and OSL bleaching characteristic: Percentage of the remaining luminescence signal after exposed to day light (left) and exposed for three hours to light transmitted through various depths of seawater (right) (note linear scale and log scale). QOSL– quartz OSL, FOSL–feldspar OSL, QTL–quart TL, and FTL–Feldspar TL (Stokes 1999).

1.5.4 Luminescence signals from minerals

During the luminescence process the traps, where the electrons are accumulated in the energy levels below the conduction band (CB), can vary depending on how is the depth of the energy below the CB, how are the stimulation sources, either thermal or optical, and also depending on the energy characteristics, temperature and wavelength. Therefore, these factors have an effect on the luminescence characteristics of different minerals and related to different methods, as explained below.

Quartz TL peak: Wintle (1997) concluded that there are three dominant temperature peaks apparent in quartz thermoluminescence, at 383 K, 598 K, and 648 K. The 383 K can be found in all quartz minerals, but because of the low stability of 383 K, this peak is not used for dating. In contrast, the 598 K and 648 K have higher stability. However, because the 648 K is bleaching slower than the 598 K, and the saturation is at lower doses, the 598 K is widely used. The 598 K could be used for dating up to millions of years. Moreover, the 598 K TL peak is quite rapidly than others bleached even 500 nm wavelength. The wavelength emitted for various temperatures is shown in Figure 1.15.

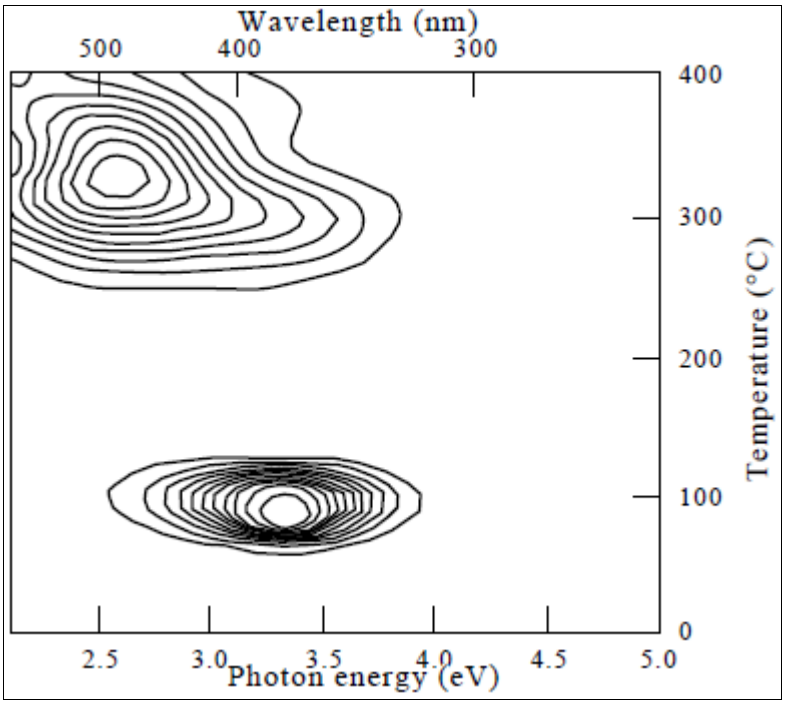

Figure 1.15 TL signal of different wavelengths emitted from quartz at different temperatures (Scholefield et al. 1994).

Feldspar TL peak: Wintle (1997) concluded that there are two dominant temperature peaks in feldspar thermoluminescence, 553 K and 603 K. For potassium feldspar, luminescence with 390–440 nm wavelength is emitted, and 560-570 nm wavelength for plagioclase feldspar.

Quartz OSL: From the observation of OSL signals in quartz when irradiated crystal were exposed to visible light it was found that the OSL production is

presented clearly at 365 nm (Huntley et al. 1991; Wintle 1997) as shown in Figure 1.16a.

Feldspar OSL: The feldspar OSL production clearly occurs at about 400 nm (Huntley et al. 1991) as shown in Figure 1.16b. They emit in three bands at 330 nm, 400 nm (mainly in K-feldspar), and 570 nm (mainly Na-feldspar).

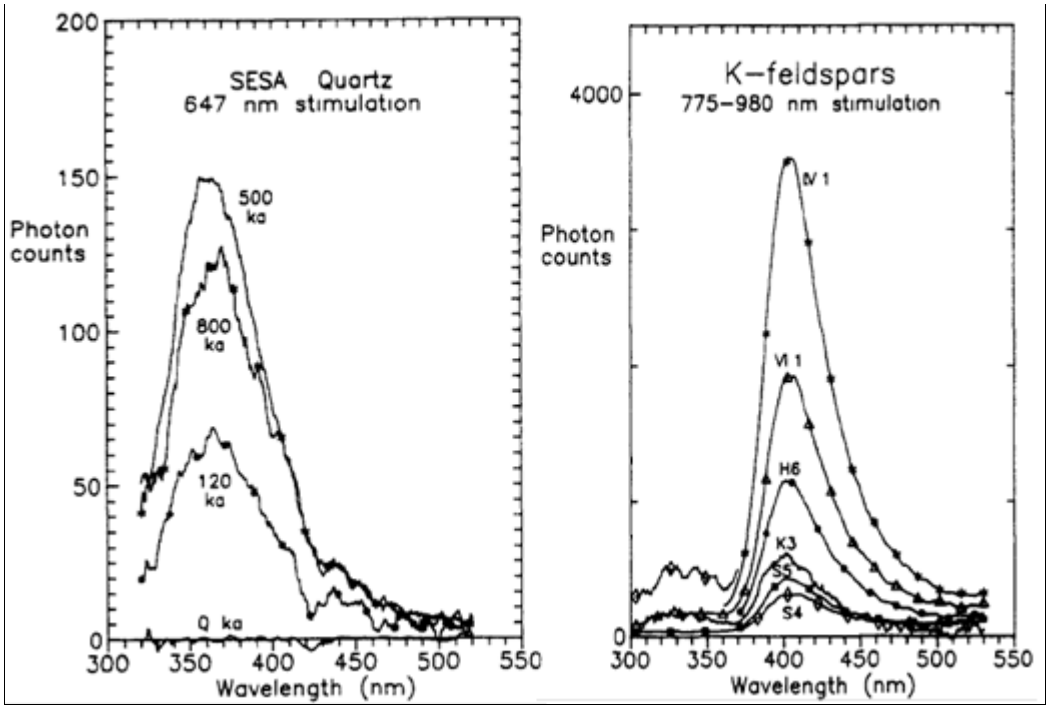

Figure 1.16 Left: Apparent OSL signal of quartz at various age ranges (647 nm light stimulated); Right: apparent OSL signal of several Finland K-feldspars (775-980 nm light stimulated) (Huntley et al. 1991).

CHAPTER 2

METHODOLOGY

2.1 Fieldwork

Two main field surveys in May and October 2012 were carried out in the study area of western Surat Thani Province for identifying locations of paleoearthquakes, between UTM 0495000 and 0523000 East, and UTM 1015000 and 1031000 North. Before the field surveys previous studies, geological maps as well as Google Earth satellite images were analyzed in order to identify possible outcrop locations. Main outcrops of subsurface sediment and rock formations were mainly quarries, active as well as abandoned and road cuts. In one case a small trench has been made using an excavator. From the field surveys finally three locations were chosen for this study, three places in Vibhavadi District (V1, V2 and V3) and two locations in Tha Chang District (TC and CTR) as shown in Figure 2.1.

At the selected sites the lithologies, structures, stratigraphy, and general environment were studied and recorded. Detailed photos were taken and sketching and drawing by hand were done by making grids with ropes over the exposed structures, if accessible. Geological investigations were carried out, for example the strike directions of faults were determined from slickensides in the vicinity. Furthermore, a small trench was done at CTR site for observing the structures and collecting samples. At all the five sites chosen for this study TL and/or OSL samples were taken with multiple samples from one site as different stratigraphic layers have been sampled.

2.2 TL dating of sediment

2.2.1 Sampling method

TL samples were collected in the night time for protecting the sediment material from light exposure by using a cylindrical steel sample holder (Figure 2.2), 10 centimeters in diameter and 50 centimeters long. Samples were taken from different layers identified at the outcrops wall in mainly horizontal direction. Both sides of the open steel cylinders were sealed against light during the transport until further processing in the laboratory.

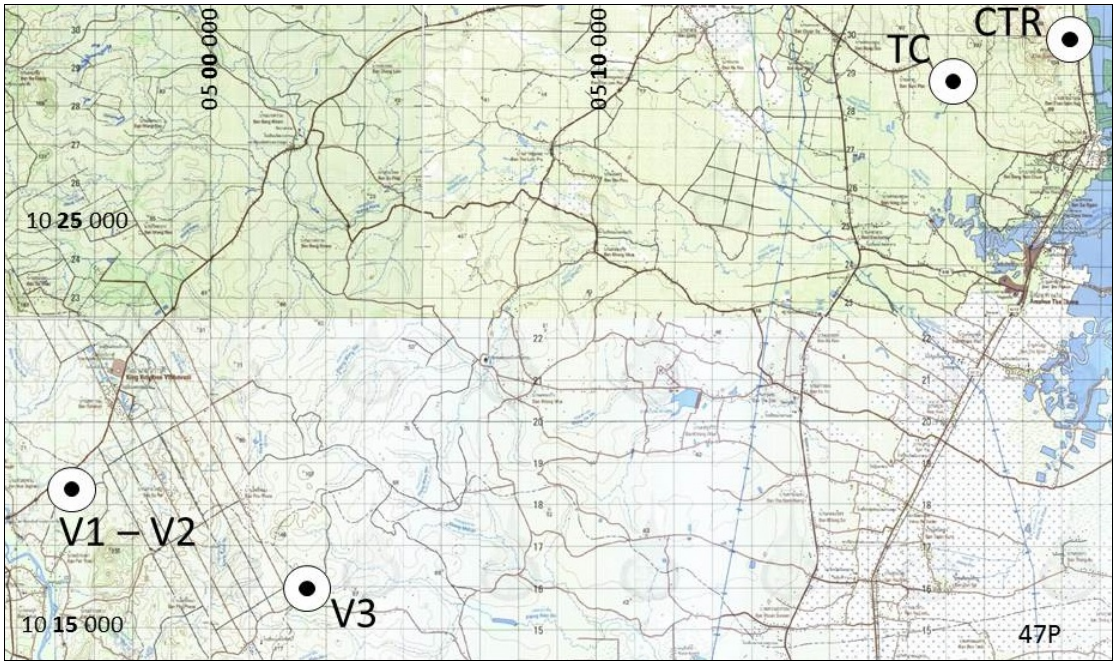

Figure 2.1 Study locations in Surat Thani province: V1, V2, and V3 are in Vibhavadi district; TC and CTR are in Tha Chang district (after RTSD 2003(a), RTSD 2003(b), RTSD 2004 and RTSD 2005)

Collected samples were separated into two parts; the first part was used to determine dose rate (this part can be processed under normal light) and the second part, which needed to be processed under red light for luminescence measuring process.

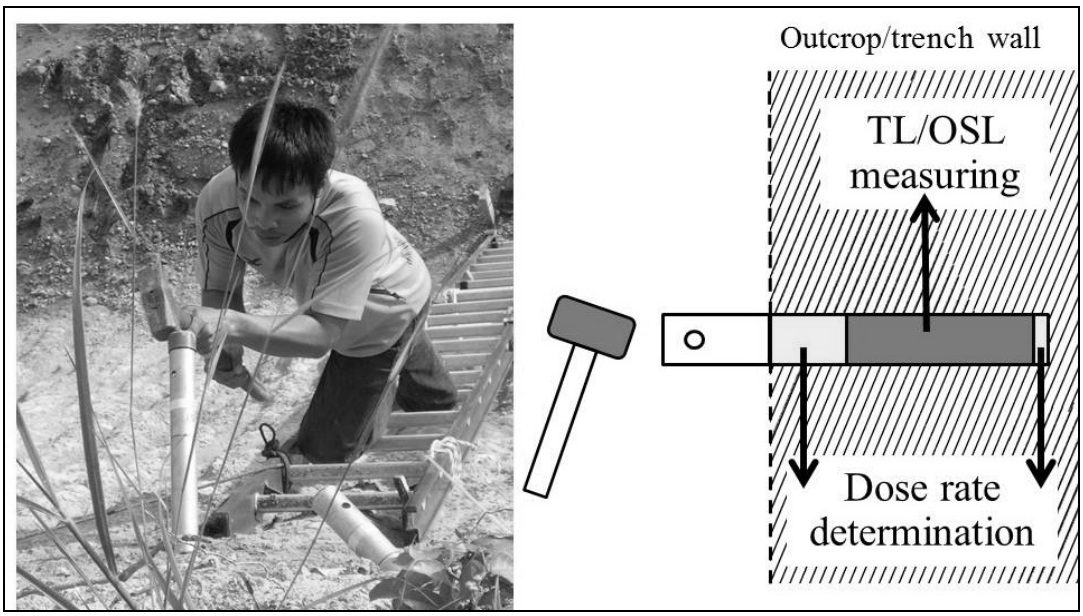

Figure 2.2 Sample holders in an outcrop wall (left); the middle part of the collected sediment was used for luminescence measuring, and the outer parts were used for dose rate determination (right).

2.2.2 Dose rate determination

Many approaches can be applied to determine dose rate such as dosimetry in situ measurement (Kitis et al. 1982), spectrometry in situ measurement (Lian and Huntley 2002), or laboratory analysis of activity (Preusser et al. 2008). The first two approaches need relatively more time as they are done during fieldwork. For this study the laboratory analysis was selected.

The activity analysis of the natural ionizing radiation is an important factor for the TL age calculation. Elements analysis techniques can be used to determine the natural three elements, potassium, uranium, and thorium, for example gamma spectrometry, alpha counting, and inductively coupled plasma-mass spectrometry (ICP-MS). First, samples were dried and milled in order to get a smaller grain size that was needed for all analysis.

In this work, gamma spectrometry was used to determine the dose rate. Gamma spectrometry is a high performance technique to determine the activity of nuclear elements that emit gamma ray. A total of 116 grams of milled samples were

kept in a sealed container for a period of one month in order to get the gas Radon into equilibrium inside the container. Then a gamma ray spectrometry was carried out to determine the amount of U-238, Th-232, and K-40 by using a high-purity germanium (HPGe) detector at 1.460 MeV for K-40, 1.760MeV or 0.609 MeV of Bi-214 (U-238) and 2.615 MeV of Tl-208 or 0.911 MeV of Ac-228 (Th-232), as shown in Figure 2.3. The three elements are used for calculating the annual dose or dose rate (D). The specific activity of the sample (concentration of nuclide) are calculated as following

$$a\ (Bq/kg) = kCn \qquad 2.1$$

where $k=1/\varepsilon P\gamma Ms$, a is the specific activity of the sample in Bq/kg, Cn is the count rate at a certain peak, ε is a detector efficiency, Pγ is the percentage of gammas per disintegration of this nuclide for a transition at energy E, and Ms is the mass in kg of the measured sample. The detector efficiency, ε, can be determined by using known activity of samples and the number of counts that appeared on the spectrum. After ε at the interesting energy level and the counts of the sample are known, the activities of each element in a sample are also known. For using the activities in the dose rate calculation they have to be changed into concentration units, ppm or percent, with 1 ppm U is 12.35 Bq/kg U, 1 ppm Th is 4.06 Bq/kg Th, and 1 % K is 313 Bq/kg K (Aboelkhair and Zaaeimah 2012).

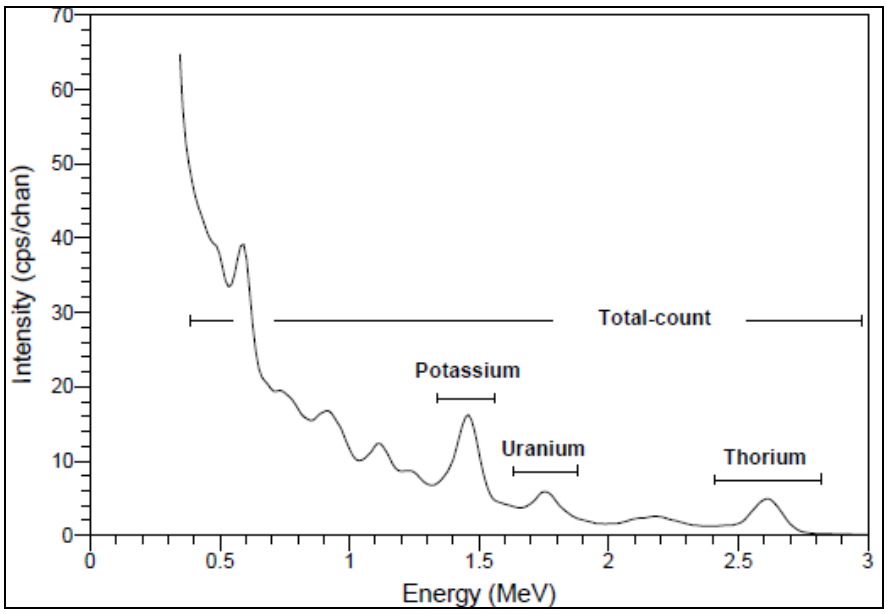

Figure 2.3 Typical gamma ray spectrum showing the positions of the conventional energy windows (IAEA 2003).

To determine the efficiency of the detector a standard with known activity is used. For this study, the 96.62 g IAEA Soil6 sample from Hatyai Campus was used, which has an activity of 19,050 Bq/kg (1840.61 Bq). Five energy levels from Ra-226 and the calculation of their efficiencies are shown in Table 2.1. The efficiency at its energy was plotted in Figure 2.4 and determined following the relationship shown in Equation 2.2.

$$Eff = 0.0013*(E)^{-0.465} \qquad 2.2$$

Table 2.1 Calculation of standard efficiency IAEA soil6 after six hours measurement. Pγ is the percentage of gammas per disintegration of this nuclide for a transition at energy E; A0 is activity of known sample.

Nuclide	A0 (dps)	Half life (s)	Intensity (Pγ)	E(keV)	Net Area	cps = Net Area/21600	Theoritical = Ao* Pγ	Eff= cps/Theoritical
Pb-214	1840.61	1608	0.192	295.21	646	0.02991	353.3973	8.46283E-05
Pb-214	1840.61	1608	0.372	351.92	1428	0.06611	684.7073	9.65538E-05
Bi-214	1840.61	1194	0.463	609.31	1357	0.06282	852.2029	7.37196E-05
Bi-214	1840.61	1194	0.151	1120.29	293	0.01356	277.9323	4.88062E-05
Bi-214	1840.61	1194	0.158	1764.49	260	0.01204	290.8165	4.13905E-05

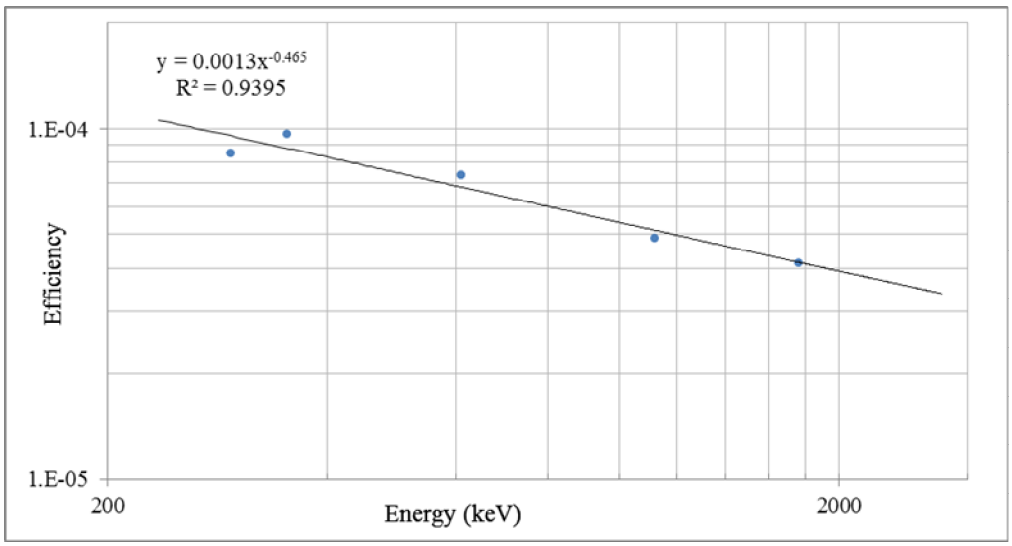

Figure 2.4 Efficiency versus energy (in logarithm scale) and related equation.

In this study, the energy of K, U, Th were used for the determination of the efficiency. The 1,764 keV peak of Bi-214 and 2,614 keV peak of Tl-208 were used to determine the equivalent of U and Th, respectively and 1,462 keV peak for K-40. The efficiency at each energy level was calculated using Equation 2.2. Therefore, at 1,764 keV the efficiency is 4.157×10^{-5}, at 2614 keV it is 3.462×10^{-5}, and at 1,462 keV it is 4.536×10^{-5}.The 116 gram part of each sample, which was kept in a sealed container, was measured. The k values of the three isotopes are k_{eqU} = 13,042.14, k_{eqTh} = 2,489.79, and k_K = 17,277.18. These k values will be used to determine the activity using Equation 2.1.

2.2.3 Cosmic dose rate

The determination of the cosmic dose rate was presented by Prescott and Hutton (1994), which is widely used. First, the dose rate D_0 at the depth of sampling was determined using following equation.

$$D_0 = \frac{C}{((x+d)^{\alpha}+a)(x+H)}\exp(-Bx) \qquad 2.3$$

where D_0 is in Gy/ka and x is in hg/cm^2 (100 g/cm^2), C = 6,072, B = 5.50×10^{-4}, d = 11.6, a = 75, α = 1.68, and H = 212, and where x can be determined

from the assumed density of the sediment samples of 2.50 g/cm^3 and the depth of the sample position in centimeter. For example, if a sample was collected at 100 centimeter depth, x = 2.50 g/cm^3 x 100 cm = 250 g/cm^2 = 2.50 hg/cm^2.

As the cosmic ray depends on the geomagnetic field, the correction of the geomagnetic latitude is needed. The conversion from geographic latitude (θ) and longitude (ϕ) to geomagnetic magnitude (λ) is presented in Equation 2.4. The geomagnetic latitude is used to determine the constant values, J, F, and H, following Figure 2.5, which is needed for the calculation of the cosmic dose rate in Equation 2.5. The real cosmic dose rate D_c is presented in Gy/ka, where h is altitude in km.

$$\sin\lambda = 0.203\cos\theta\cos(\phi - 291) + 0.979\sin\theta \qquad 2.4$$

$$D_c = D_0[F + J\exp(h/H)] \qquad 2.5$$

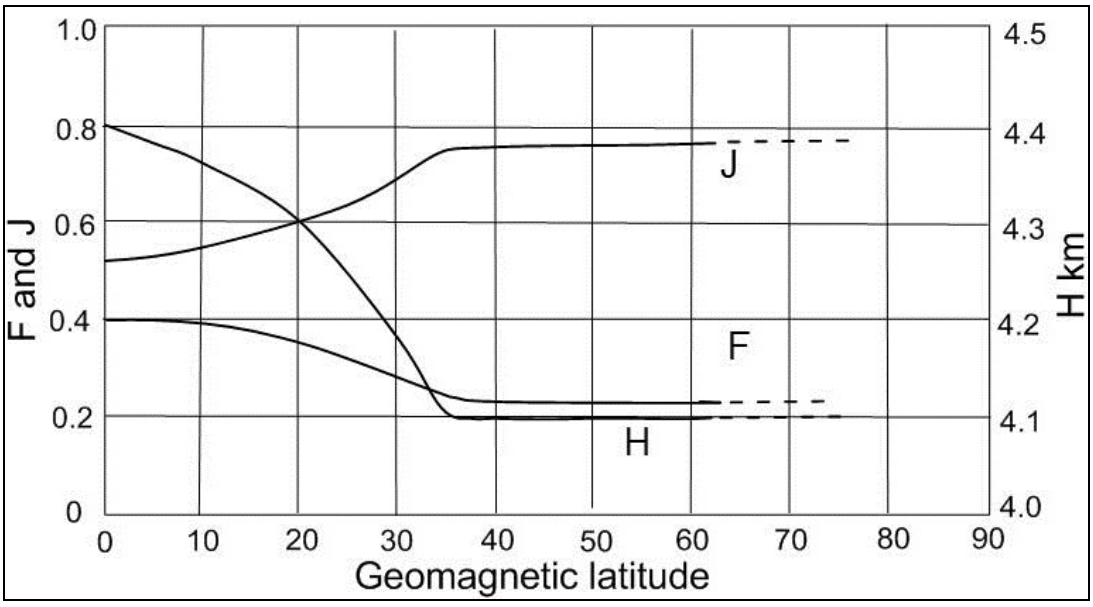

Figure 2.5 Determination of J, F, and H constant values to correct the geomagnetic latitude (redrawn from Prescott and Hutton 1994).

2.2.4 Dose rate calculation

Aitken (1985) offered a way to determine the dose rate from the concentration of these elements using the conversion factors (constant values), which were developed by Guérin et al. (2011) as shown in Equation 2.6a and b. For the determination of the net external dose rate after a correction for the water content is shown in Equation 2.6c.

$$D_\beta = 0.0277\ Th + 0.1457\ U + 0.7982\ K \quad (2.6a)$$

$$D\gamma = 0.0479\ Th + 0.1116\ U + 0.2491\ K \quad (2.6b)$$

$$D_{ext} = \frac{D_\beta}{1+1.25WF} + \frac{D_\gamma}{1+1.14WF} \quad (2.6c)$$

D_{ext} is net external dose rate in Gy/ka, which is calculated from the beta dose rate (D_β), and the gamma dose rate (D_γ) after corrected for water content (weight of water over dry weight) W in the sediment, whereas F is the fraction of water saturation in the soil. So, in Equation 2.6c, no value for F is assumed (Aitken 1985). For Th, U, and K the concentration of the radioactive element (Th, U, and K respectively) is in ppm, for Th and U, and in percent for K.

In case of quartz luminescence, the internal dose rate can be skipped (Preusser et al. 2008) because there is trace radioactive element in the crystal. Therefore, the net dose rate, D, can be calculated using the external dose rate and cosmic dose rate following Equation 2.7.

$$D = D_{ext} + D_c \quad (2.7)$$

For example, sample BT1177 with 9.82 ppm Th, 2.52 ppm U, and 0.487% K, and with 6.7% water content, D_β is 0.0277x9.82 + 0.1457x2.52 + 0.7982x0.48 = 1.027 Gy/ka. $D\gamma$ is determined accordingly. Using Equation 2.6c and 2.7 the total dose rate is determined using W=0.067, F=0.8 and D_c=0.155, so D_{ext} and D is 1.791 and 1.946 Gy/ka, respectively.

2.2.5 Sample preparation

All sample preparation procedures were done in a dark room under red light conditions. Field collected samples were sieved. The 90-200 micron fraction was used as a coarse grain sample. Samples were treated with 10% or less hydrochloric acid (HCl) (high concentration could generate heat during the reaction) until the reaction was finished for removing all carbonate material.

Treated samples were separated by using density liquid, tetra–bromoethane (density 2.967 g/cm^3) and dipropylene glycol (density 1.021 g/cm^3). For the first density separation procedure, the 2.70 g/cm^3 density liquid was mixed with the cleaned minerals for separating the heavy minerals. The minerals were separated into two parts, higher and lower than 2.70 g/cm^3. The lower part, which has a density of less than 2.70 g/cm^3 was applied to the 2.58 g/cm^3 heavy liquid for the separation of quartz (>2.58 g/cm^3) and feldspar and others (<2.58 g/cm^3). Finally, in order to get a bright TL signal, the interesting minerals (quartz or feldspar) were etched using hydrofluoric acid (HF) for removing the minerals surface, where mostly effected by any alpha particle. A diagram summarizing the preparation and treatment steps is given in Figure 2.6.

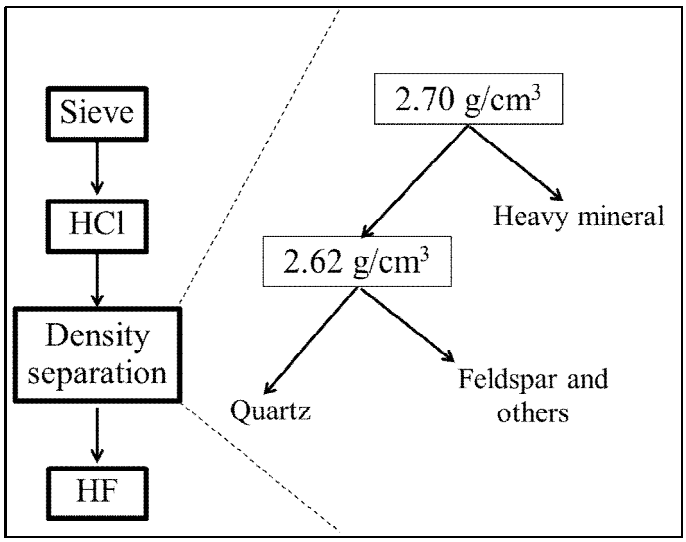

Figure 2.6 Steps for the preparation of quartz for luminescence measurements; treatment and density separation.

2.2.6 Measurement and processing of multi-aliquot additive dose TL

Thermoluminescence is a luminescence emitted by thermal stimulation. A Harshaw 3500 TL Reader was used to measure the TL signal at the Physics Section, Department of Science, Faculty of Science and Technology, PSU, Pattani Campus. The samples were stepwise heated up with 25 °C per second until 600 °C was reached. All samples were irradiated at the Office of Atoms for Peace in Bangkok, Thailand.

There are two main techniques to determine the equivalent dose, ED, multi-aliquot and regeneration technique. The multi-aliquot technique (additive dose) is a method where artificial radiation is added to the natural level to simulate a future situation. After the present and future levels are known, extrapolation method is used to determine the starting point when the mineral was reset the last time in the past as shown in Figure 2.7.

In this study, every sample was irradiated from 50 to 1,500 Gy. Plotting the deconvoluted signal with the artificial dose an equation fitted can be drawn. The interception of the signal and residual level is called equivalent dose or accumulated dose (ED). The separated quartz was bleached for 20 hours in the sunlight in order to determine the residual level of quartz after bleached by the sun.

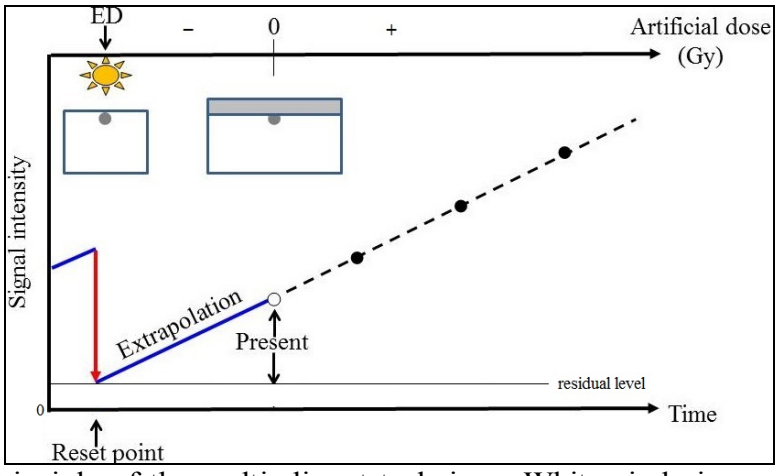

Figure 2.7 Principle of the multi-aliquot technique. White circle is present (natural) signal, black circles are artificial signals added to the natural signal.

Glow curve deconvolution

The measured TL signal can be quite complex as shown in Figure 2.8, as it could show four or more peaks because of more electron traps type overall. For the TL signal analysis a deconvolution software was used; here the GlowFit v1.1 freeware, which was developed and presented by Puchalska and Bilski (2006). The main advantage of GlowFit is the ability to resolve complex TL glow curves consisting of strongly overlapping peaks. The GlowFit provides the intensity for each temperature peak. The area under each peak is calculated and used as the intensity of the artificial dose as shown in Figure 2.7.

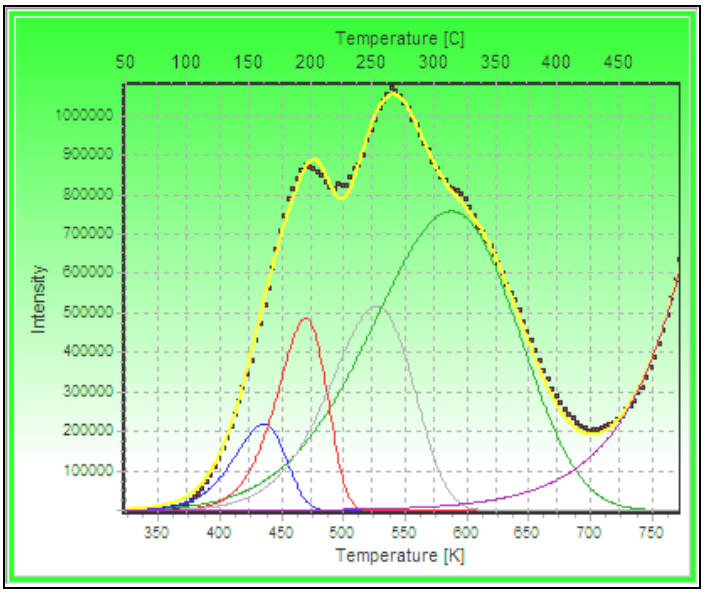

Figure 2.8 GlowFit v1.1 deconvolution result. The laboratory signal (dots) are deconvolved for each temperature peak (blue, red, gray, and green lines), and the total deconvolved results (yellow line) of sample TL08. The violet line is the black body radiation.

2.2.7 Age calculation

It was assumed that the dose rate, D, to a mineral from the ionizing radiation of the environment, external, internal, and cosmic radiation, was constant. The accumulated dose or equivalent dose, ED, can be estimated by multi aliquot and a

regeneration technique, which is presented in the previous section. The age of sample can then be determined by following Equation 2.8.

$$Age = \frac{ED}{D} \tag{2.8}$$

The error of age can be estimated from Equation 2.8 by using partial derivative method and the Equation 2.9 can be used.

$$\Delta Age = \left|\frac{\partial Age}{\partial ED}\right| \cdot \Delta ED + \left|\frac{\partial Age}{\partial D}\right| \cdot \Delta D$$

$$\Delta Age = \frac{\Delta ED}{D} + \frac{ED \cdot \Delta D}{D^2} \tag{2.9}$$

2.3 OSL dating of sediment

For the OSL dating some of the operating steps are similar to the TL steps, like the sampling method, cosmic dose rate determination, dose rate calculation, and age calculation. However, for the sample preparation the high density liquid was made from a sodium polytungstate (NST) solution, whose density depends on its concentration.

2.3.1 Dose rate determination

For the OSL dating thick source alpha counting was used for the determination of the U and Th content in the sediments, and ICP-MS was applied for the determination of the K content.

Thick source alpha counting (TSAC) is a technique for determining the concentration of radioactive elements, which are emitting alpha particles in sediments, such as in the uranium series. As an alpha particle can move a maximum of 25 μm, this technique uses a sample source with a thickness of more than 25 μm (Aitken 1985) as shown in Figure 2.9 (a). The dried-crushed samples, which have a particle

size of less than 63 μm, were prepared as described above and then put into trays of a ZnS (Ag) scintillator as shown in Figure 2.9 (b). The ZnS (Ag) scintillator can emit light when it is stimulated by alpha particles in the samples (Michael and Zacharias 2000). All samples were stored for a minimum of one month in order to reach equilibrium of the gas radionuclides before the samples were measured.

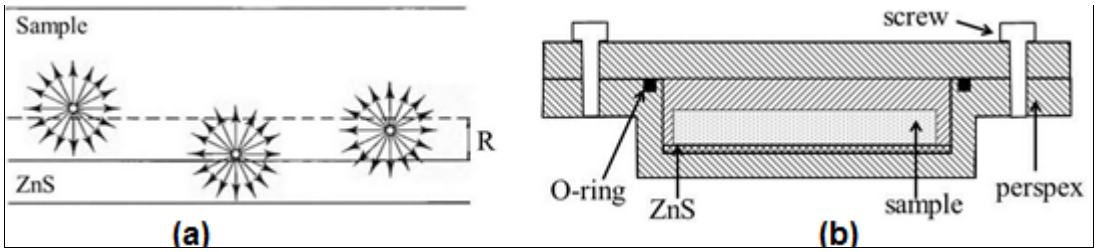

Figure 2.9 (a) TSAC idealized sketch (Aitken 1985) with only particles at the distance R (approx. 25 μm) from the bottom are converted to light emission; (b) practical tray for the measurement of TSAC (Soumana et al. 1997).

ICP-MS is a spectroscopy technique which is used for the determination of the potassium 40 content for the OSL dating. Wolf (2005) described the principles of the ICP-MS to determine the elements. ICP-MS combines a high-temperature ICP (inductively coupled plasma) source with a mass spectrometer. The ICP source converts the atoms of the elements in the sample to ions. These ions are then separated and detected by the mass spectrometer. In a magnetic field the ion of each element, which has a different mass, has a circular motion for which the radius is varying with the mass. An overview of the ICP-MS principle is shown in Figure 2.10.

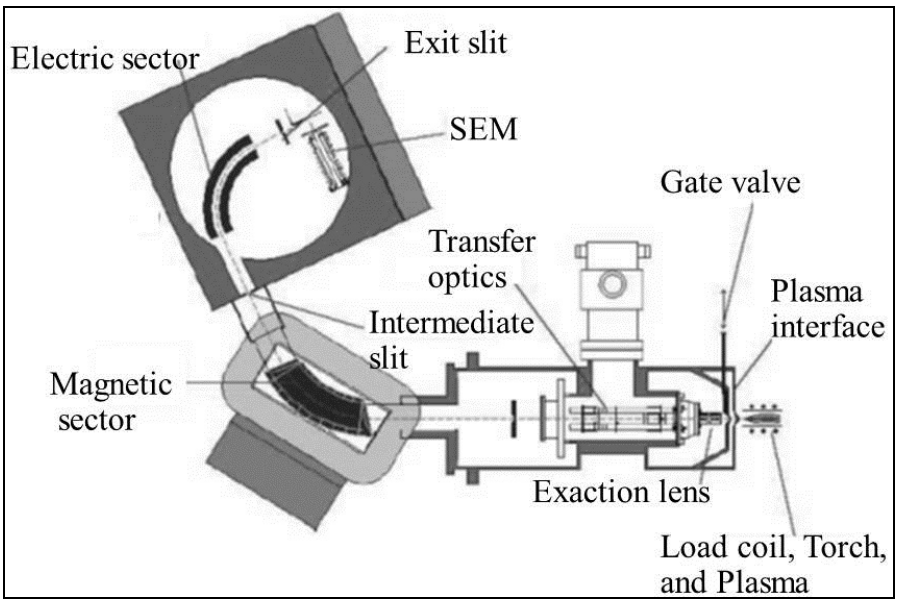

Figure 2.10 Schematic diagram of ICP-MS (Wolf 2005).

2.3.2 Measurement and processing of single aliquot OSL

OSL is the emission of luminescence light by visible light stimulation, blue light in this study. A Risø TL/OSL reader was used in this study at the University of Bayreuth, Germany. This instrument has its own irradiation system, which is $^{90}Sr/^{90}Y$. The concept of this measurement is shown in Figure 2.11.

Single-aliquot regeneration

The single-aliquot regeneration (SAR) method involves the interpolation and measurement of the dose of the ionizing radiation that produces the same luminescence signal than a signal that was measured from the sample in its natural state (Fattahi 2009). In principal, the regeneration method is simulating the luminescence signal since the time it was bleached since it has received the natural ionizing radiation (here artificially in laboratory). The natural signal intensity is then used in the comparison with the interpolating graph as an ED as shown in Figure 2.12.

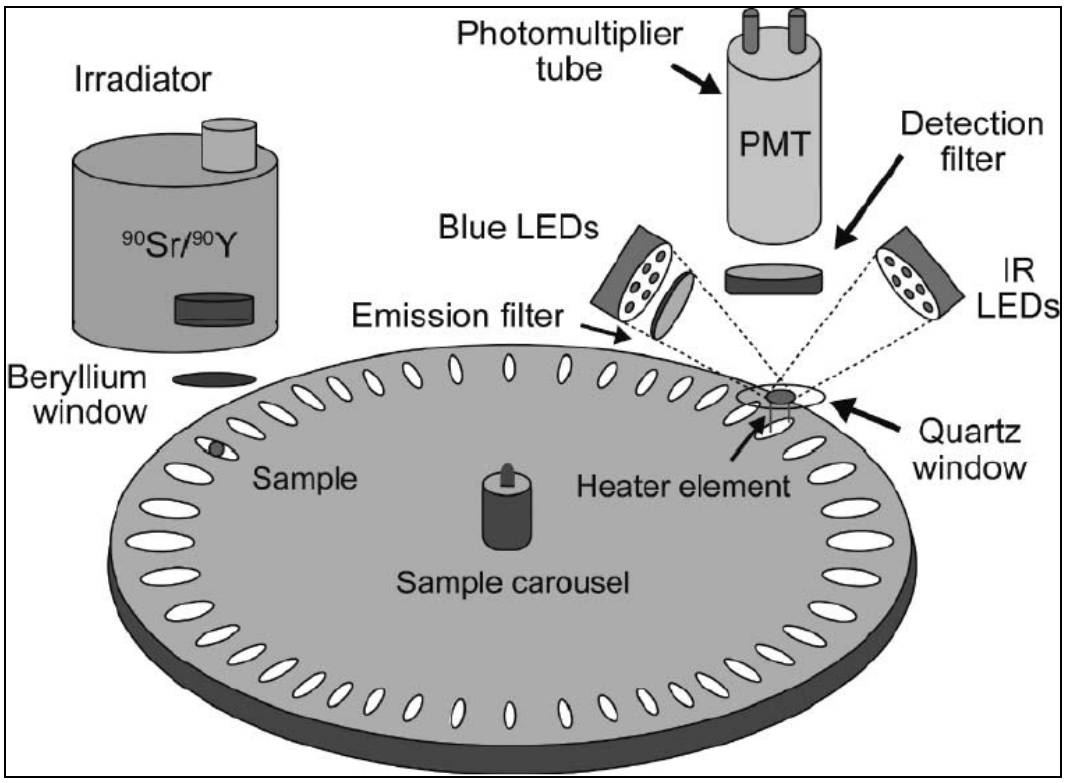

Figure 2.11 Basic features of a Risø OSL reader (Preusser et al. 2008).

Step measurements

Preusser et al. (2008) described the step measurements for the regeneration technique as shown in Figure 2.13. After bleaching was carried out for each step sensitivity changes can occur. A test dose (Tx) step is necessary by the irradiation of a low fixed dose for each generative dose. It is needed for normalizing the interesting signal (Lx) into Lx/Tx. For a suitable fitting a difference between the regenerative dose points (plus a zero point) is required (Preusser et al. 2008). To avoid possible errors, Preusser et al. (2008) suggested to measure two times the lowest regenerative dose (cycle 2 and 6 in Figure 2.12). If they show more than 10% deviation from unity, the data can be discarded.

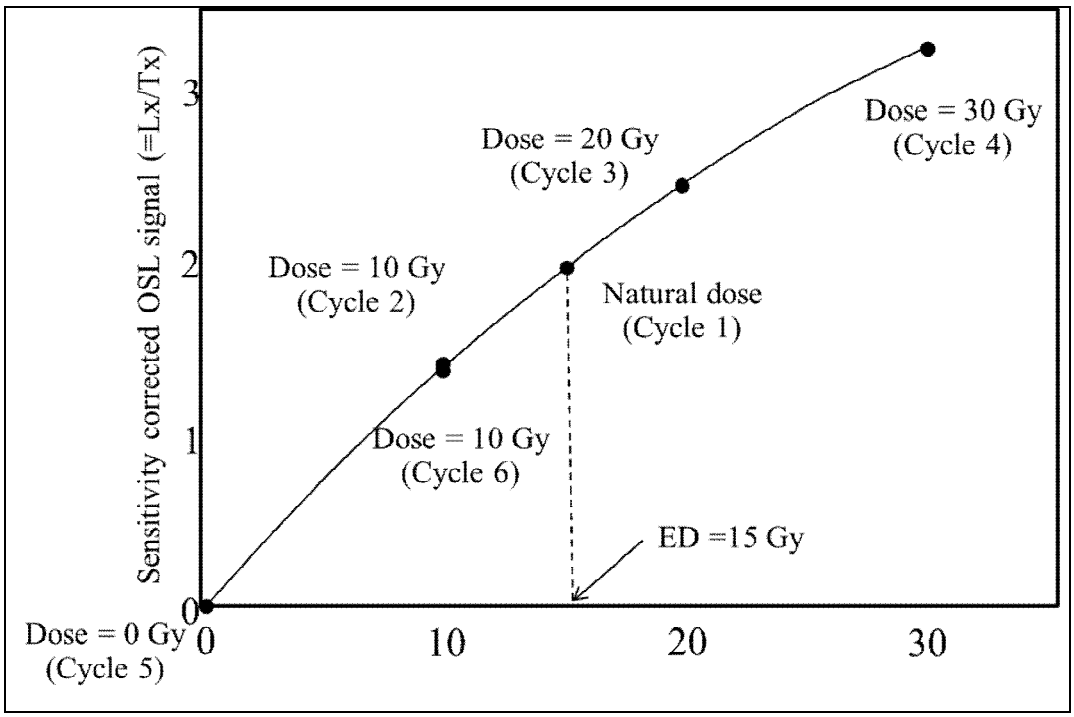

Figure 2.12 Principle of the regeneration method; cycle 1 is the natural luminescence level, cycles 2–4, and 6 are bleached and make artificial irradiation, cycle 5 shows bleached signal (after Preusser et al. 2008). In this case ED is 15 Gy.

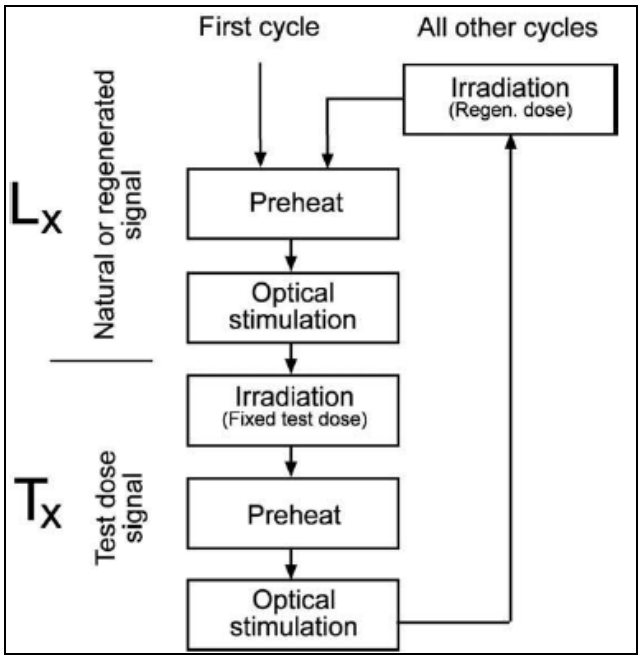

Figure 2.13 Step measurement of regeneration technique (Preusser et al. 2008).

Age model

Because the SAR method can give several values of ED, a statistical analysis is necessary to be carried out. Galbraith and Roberts (2012) gave recommendations about the statistical aspects of the equivalent dose and error calculation and the display of results in OSL dating. The age model is a statistical analysis of the ED. Five age models were presented by Galbraith and Roberts (2012): 1) Common age model, suitable for well bleached grains, the distribution curve is approximately normal Gaussian with no overdispersion, 2) Central age model, CAM, likely the common age model but could be overdispersed, 3) Minimum age model, MAM, for colluvial sediments which show incomplete bleaching, 4) Maximum age model, for fully bleached sediments like aerial sediment, 5. Finite mixture model, which is used in cases where there are more than two ages in a sediment sample. The statistical model was run by the R-studio software with luminescence package (Kreutzer et al. 2012).

2.4 C-14 dating

Ancient plant material was found in Vibahvadi district, outcrop V1. Radioactive carbon dating was used to determine its age by following the ASTM D6866-06a (ASTM International Standards Worldwide 2013). For this study the analysis was carried out by the Thailand Institute of Nuclear Technology (TINT), Nakorn Nayok, Thailand. The ASTM D6866-06a is a standard test method for determining the biobased content of natural range materials using radioactive carbon and isotope ratio mass spectrometry analysis.

C-14 is a radioactive isotope that is formed in the upper atmosphere. The ratio of the C-14/C-12 in living plants is a constant value. After a plant is dead the living processes in the plant are stopped and by this the intake of new C-14. Then the C-14 decays, so the amount of C-14 decreasing according to a half-life of 5,730 years. The amount of C-14 after the biological processes have been stopped is shown in Figure 2.14. The equation to calculate the age from the remaining C-14 content in the

organic matter is shown in Equation 2.10 where age is in years, with λ =1.2097x10^{-4} year^{-1}, C is the amount of C-14 in the dated material, and C_0 is the amount of C-14 in nature.

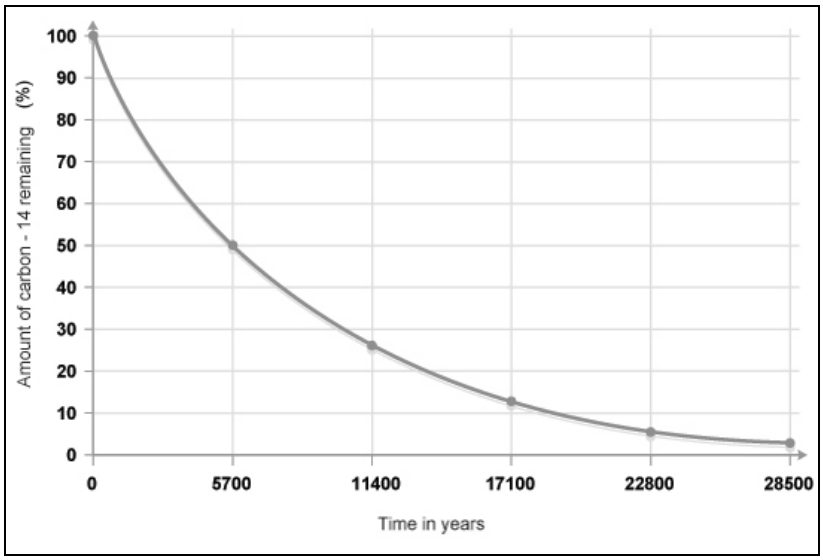

Figure 2.14 C-14 remaining in dated materials and its age (BBC 2013).

$$Age = -\frac{1}{\lambda}\ln(\frac{C}{C_0}) \qquad 2.10$$

2.5 Paleomagnitude estimation

For present earthquakes, all important parameters, location, occurrence time, and magnitude, can be determined from seismograms. However, for prehistoric earthquakes, no seismograms are available, so geological evidences are used. The location is known from a fault location, the occurrence time of a paleoearthquake can be known from dating methods, like luminescence dating in this study, and the paleomagnitude can be inferred from evidences of fault movement in the geological and environmental record. McCalpin (2009) presented several techniques for the determination of paleomagnitudes, such as surface rupture length (SRL), maximum

displacement (MD), and average displacement (AD), which were widely used. The empirical relationship is generally in the form of Equation 2.11.

$$M = a + b*\log(D), \qquad 2.11$$

where M is the paleomagnitude, D is the length or displacement, and a, b are constant values that are determined from regression lines (Wells and Coppersmith 1994) between geologic movements, such as length or displacement, and known magnitudes from historical earthquake as presented in Table 2.2.

Table 2.2 Techniques for the determination of the paleomagnitude, maximum displacement (MD), and average displacement (AD), with their regression line constant values (a, b) and their source range (Wells and Coppersmith 1994).

Method	Slip type	a	b	Standard deviation*	Displacement range (m)	Mw range
MD	Strike slip	6.81	0.78	0.29	0.01-14.6	5.6-8.1
	Reverse	6.52	0.44	0.52	0.11-6.5	5.4-7.4
	Normal	6.61	0.71	0.34	0.06-6.1	5.2-7.3
AD	Strike slip	7.04	0.89	0.28	0.05-8.0	5.6-8.1
	Reverse	6.64	0.13	0.50	0.06-1.5	5.8-7.4
	Normal	6.78	0.65	0.33	0.08-2.1	6.0-7.3

* Standard deviation of magnitude M

As the surface rupture length was not part of the scope of this study, the SRL method was not applied here. For the estimation of the paleomagnitude the displacements found in outcrops and stream offset were used.

CHAPTER 3

RESULTS

This chapter comprises the dating results and a detailed description of the five sites in Surat Thani Province where evidences of paleoearthquakes have been identified.

3.1 Dating Results

3.1.1 Radioactive elements analysis

Gamma spectrometry was used to determine the concentrations of the radioactive elements, which are used for dose rate calculation as part of the thermoluminescence age dating. From Equation 2.1, the peak areas of the interesting energies and k values were calculated as shown in Chapter 2 and were then used to calculate the activities, which are then converted into concentration of each element (U, Th, and K). The results are shown in Table 3.1. As the peak of TL12 at 2,610 keV was less than the background the peak of Ac-228 was selected for calculating the concentration of Th.

Alpha counting and ICP-MS data were used in determining the concentrations of U, Th, and K for the dose rate calculation of the OSL dating. All alpha counting results were converted from cph (count per hour) to ppm and percentages of K in the samples and shown in Table 3.2. Furthermore, the water content values for all samples are presented in Table 3.3 as well as the annual dose rate results.

3.1.2 Annual dose rate

Data from Section 3.2.1 were used in the calculation of the annual dose rate by the equations presented in Chapter 2. The errors are only presented in the total dose rate values. These results are presented in Table 3.3.

Table 3.1 Activities and concentrations of U, Th, and K based on calculations of the peak areas after removing the background.

Sample	Peak area at keV				Activity and error (Bq/kg)								Concentration and error					
	Ac-228 (911.2)	K-40 (1462)	Bi-214 (1764)	Tl-208 (2614)	Th from 911		K from 1460		U from 1764		Th from 2614		U from 1764 (ppm)		Th from 2614 (ppm)		K from 1460 (%)	
					Th	ΔTh	K	ΔK	U	ΔU	Th	ΔTh	U	ΔU	Th	ΔTh	K	ΔK
TL00	323	5	47	295	88	1	4	2	28	1	34	2	2.30	0.07	8.38	0.54	0.013	0.006
TL01	190	3	55	280	52	0	2	1	33	1	32	2	2.69	0.08	7.95	0.52	0.008	0.004
TL02	302	5	8	263	83	1	4	2	5	0	30	2	0.39	0.03	7.47	0.51	0.013	0.006
TL03	26	1	2	153	7	0	1	1	1	0	18	2	0.10	0.01	4.34	0.39	0.003	0.003
TL04	539	445	80	379	148	6	356	17	48	1	44	2	3.91	0.09	10.76	0.61	1.137	0.054
TL05	127	775	35	161	35	8	620	22	21	1	19	2	1.71	0.06	4.57	0.40	1.981	0.071
TL06	109	915	20	270	30	8	732	24	12	1	31	2	0.98	0.05	7.67	0.52	2.338	0.077
TL07	129	385	37	36	35	5	308	16	22	1	4	1	1.81	0.06	1.02	0.19	0.984	0.050
TL08	174	365	24	183	48	5	292	15	14	1	21	2	1.17	0.05	5.20	0.42	0.933	0.049
TL09	109	725	28	175	30	7	580	22	17	1	20	2	1.37	0.05	4.97	0.41	1.853	0.069
TL10	119	323	9	150	33	5	258	14	5	0	17	2	0.44	0.03	4.26	0.38	0.825	0.046
TL11	211	455	59	188	58	6	364	17	36	1	22	2	2.88	0.08	5.34	0.43	1.163	0.055
TL12	195	425	22	-	53	6	340	16	13	1	-	-	1.08	0.05	13.15	1.39	1.086	0.053
TL13	438	435	114	119	120	6	348	17	69	1	14	1	5.57	0.11	3.38	0.34	1.112	0.053
TL14	619	715	61	537	169	7	572	21	37	1	62	3	2.98	0.08	15.25	0.73	1.827	0.068
TL15	618	1035	72	466	169	9	828	26	43	1	54	3	3.52	0.09	13.23	0.68	2.645	0.082
TL16	350	595	69.9	300	96	7	476	20	42	1	35	2	3.42	0.09	8.52	0.54	1.521	0.062
TL17	802	775	87	640	220	8	620	22	53	1	74	3	4.25	0.10	18.17	0.79	1.981	0.071
TL18	545	835	78	416	149	8	668	23	47	1	48	3	3.81	0.09	11.81	0.64	2.134	0.074
TL19	279	505	28	282	76	6	404	18	17	1	33	2	1.37	0.05	8.01	0.53	1.291	0.057

Table 3.2 Alpha counting and ICP-MS results.

Sample	U (ppm)		Th (ppm)		K (%)
	U	ΔU	Th	ΔTh	
BT1168	4.24	0.41	18.59	1.37	0.699
BT1169	5.09	0.40	17.42	1.37	0.619
BT1170	2.68	0.26	8.39	0.87	0.030
BT1171	3.43	0.37	15.33	1.22	0.081
BT1172	2.35	0.27	9.33	0.91	0.023
BT1173	4.96	0.58	19.57	1.93	0.103
BT1174	1.76	0.17	6.03	0.58	0.139
BT1175	6.24	0.47	10.92	1.54	0.643
BT1176	3.07	0.36	8.60	1.19	0.397
BT1177	2.52	0.37	9.82	1.24	0.487

Table 3.3 Water content, annual dose rate (D) results of all samples.

Sample	Water fraction per dried mass	D_β (Gy/ka)		D_γ (Gy/ka)		D_c (Gy/ka)		D (Gy/ka)	
		D_β	ΔD_β	D_γ	ΔD_γ	D_c	ΔD_c	D	ΔD
TL00	0.075	0.537	0.019	0.658	0.033	0.143	0.007	1.338	0.059
TL01	0.063	0.582	0.018	0.682	0.033	0.160	0.008	1.424	0.060
TL02	0.119	0.245	0.018	0.399	0.026	0.151	0.008	0.795	0.052
TL03	0.065	0.128	0.015	0.217	0.020	0.151	0.008	0.496	0.043
TL04	0.054	1.685	0.073	1.167	0.051	0.129	0.006	2.981	0.130
TL05	0.095	1.787	0.077	0.846	0.040	0.118	0.006	2.751	0.123
TL06	0.142	1.945	0.083	0.982	0.043	0.148	0.007	3.075	0.133
TL07	0.065	1.011	0.054	0.478	0.027	0.155	0.008	1.644	0.089
TL08	0.138	0.931	0.058	0.583	0.034	0.143	0.007	1.657	0.099
TL09	0.099	1.652	0.074	0.799	0.039	0.123	0.006	2.574	0.120
TL10	0.057	0.796	0.052	0.438	0.032	0.169	0.008	1.403	0.091
TL11	0.112	1.345	0.067	0.825	0.039	0.169	0.008	2.339	0.114
TL12	0.090	1.273	0.088	0.943	0.078	0.169	0.008	2.384	0.174
TL13	0.055	1.699	0.068	1.016	0.040	0.143	0.007	2.858	0.115
TL14	0.111	2.083	0.086	1.410	0.055	0.154	0.008	3.647	0.149
TL15	0.171	2.553	0.097	1.550	0.054	0.141	0.007	4.245	0.158
TL16	0.084	1.797	0.077	1.098	0.048	0.159	0.008	3.054	0.133
TL17	0.101	2.456	0.093	1.699	0.061	0.146	0.007	4.301	0.161
TL18	0.106	2.339	0.090	1.413	0.054	0.132	0.007	3.883	0.151
TL19	0.070	1.357	0.068	0.808	0.043	0.165	0.008	2.330	0.119

Table 3.3 (cont.) Water content, annual dose rate (D) results of all samples.

Sample	Water fraction per dried mass	D_β (Gy/ka)		D_γ (Gy/ka)		D_c (Gy/ka)		D (Gy/ka)	
		D_β	ΔD_β	D_γ	ΔD_γ	D_c	ΔD_c	D	ΔD
BT1168	0.181	1.432	0.083	1.318	0.047	0.162	0.008	2.911	0.055
BT1169	0.173	1.465	0.082	1.346	0.045	0.162	0.008	2.973	0.053
BT1170	0.050	0.616	0.060	0.686	0.045	0.151	0.008	1.453	0.053
BT1171	0.089	0.908	0.080	1.058	0.053	0.143	0.007	2.110	0.060
BT1172	0.055	0.587	0.062	0.688	0.047	0.160	0.008	1.435	0.055
BT1173	0.069	1.260	0.129	1.439	0.071	0.151	0.008	2.850	0.079
BT1174	0.061	0.503	0.038	0.497	0.031	0.190	0.010	1.190	0.041
BT1175	0.075	1.604	0.103	1.309	0.049	0.143	0.007	3.056	0.056
BT1176	0.056	0.949	0.081	0.821	0.051	0.184	0.007	1.954	0.058
BT1177	0.067	0.963	0.083	0.828	0.052	0.155	0.008	1.946	0.060

3.1.3 Equivalent dose and age

The equivalent dose of the TL multi-aliquot method is presented in Table 3.4 with an example shown in Figure 3.1, here sample TL11. The growth curve was fitted by an exponential rise to maximum equation, y = y0 + a(1-exp(-bx)). Residual level (dashed line) is 1.69E6. The interception of the growth curve and the linear residual level is the ED, in this case 42.7 Gy.

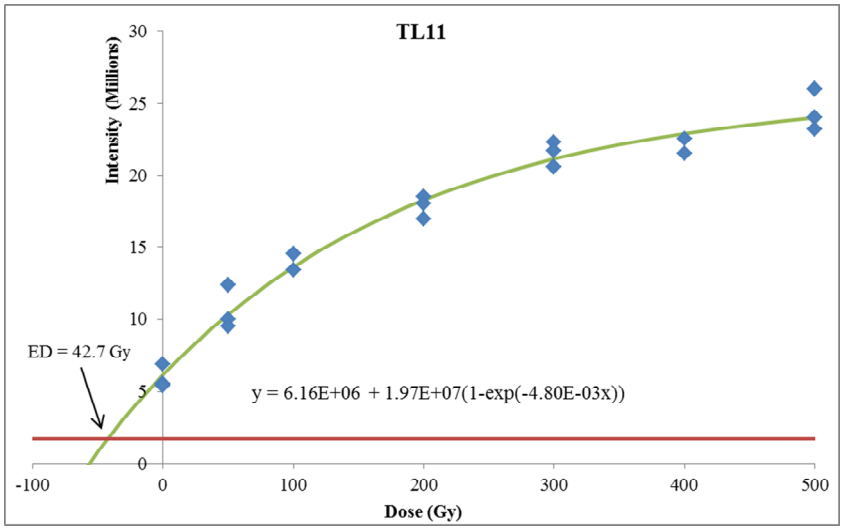

Figure 3.1 TL result of sample TL11: The growth curve was fitted by an exponential rise to maximum equation, y = y0 + a(1-exp(-bx)). Residual level (dashed line) is 1.69×10^6. The interception of the growth curve and the linear residual level is the ED, in this case 42.7 Gy.

Table 3.4 Equivalent dose and ages calculated from TL multi-aliquot method.

Sample	ED (Gy)	Age (ka)	Δage
TL00	73.0	54.6	35.2
TL01	78.7	55.2	12.5
TL02	140.3	98.6	14.1
TL03	28.9	58.2	20.0
TL04	117.9	39.5	6.6
TL05	393.9	143.2	18.3
TL06	306.7	99.7	11.8
TL07	116.4	70.8	15.9
TL08	129.4	78.1	15.0
TL09	90.5	54.6	7.3
TL10	25.2	17.9	6.2
TL11	42.7	18.2	5.3
TL12	44.8	18.8	5.1
TL13	99.4	34.8	7.0
TL14	151.1	41.4	13.1
TL15	148.8	35.1	4.4
TL16	32.0	10.5	3.6
TL17	274.2	63.8	12.4
TL18	447.7	115.3	26.5
TL19	24.4	10.5	4.0

For the equivalent dose of the OSL single aliquot, each sample was measured with 19 or more individual aliquots and fitted using an exponential function for determining the ED (De). Figure 3.2 presents an example from BT1169, which has 19 aliquots. Note that in the graph ED is presented in seconds, which was the time of artificial irradiation. The source parameter used to convert from ‘second’ to ‘Gy’ was 0.1314 Gy/s. For every ED a distribution curve was plotted before using any statistical analysis (age model). Three age models were applied to the data, central age model, common age model, and minimum age model. The results of the age models are presented in Table 3.5.

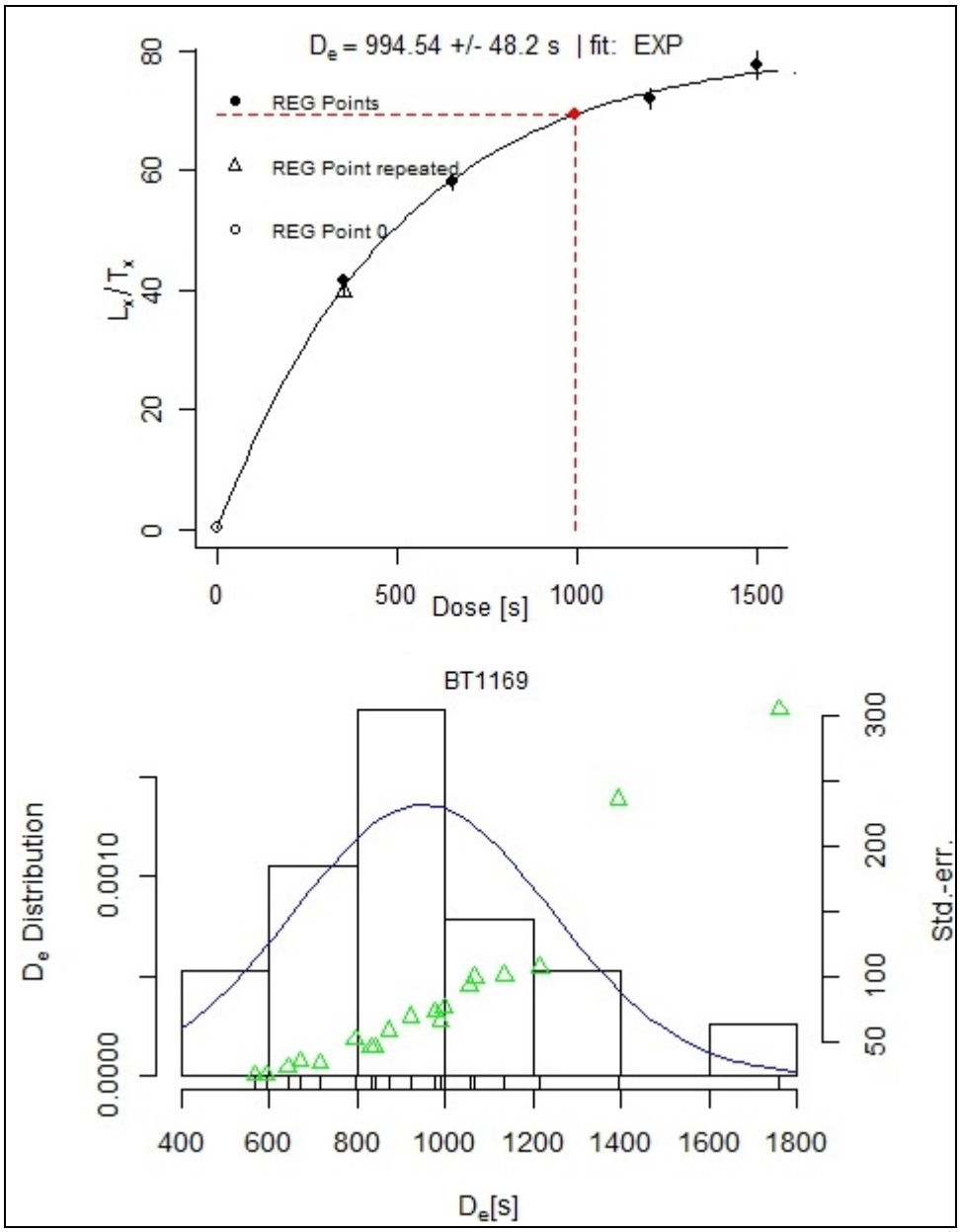

Figure 3.2 Top: Lx/Tx is the sensitivity corrected OSL signal of one aliquot of Sample BT1169 fitted by an exponential equation for ED or De determination, which has ED=994.54 s. Note: REG Points - OSL data points of each dose, REG Point Repeated - error checking, repeating a measured point with the same dose, REG Point 0 - bleached measurement. Bottom: Histogram of 19 aliquots of sample BT1169 before using any age model.

Table 3.5 Equivalent dose and age calculated from OSL regeneration data and different statistical analyses applied. MAM3 is the minimum age model, CAM is central age model.

Sample	ED (Gy)							Age (ka)						
	No model		MAM3**			CAM		No model		MAM3**			CAM	
	ED	ΔED	Mid	Min	Max	ED	ΔED	Age	ΔAge	Mid	min	max	Age	ΔAge
BT1168	Saturated		-	-	-	-	-	-	-	-	-	-	-	-
BT1169*	113.0	35.8	84.1	76.6	92.2	117.2	7.14	38.00	13.78	28.30	25.76	31.00	39.41	2.64
BT1170	18.8	2.9	16.4	14.5	17.4	20.1	0.78	12.93	3.01	11.28	10.00	11.94	13.85	0.68
BT1171	22.9	4.9	19.3	16.6	20.3	24.3	1.78	10.84	3.02	9.15	7.88	9.63	11.53	0.94
BT1172	4.51	0.55	3.93	3.78	4.57	4.67	0.14	3.14	0.64	2.74	2.63	3.18	3.25	0.13
BT1173	24.2	4.5	20.7	18.4	21.5	24.1	0.85	8.51	2.21	7.25	6.45	7.55	8.46	0.38
BT1174	0.99	0.73	0.19	0.17	0.20	0.7	0.15	0.83	0.67	0.16	0.14	0.17	0.59	0.13
BT1175	21.5	6.0	15.0	13.6	15.8	21.1	1.01	7.03	2.32	4.89	4.45	5.17	6.89	0.38
BT1176	3.57	1.18	1.78	1.57	2.00	4.2	0.57	1.83	0.73	0.91	0.80	1.02	2.17	0.31
BT1177	4.84	1.39	2.86	2.67	3.09	4.9	0.32	2.48	0.90	1.47	1.37	1.59	2.53	0.19

* BT1169 has skewness = 0.025 that is close to symmetry, it was suitable to be run by common age model. ED ran by central age model = 101.90±1.49 Gy and 34.28±0.71 ka age. **MAM3 gave non-symmetric errors.

3.2 Locations of paleoearthquakes

3.2.1 Vibhavadi sites V1 and V2

The Site V1 and V2 are located in Vibahvadi District, Surat Thani Province. This area was an old sand pit surrounded by a small village and rubber trees. DMR (2007) already worked in the area but at a location nearby and they presented a topographic map shown in Figure 3.4 with the Klong Marui Fault shown. According to the authors the KMFZ is a left lateral strike-slip fault. The authors also show a change of a stream with 18 meters left lateral horizontal displacement, however this direction is not parallel to the proposed fault line.

The fault zone at V1 site also appeared further below at the artificial pool. It was white sandy clay in-between the sandstone layer, similar to the pit wall (see Figure 3.3). When combining the direction at the pit wall and at the pool the direction of the fault could be determined with 145-325 or NW–SE (Figure 3.3). GRC (2013) additionally defined the fault zone in this area by using seismic reflection surveys (Figure 3.4) with three seismic sections shown in Figure 3.5. The fault zone with several faults appeared in the seismic sections. A correlation indicates a NW–SE direction, which correlates to the fault zone found in the outcrops nearby (this study) and is also parallel to the stream offset founded by DMR (2007) earlier.

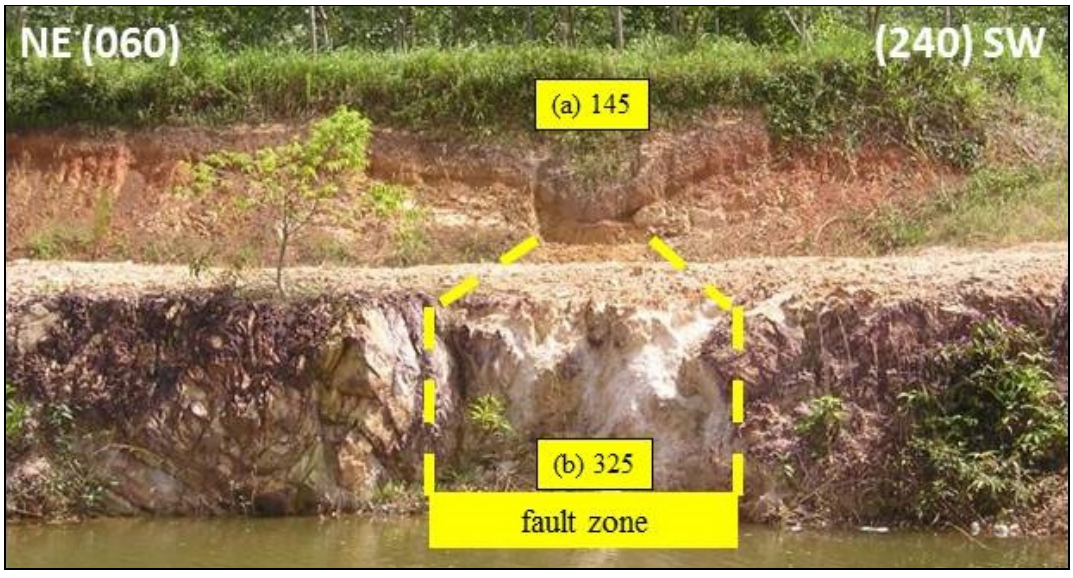

Figure 3.3 Fault zone at V1 site which has a strike direction of 145-325. a) outcrop at the pit wall, b) outcrop at the pond level below and about 15 away from a).

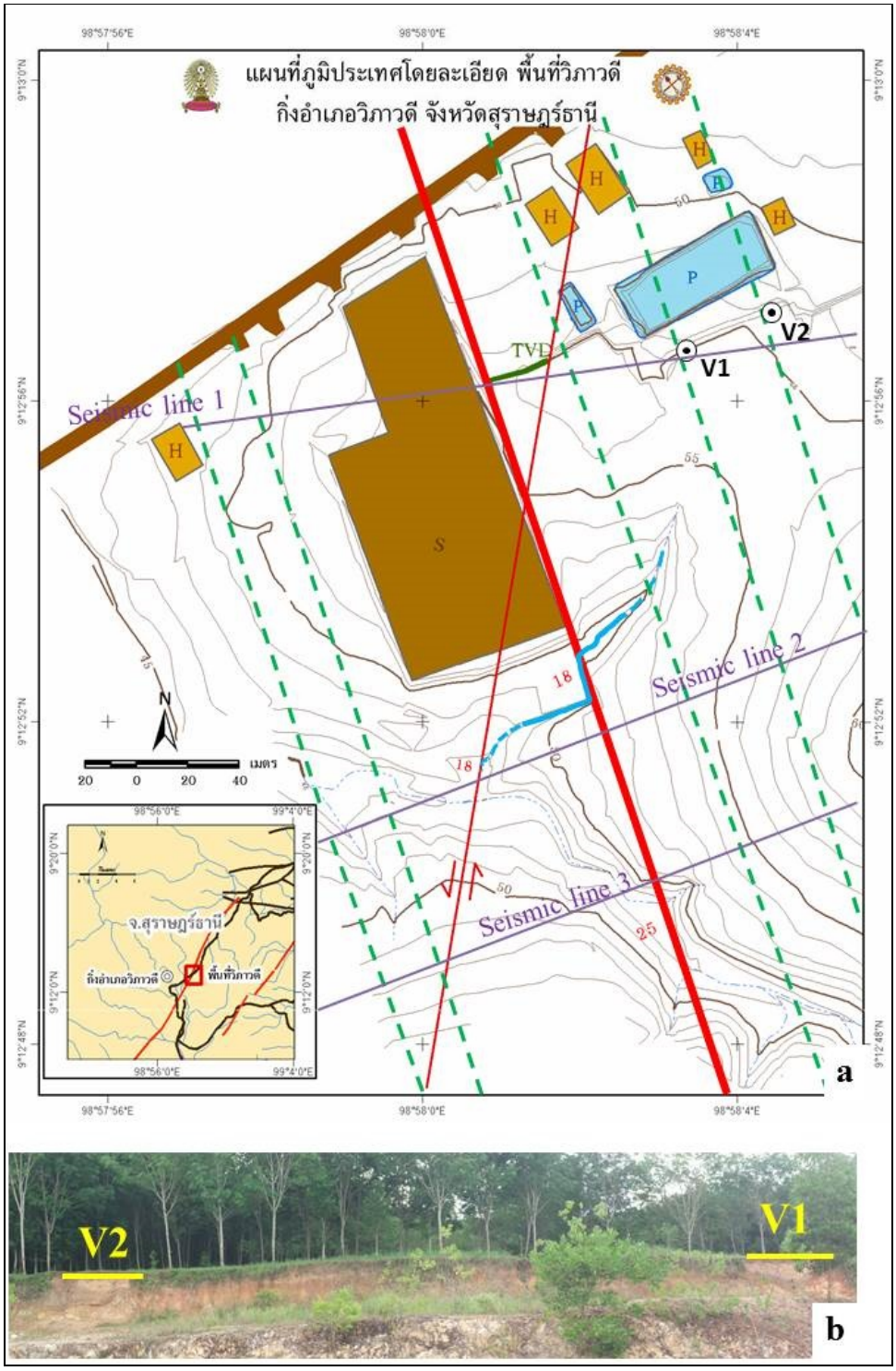

Figure 3.4 (a) Topographic map of V1 and V2 site (after DMR, 2007): H are houses, S is a school, P are pools, green line was the fault defined seismic investigations (see GRC 2013). V1 and V2 are trenches. Numbers on the isolines are elevations above sea level. (b) Overview of the V1 and V2 (photo to SE direction).

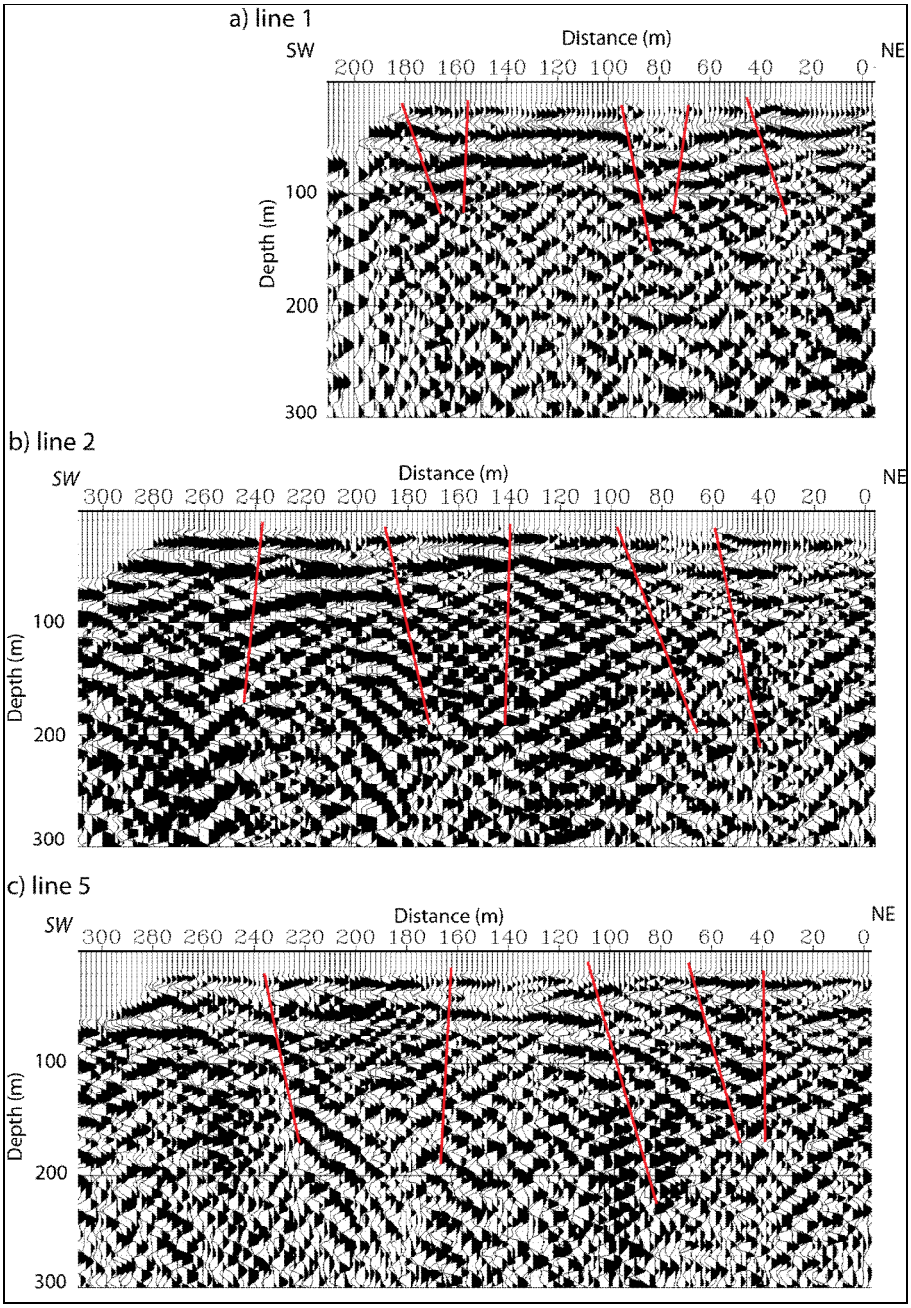

Figure 3.5 Seismic reflection sections acquired in the area of V1 and V2 by GRC (2013). For survey locations see Figure 3.4. Red lines indicate faults interpreted by GRC (2013).

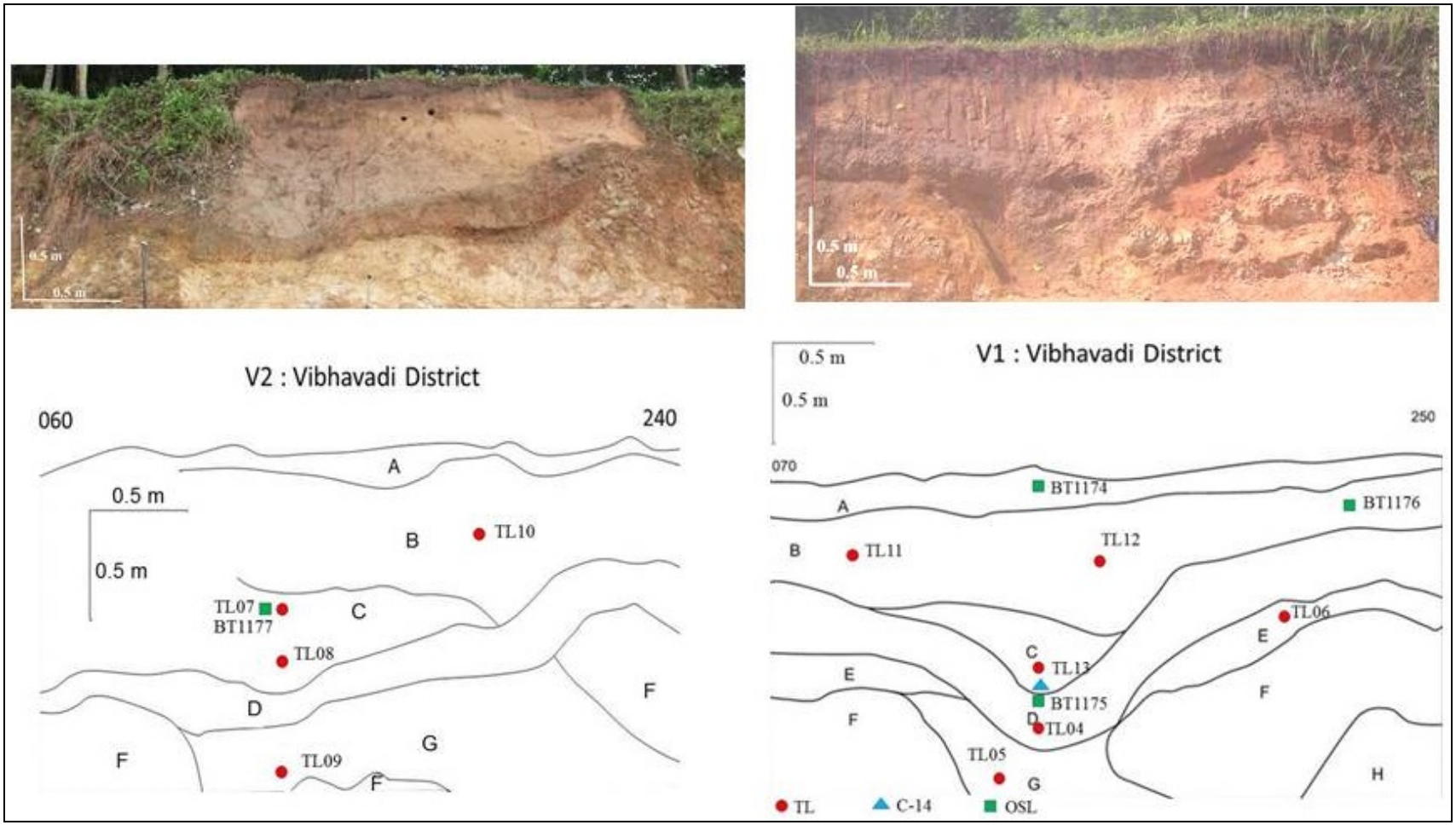

Figure 3.6 Photo and schematic diagram to SE showing the sedimentary units of V1 and V2 in Vibhavadi district including the sample locations and numbers used for age dating (circles = TL sample, square = OSL sample, and triangle = C-14 sample).

The V1 is located at UTM 496436 1018697 and 50 m above sea level. Eight sedimentary units were found, from A to H (Figure 3.6), as described in Table 3.6. Moreover, the plant material for C–14 dating was found at the bottom of unit C. The V2 site is 36 meters to the East of V1 (UTM 496480 1018722) and 49 m above sea level. The description of each layer is also presented in Table 3.6.

Table 3.6 Description of V1 and V2 sedimentary units.

Unit	Description
A	Black top soil
B	Light brown clayey sand
C	Brown-grey colored and medium plastic clay, with black grains and black plant material
D	Dark-grey, slightly orange gravel with a few black grains and black plant material
E	Red to ocher colored medium plastic clay
F	Fractured white-yellow sandstone
G	Yellow-white sandy clay
H	Medium plastic white-grey-yellow silty clay

Dating results presented in the previous part are shown in Figure 3.7 and 3.8 for both TL and OSL result in V1 and V2. TL results are in Pleistocene but OSL are in Holocene. For further discussion see Chapter 4. Moreover, C-14 results based on plant material collected from layer C and D of V1 gave an age of 510±150 years.

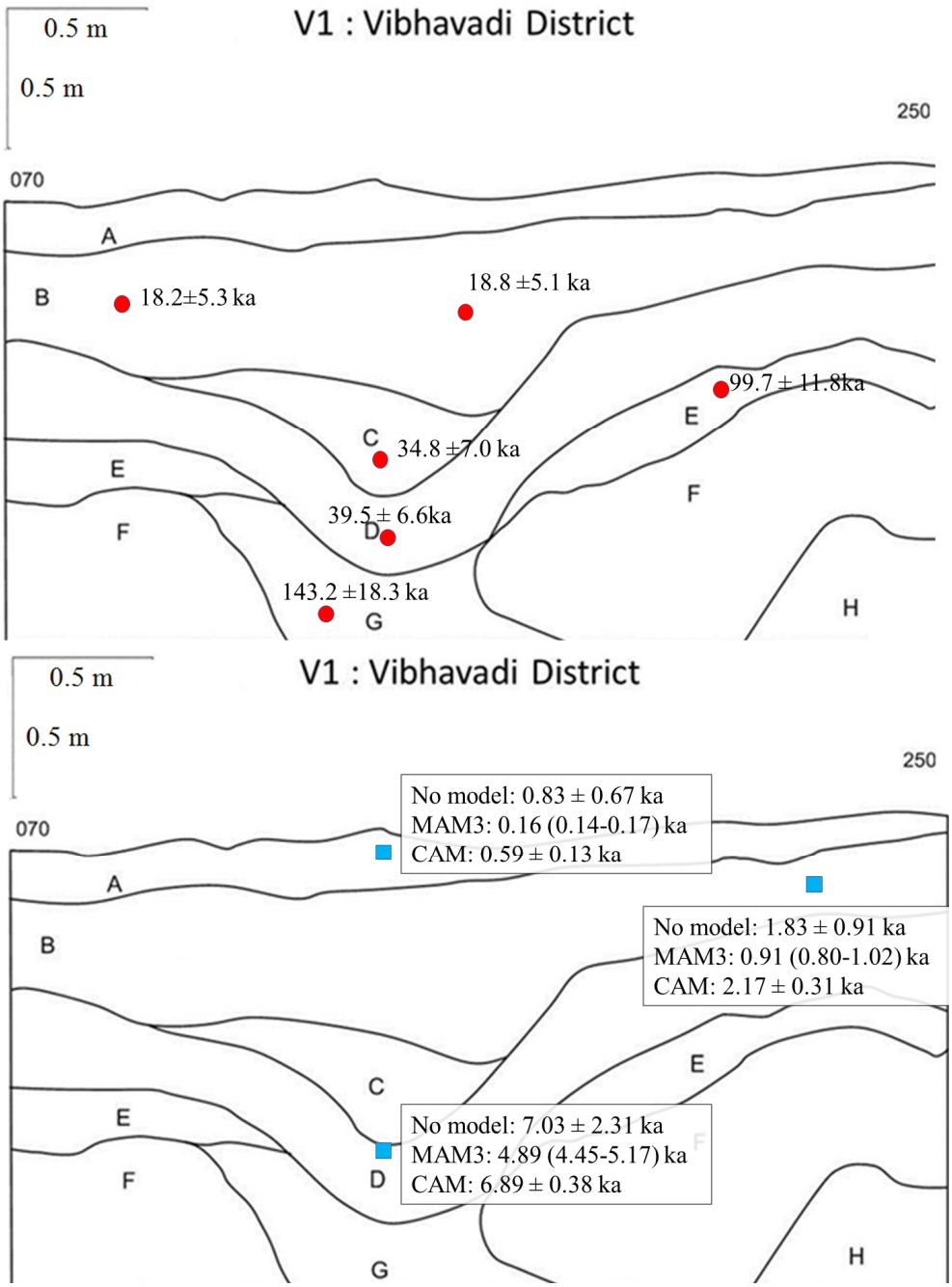

Figure 3.7 Vibahvadi V1 site: TL dating results (top) and OSL dating results with different age models (bottom).

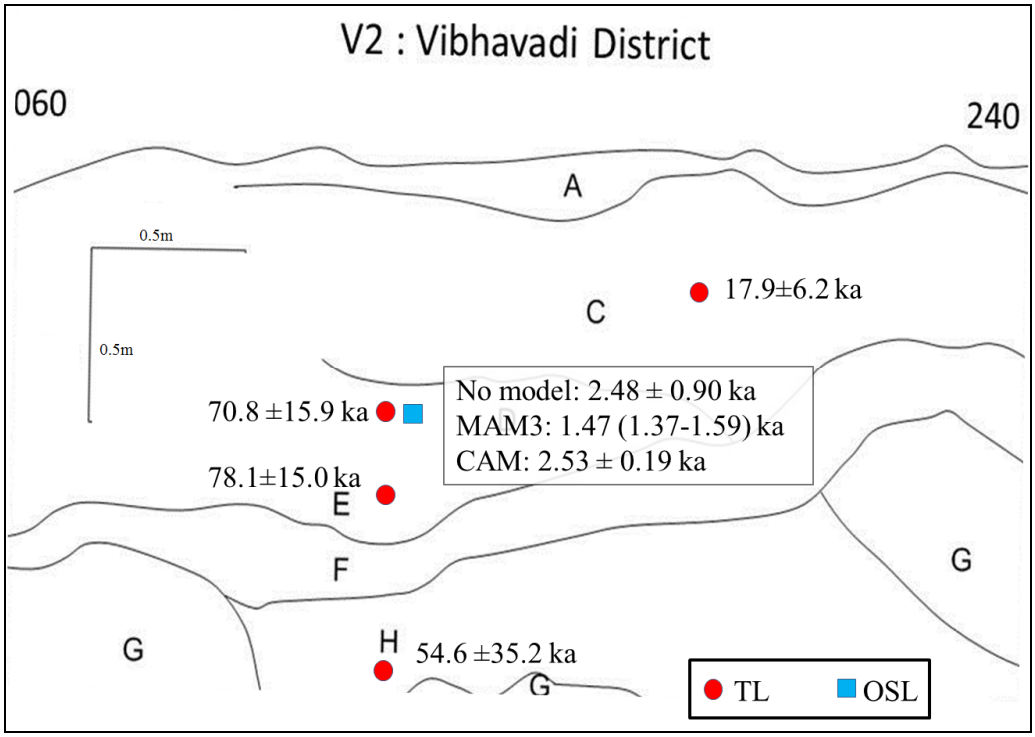

Figure 3.8 Vibahvadi V2 site: TL dating results and OSL dating results with different age models.

3.2.2 Vibhavadi site V3

Vibhavadi site V3 is in Vibhavadi District, Surat Thani (UTM 501985 1015938), 105 m above sea level. The site is an old sand pit developed from a road cut with a wall of about six meter height (see Figure 3.9 and 3.10). At the V3 site only samples for TL dating were collected, with sample numbers TL14 to TL19 as presented in Figure 3.10.

The lithological units of the V3 site and the locations where the samples were collected for the age dating are also presented in Figure 3.10. The A layer is brown top soil, B is yellow silt, C is gravel and brown silt, D is brown silt, E is light brown silt, F is orange silt, G is brown grey clay, H is brown clay with gravel, I is red brown clay, and J is white clay with weathered rock. A normal fault was identified where the fault plane was marked by white clay. The orientation of the fault was 282/55 (dip direction/dip angle) with about 50 cm vertical movement of the hanging wall downwards to NW (normal fault).

Figure 3.9 Site V3: Fault with white clay apparent on the plane with an orientation of 282/55 (dip direction/dip angle) and a vertical movement of about 50 cm.

There was a discontinuity of the gravel and brown silt layer (unit C). Moreover, there was another fault where white clay appeared on the plane presented as a dashed line in Figure 3.10. The dating results are presented in Figure 3.11.

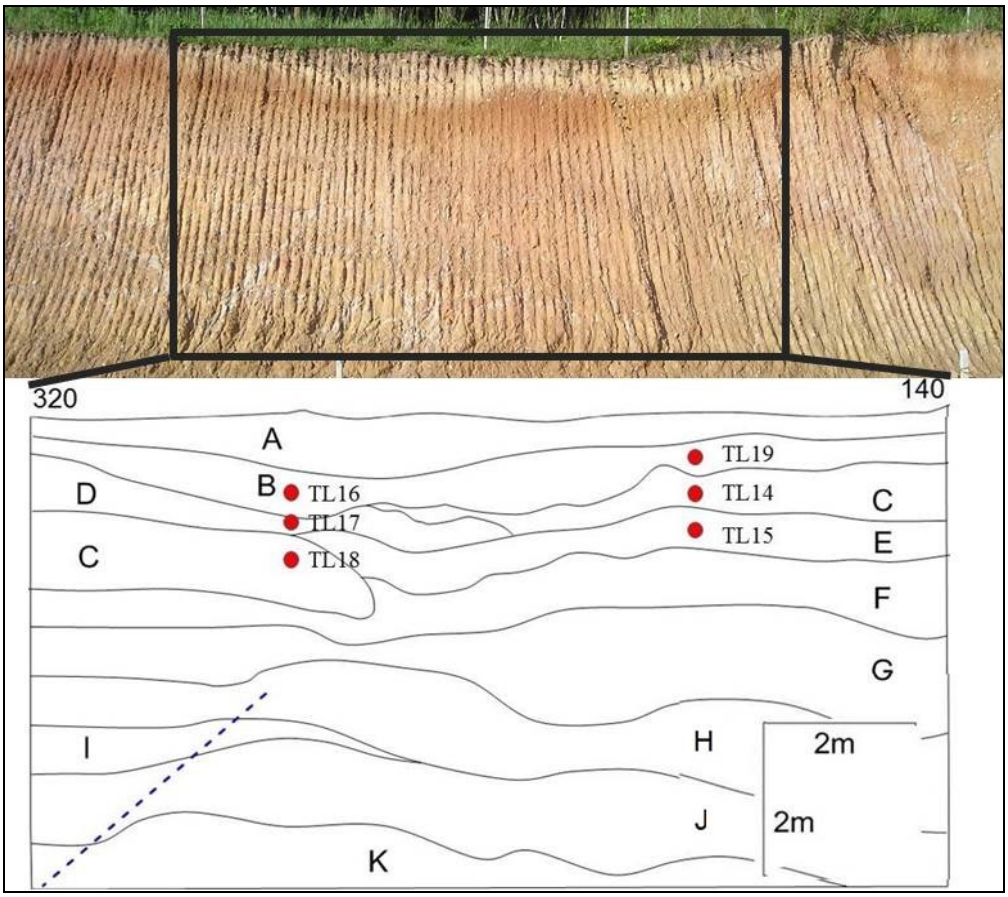

Figure 3.10 Stratigraphy of V3; A is brown top soil, B is yellow silt, C is gravel and brown silt, D is brown silt, E is light brown silt, F is orange silt, G is brown grey clay, H is brown clay with gravel, I is red brown clay, J is white clay with weathered rock, and dash line is a fault with white clay.

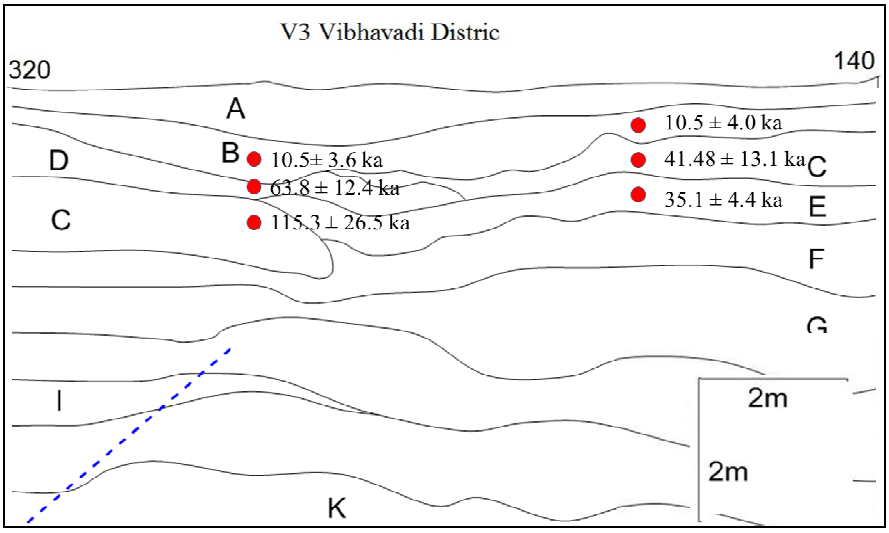

Figure 3.11 TL sample locations and dating result at site V3.

3.2.3 Tha Chang site TC

Site TC is in Tha Chang district, Surat Thani (UTM 519313 1028702), 35 m from sea level. Normal faults were found in this area on the faulted structures as shown in Figure 3.13. Both TL and OSL were collected for dating. This location is in the rubber tree farm. An overview map is presented in Figure 3.12.

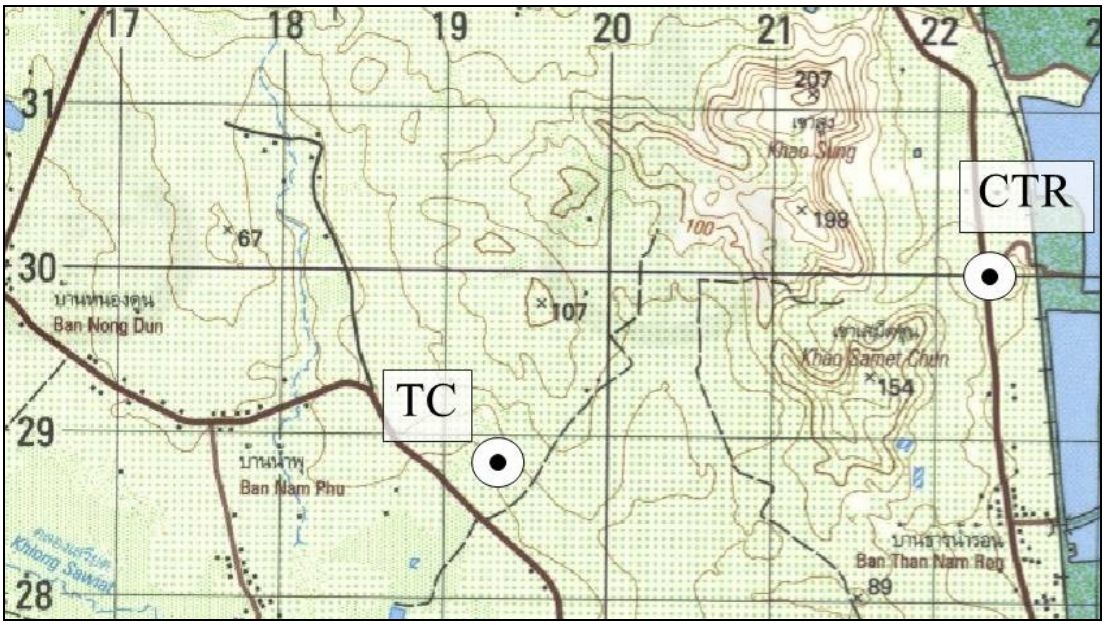

Figure 3.12 Topographic map with the location of TC and CTR site in Tha Chang district of Surat Thani Province (modified from RTSD 2005).

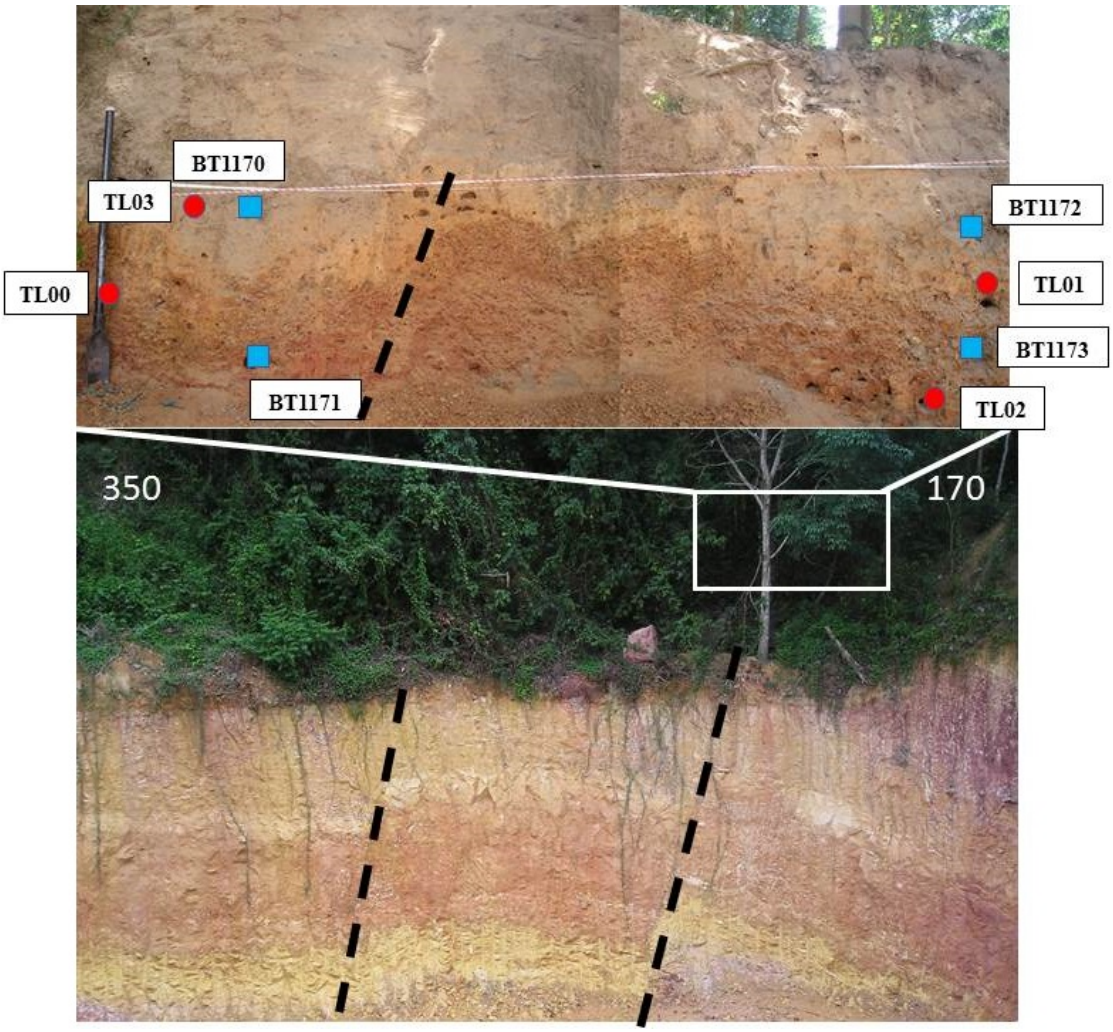

Figure 3.13 Overview of TC with clearly visible faults with the sample locations as well as the sample numbers.

Two different layers of sediment were found; in the upper part silty sand and in the lower part silt with small rock fragments. Eight samples were collected for dating, four for TL and four for OSL dating. Stratigraphic and dating results, both TL and OSL, are presented in Figure 3.14. Several age models were applied and presented here, but will be discussed in the next chapter.

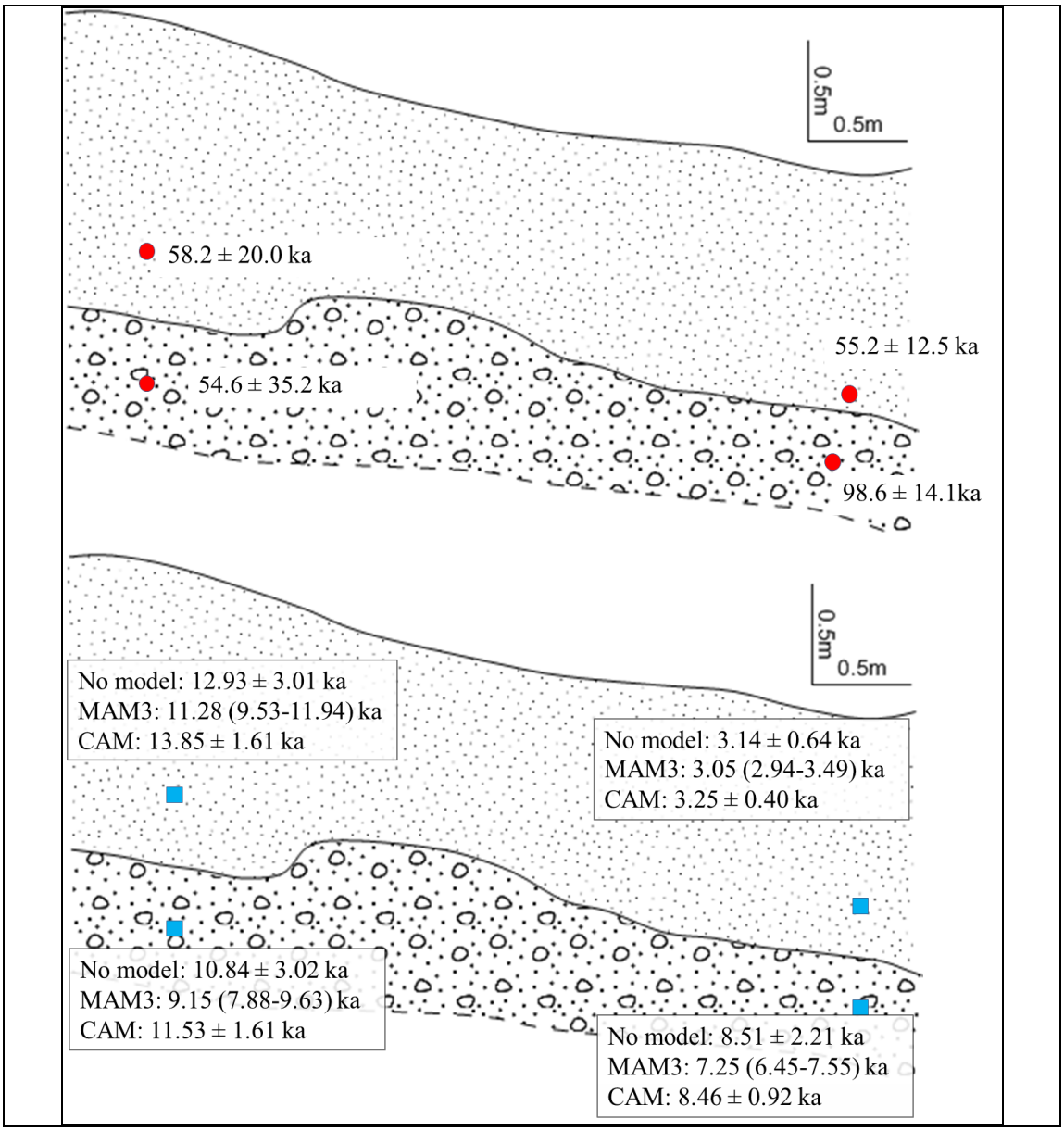

Figure 3.14 Stratigraphic and dating results: top is TL and bottom is OSL; upper sediment layer is silty sand, lower layer is silt with small rock fragments.

3.2.4 Chaiya–Tha Chang site CTR

The Chaiya – Tha Chang site (CTR) is east of the road from Tha Chang to Chaiya in Tha Chang district, Surat Thani (UTM 522312 1030008) at 28 m above sea level (Figure 3.12). A large normal fault dipping north was apparent (5.5 m approx. minimum displacement), but no strike direction could be determined.

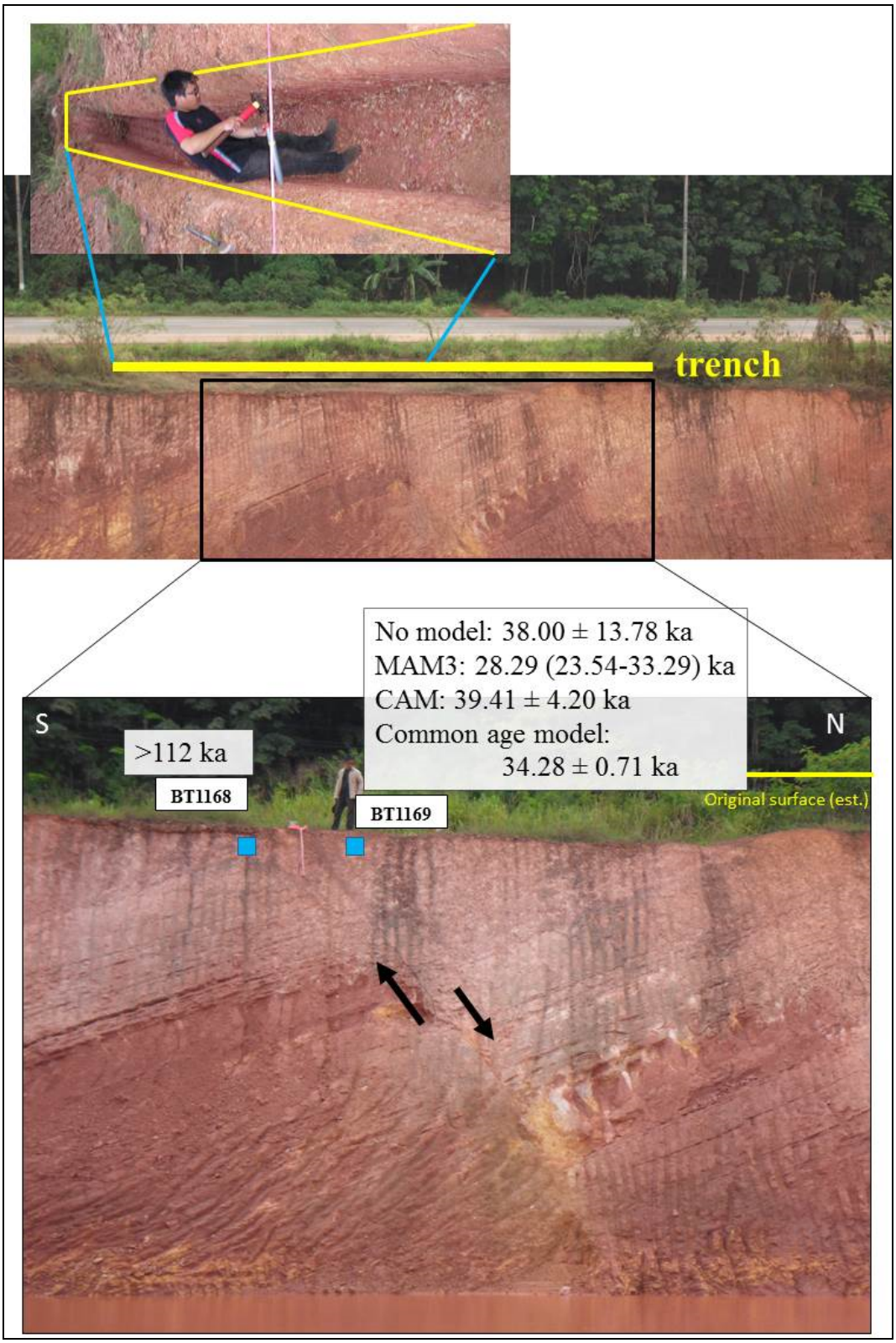

Figure 3.15 Trenching work at the CTR site (top) with a site overview of the quarry wall near Chaiya –Tha Chang road (middle) and a more detailed photo with the OSL dating results (bottom).

In the area approximately 1.5 m of the original upper near surface sediment layers were removed by quarry activities according to local people. A one–meter deep and 12 m–long trenching was done parallel to the wall. In the trench the upper layer appeared to be red white clay, which was above the siltstone layer that can be seen in the wall shown in Figure 3.15. In the trench the fault could not be identified, maybe because of near surface weathering and bioturbation. Therefore the samples for OSL dating were collected from two sides of the fault which was extrapolated from the wall also shown in Figure 3.15.

CHAPTER 4

DISCUSSION AND CONCLUSION

The results presented in the previous chapter are discussed, especially the TL and OSL data with respect to their quality. For each paleoearthquake site a time line has been drawn with a discussion on the paleomagnitude. At the end conclusions have been drawn together with some outlook for the future.

4.1 TL and OSL data

4.1.1 Discrepancies of TL and OSL data

The results of the TL dating at PSU Pattani gave age values that are significant different from other results, OSL from the laboratory in Bayreuth/Germany and the C-14 data from DMR (2007). All TL values are more than five times (up to eighteen times) higher than the other ones. Several possible error sources that might have been the reason for that have been checked.

First, the irradiation part carried out at the Office of Atoms for Peace (OAP) was checked by measuring OSL from dosed quartz. One of the TL samples prepared for the laboratory in Pattani for TL measurements was used to measure the OSL signal at Bayreuth and it gave an age close to the OSL age. However, the equivalent dose of TL is still quite high when compared to OSL.

Second, the detection of the thermoluminescence signal that was measured was emitted from heated quartz. Looking into the occurrence of the TL signal, each defect point in a quartz crystal has specific properties; the energy below the conduction band where the electrons are trapped (trap depth) and the temperature stimulating the electrons from escaping from the traps. The quartz samples collected from the study areas could have complex properties, e.g. the temperature peak of interest is very close with other peaks (Aitken, 1985; Preusser et al., 2009). Further, it could be possible that the deconvolution software cannot separate each peak that

appeared in the TL signals. Moreover, the temperature of interest is affected by the incandescence signal (Fleming, 1979; Aitken, 1985; Wintle, 1997).

Finally, as the OSL method itself has an advantage in age dating likely easier for bleached (Figure 1.4), controllable stimulated wavelength light OSL (TL requires temperature increase) (Aitken, 1998) and with the equipment used in Bayreuth and the experienced staff there it is more likely that the OSL ages are more realistic. These ages would correlate with the C–14 data from DMR (2007). It might also explain that TL ages are published in the report of DMR (2007) but not further used in the presentation of the results and in the conclusions.

4.1.2 OSL age models

For the final proceeding of the OSL data age models were applied, however different ones (see Section 2.2.6 and 3.2.2). Basically, physical and statistical reasons were applied in this process. In the following the process of applying an age model is discussed for each sample.

Sample BT1168 has a saturation ED and the curve started to saturate at approximately 300 Gy and using a dose rate of 2.911 Gy/ka the age of sample BT1168 is therefore more than 100 ka. As the distribution curve of sample BT1169 was mostly symmetric (skewness 0.025), the central age model was used and resulted in an age of 34.28±0.71 ka. As sample BT1171 is a colluvial sediment (probably not completely bleached), the MAM3 age model, which is giving a minimum age value is used. Therefore, the OSL age for this sample is 9.15 ka, with a 68% confidence between 7.88 ka and 9.63 ka. For consistency, sample BT1170 was located above BT1171. The CAM model, which gave a higher age was not reasonable to be used. Therefore, its age is 11.28 ka with a 68% confidence between 9.53 ka and 11.94 ka. As the sampling locations of sample BT1172 and BT1173 were under a tree where bioactivities might have occurred from the roots of the tree, the MAM3 was not reasonable to be used. Therefore the CAM model was selected. The age of sample BT1172 then is 3.25±0.04 ka and the one of sample BT1173 is then 8.46±0.92 ka. Sample BT1174 was top soil and the BT1176 sample was close to it. Both samples

were probably disturbed by bioactivities, so also here MAM3 model was not suitable. CAM was selected. The age of sample BT1174 is then 0.59±0.16 ka and for sample BT1176 an age of 2.17±0.0.44 ka was determined. The BT1177 sample was in the same layer with BT1176. Therefore, CAM model was selected. The BT1177 age is 2.53±0.35ka. For sample BT1175, DMR (2007) dated a sample in the close vicinity that gave an age of 6.0 ka using C-14 method. The CAM model in this study gave a consistent value with an age of 6.89±0.69 ka.

4.1.3 Equivalent dose and age relationship between TL and OSL

The number of OSL samples is limited in comparison to the TL samples, however as outlined above there is a significant difference in the age values between both methods. For some sample locations TL and OSL data are available. Assuming that for any reason there might be systematic difference between the TL and OSL data, a correlation between both is attempted. However, not the age values itself, which include age models for the OSL data, are used rather then the ED values from both methods are compared.

For following samples TL and OSL data for the equivalent dose (ED) were available and used for the comparison: TL00 and BT1171, TL01 and BT1172, TL02 and BT1173, TL03 and BT1170, TL13 and BT1175, and TL10 to TL12 and BT1176. The relationships are presented in Figure 4.1. The eight data points do not show a consistent relationship; rather they could be fit with two trend lines, a polynomial and a linear trend line. From relationship in Figure 4.1, the linear trend line is related to the samples, which have a higher ED value for OSL. In contrast, the lower ED values from OSL have a polynomial relationship with an R^2 value of 0.9997. However, if the polynomial relationship would not be used and a linear trend line would be used instead, the R^2 would be 0.8 approximately. Therefore, the lower zone in Figure 4.1 will be used with a polynomial fit.

Using available data related to the lithologies of the samples, the two different trend lines could not be related to the sampling site, or to the grain size, or to

the age. Therefore it might be possible that the reason for this difference lies in the TL properties as presented in the previous section.

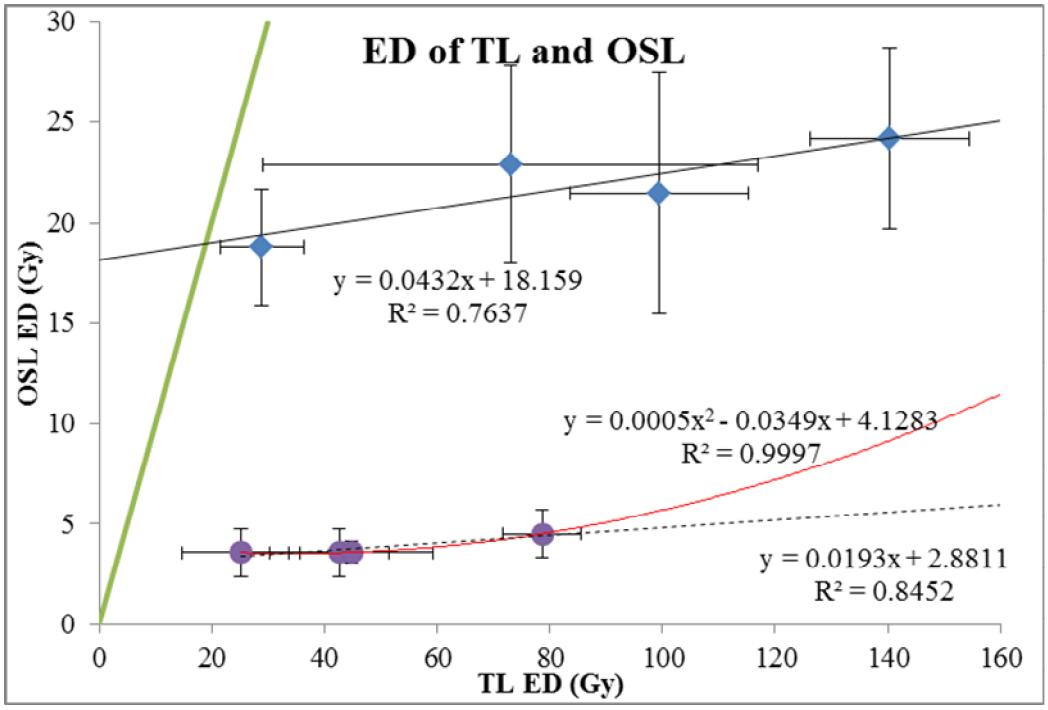

Figure 4.1 Relationship of ED between TL and OSL data for sample where the sample location is close to each other.

Using the relationships shown in Figure 4.1, the TL ages from locations where no OSL data are available, were converted into "OSL ages" (converted TL, cTL), which are presented in Table 4.1. These ages could be used as rough estimates in the interpretation by considering the consistency with ages from other layers above and below presented in Chapter 3.

Table 4.1 Original TL ED and ages, converted TL ED and ages from the two relationships shown in Figure 4.1; ED in Gy, ages in ka. Bold indicates samples and data used to establish the relationships

Location	Sample	Former		linear		Quadratic	
		ED	Age	ED	Age	ED	Age
TC	**TL00**	73.03	54.58	21.31	15.93	4.25	3.17
	TL01	78.65	55.23	21.56	15.14	4.48	3.14
	TL02	140.34	98.55	24.22	17.01	9.08	6.38
	TL03	28.87	58.20	19.41	39.13	3.54	7.13
V1	TL04	117.88	39.54	23.25	7.80	6.96	2.34
	TL05	393.94	143.20	35.18	12.79	67.97	24.71
	TL06	306.68	99.73	31.41	10.21	40.45	13.15
V2	TL07	116.40	70.80	23.19	14.10	6.84	4.16
	TL08	129.38	78.08	23.75	14.33	7.98	4.82
	TL09	90.46	54.59	22.07	13.32	5.06	3.06
	TL10	25.15	17.93	19.25	13.72	3.57	2.54
V1	**TL11**	42.66	18.24	20.00	8.55	3.55	1.52
	TL12	44.79	18.79	20.09	8.43	3.57	1.50
	TL13	99.41	34.78	22.45	7.86	5.60	1.96
V3	TL14	151.09	41.43	24.69	6.77	10.27	2.82
	TL15	148.81	35.05	24.59	5.79	10.01	2.36
	TL16	32.03	10.49	19.54	6.40	3.52	1.15
	TL17	274.20	63.75	30.00	6.98	32.15	7.48
	TL18	447.73	115.31	37.50	9.66	88.74	22.85
	TL19	24.41	10.48	19.21	8.25	3.57	1.53

4.2 Paleoseismological analysis of Vibhavadi site V1 and V2

4.2.1 Paleoearthquake scenario

A consistent pattern of the converted TL ages of the sandy clay in–between the sandstone layer indicate that there was already a fault zone before 35 ka. Until approximately 6.89 ka, the sandstone and clay layer was covered by a dark-grey gravel layer. The first paleoseismological event occurred between 2.53–6.89 ka before present. It was likely a left lateral strike slip fault based on the horizontal displacement of the stream which an extensional environment, see Figure 4.3(c).

From this result the SWW (250) side of the sandstone layer was moved relatively up one meter vertically along the fault, at V1 and at V2. After this earthquake event, the clay layer was settled over the gravel layer at around 2.53 ka before present. The light brown clayey sand was continuously settled over the clay and the gravel layer around 2.17 ka ago. The second paleoearthquake event occurred between 0.59 and 2.17 ka (Figure 4.3 (e)). It is assumed that it is also an oblique left lateral strike slip fault in an extensional environment. The SWW of the fault side was relatively moved down and so that the clay layer at the NEE side moved up approximately 0.4 m vertically. After that, the black topsoil occurred and appeared until today.

4.2.2 Magnitude of paleoearthquakes

From the scenario in Figure 4.3 there were two paleoseismic events, with the first event occurred between 2.53 and 6.89 ka. Here the minimum displacement in vertical direction was approximately 1 meter. Estimating the paleo-magnitude for a strike slip environment using Equation 2.11, it gives a Mw value of 6.8 for maximum displacement (MD), and Mw of 7.0 for average displacement (AD). The second event occurred between 0.59 and 2.17 ka, and a minimum displacement appeared in vertical direction of approximately 0.5 meter. Using Equation 2.11 for strike slip environment for the estimation of the paleomagnitude, it gives Mw of 6.6 for maximum displacement (MD), and Mw of 6.7 for average displacement (AD). However, there was no evidence of horizontal displacement at the outcrops.

From the topographic map presented by DMR (2007) and also confirmed during the fieldwork was an 18 meter horizontal displacement of a stream channel in left lateral direction (see also Figure 3.3). This displacement value could be the result of a single movement or it could be part of multiple movements. Using Equation 2.11, this evidence could produce an earthquake magnitude of up to 7.8 in moment magnitude scale during single movement. However, there is no evidence to support that it was the result of a single event or of multiple events. The magnitude and displacement relationship is presented in Figure 4.2.

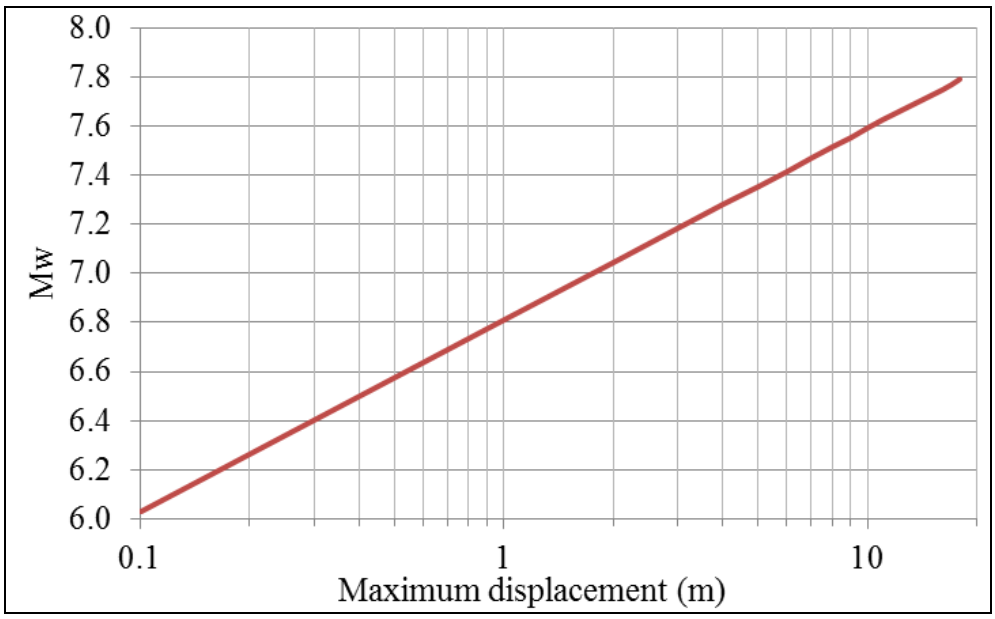

Figure 4.2 Relationship between moment magnitude and maximal displacement for the 18 meter horizontal displacement of a stream channel in left lateral direction at Vibhavadi site V1 and V2. A single event with 18 m horizontal displacement would generate a Mw 7.8 earthquake.

4.2.3 Conclusion

From the geological observations at the outcrops, and the horizontal displacement of the stream channel together with the seismic reflection results from GRC (2013), the V1 and V2 site show a fault zone with several NNW–SSE striking left lateral strike slip faults. The geological records show two paleoseismic events. The last event occurred between 0.59 ka and 2.17 before present with a minimum Mw of 6.6 and a maximum of 7.8. The older event occurred between 2.53-6.89 ka with a Mw of more than 6.8.

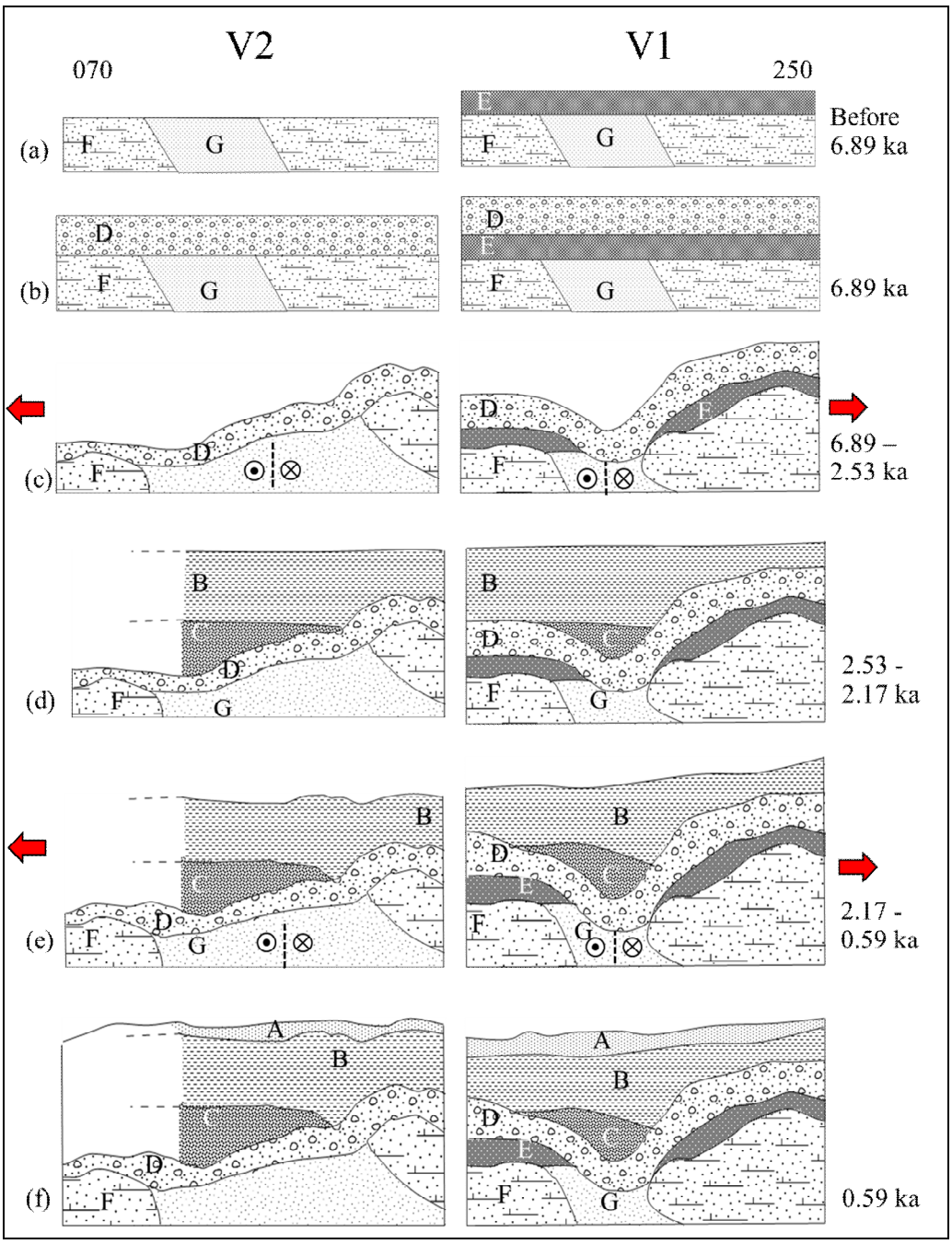

Figure 4.3 Geological and paleoearthquake scenarios for V1 and V2 with two paleoseismic events (see also Figure 3.6 in Chapter 3).

4.3 Paleoseismological analysis of site V3

4.3.1 Paleoearthquake scenario

As for this outcrop no OSL data are available, therefore the original and (oTL) converted TL (cTL) are used for the scenario of the geological events in

the past (see Table 4.1). Before 115.3 / 9.66 ka (oTL/cTL) the brown silt with gravel layer was deposited. Between 63.7-115.6 / 6.98–9.66 ka there was a paleo-seismological event (Figure 4.4 (b)). It is a normal due to an extensional system with an orientation of 282/55 (dip angle/dip direction). Further, the brown silt layer with gravel is not continuing, and the SE side was relatively moved up. At around 63.7 / 6.98 ka before present the brown silt layer over gravel was settled. Between 63.7-41.4 /2.88–6.98 ka the gravel layer was eroded and a brown silt layer was deposited. After that, the yellow silt was deposited over the brown silt layer (10.5–41.4 / 1.15–2.82 ka before present) and later topsoil followed at 10.5 ka to present /1.15 to present, respectively.

4.3.2 Magnitude of paleoearthquakes

The displacements observed in the unconsolidated sediments of the outcrop V3 give six displacement values (in Figure 4.5), with 0.8, 0.6, 0.3, 0.5, 1.7, and 1.3. Calculations using maximum displacement method using 1.7 m and using the average displacement method (0.9 m) give a paleomagnitude (Mw) of 7.0 for both methods.

4.3.3 Conclusion

Here at site V3 an extensional normal fault could be observed with an orientation of 282/55 (dip angle/dip direction) or a strike direction of NNE–SSW as the result of a paleoseismological event. This event has a Mw value of minimal 7.0. As no OSL ages are available here this event has occurred between 87.9–127.6 ka (oTL) or between 7.08–8.81 ka (cTL).

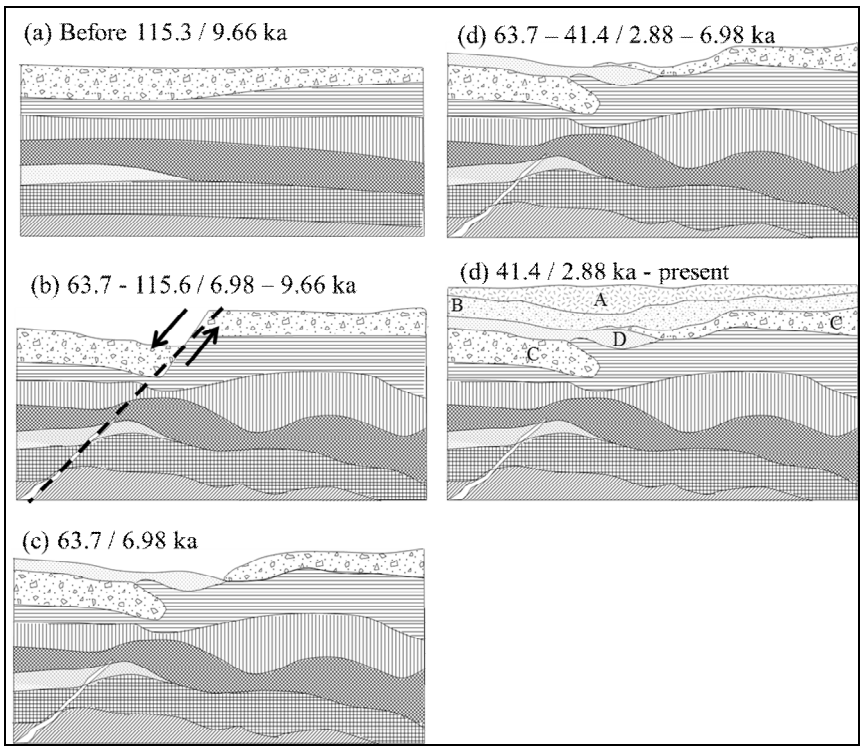

Figure 4.4 Scenario of site V3 with one paleoseismological event. Ages are original TL ages and converted TL ages (see Table 4.1).

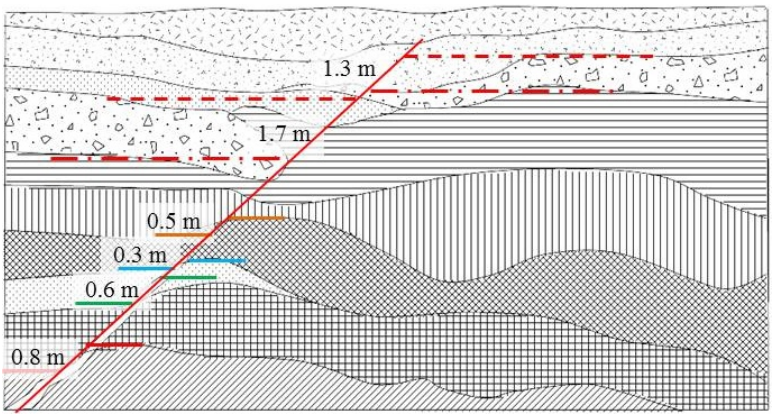

Figure 4.5 Schematic drawing of the displacement of the sedimentary layers at site V3 (see also Figure 3.10 and 3.11).

4.4 Paleoseismological analysis of site TC

4.4.1 Paleoearthquake scenario

The OSL age results of the samples from two layers of site TC are close in value. It could be assumed that the upper silty sand has a relatively high sedimentation rate resulting in the small difference in OSL ages. The age boundary of

error was used for describing the scenario of this fault. The lower silt layer with small rock fragments was deposited more than 9.63 ka ago. After that, the upper silty sand layer was deposited between 9.53 and 9.63 ka before present. From 9.53 ka to present, there was a paleoseismological event (Figure 4.6 (c)), a normal fault in an extensional environment, likely with a left lateral sense of movement and with a NNE–SSW strike direction according to the geological observations in the field. Later the surface was eroded and that has smoothened the surface until present.

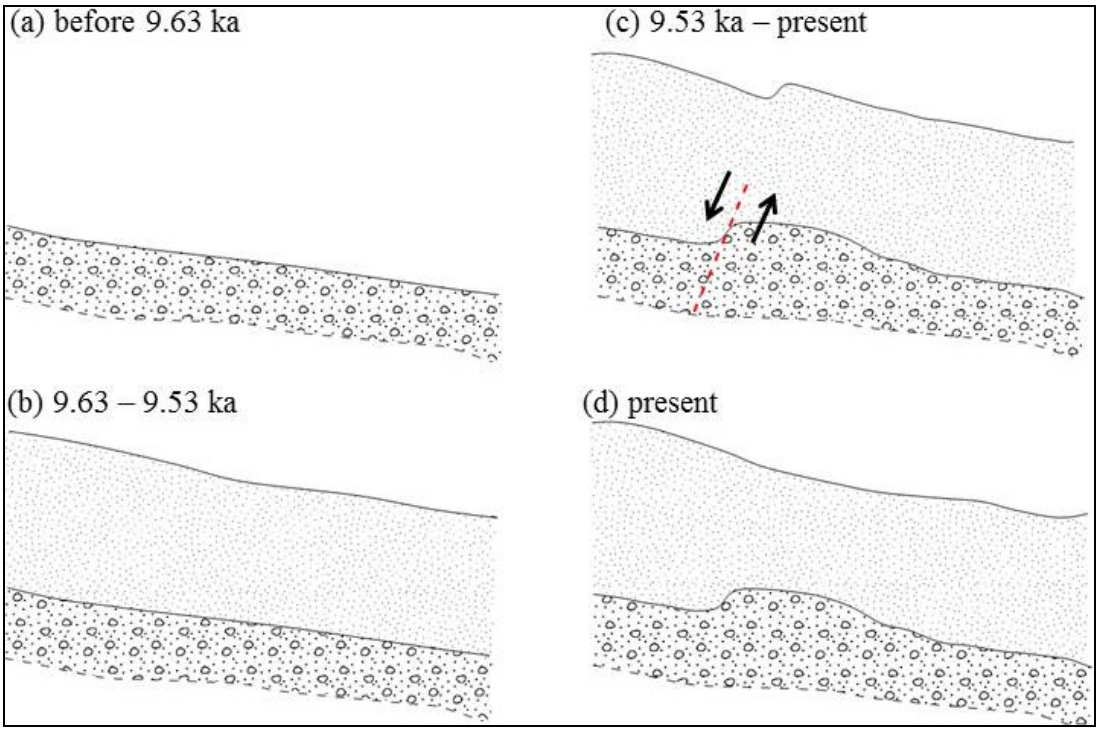

Figure 4.6 Scenario of TC with a paleoseismological event in Holocene.

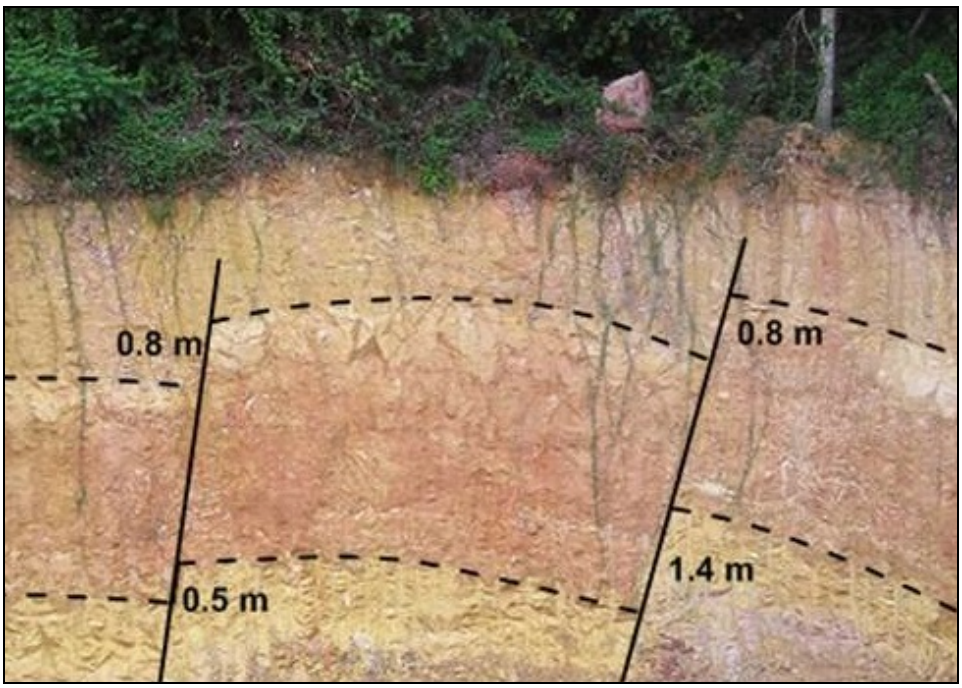

Figure 4.7 Vertical displacements of rock layers in the outcrop under the sampling location.

4.4.2 Magnitude of paleoearthquakes

The vertical displacement of the unconsolidated sediment found at site TC gives a value of approximately 0.2 m. Further, displacements of the rock layers beneath were also found (Figure 4.7), which have vertical displacement values of 0.2, 0.5, 0.8, 0.8, and 1.4 m. Both maximum displacement (1.4 m) and average displacement (0.74 m) were used to calculate the paleomagnitude. Both methods give an Mw value of 6.9.

4.4.3 Conclusion

The fault at site TC in Tha Chang district is likely strike slip fault with extensional character. A paleoseismic event occurred between 9.53 ka to present. Its strike direction is NE-SW. The minimum Mw value for this event is 6.9. However, this value could be higher because this value was calculated from the vertical displacement of the strike slip fault that usually has more a horizontal displacement.

4.5 Paleoseismological analysis of site CTR

4.5.1 Paleoearthquake scenario

The tilting and consequently dipping south of the layers, mainly layers of unconsolidated white-red clay and siltstone layers, which were observed in the outcrop occurred more than 112 ka before present (see also Figure 3.15). Between 34.3 and 112 ka there was extensional tectonic with a possible strike slip environment resulting in a north dipping fault seen in the outcrop. After that sediments from higher altitudes were transported and deposited at the lower part as shown in Figure 4.8 (c). This is a reason why trenching could not find any changes of sediments but the OSL measurements gave different ages.

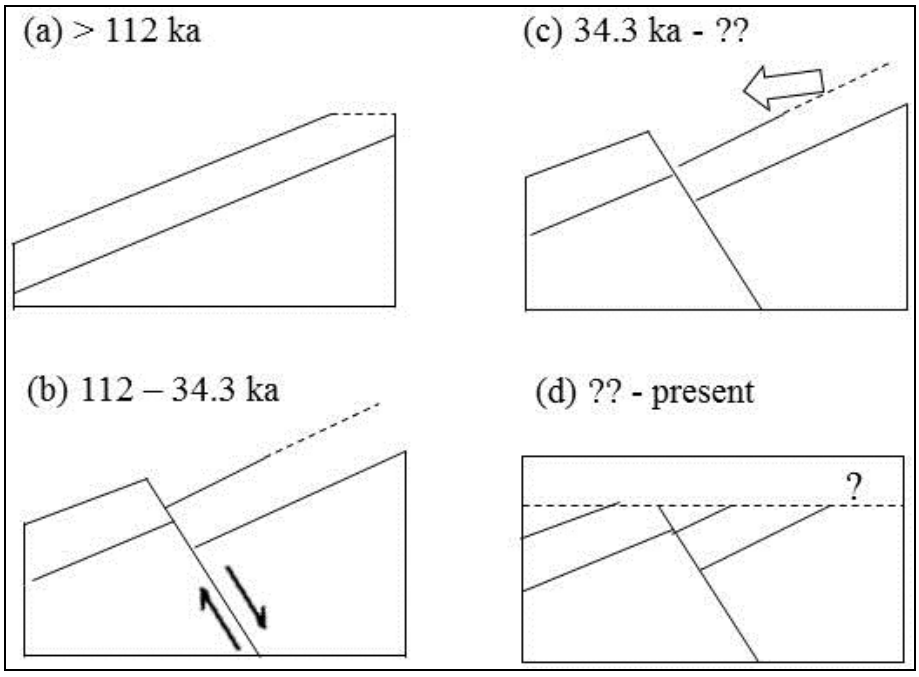

Figure 4.8 Scenario of CTR with a paleoseismological event in Pleistocene.

4.5.2 Magnitude of paleoearthquakes

The normal displacements of 4.0, 4.1, and 4.1 m redrawn from the photo in Figure 3.15 and presented in Figure 4.9 were assumed to be from a single event. The AD (4.07 m) method gives a Mw value of 7.6 and the MD (4.1 m) one a Mw of 7.3. Therefore, the minimum magnitude in this area was 7.3 on the moment magnitude scale.

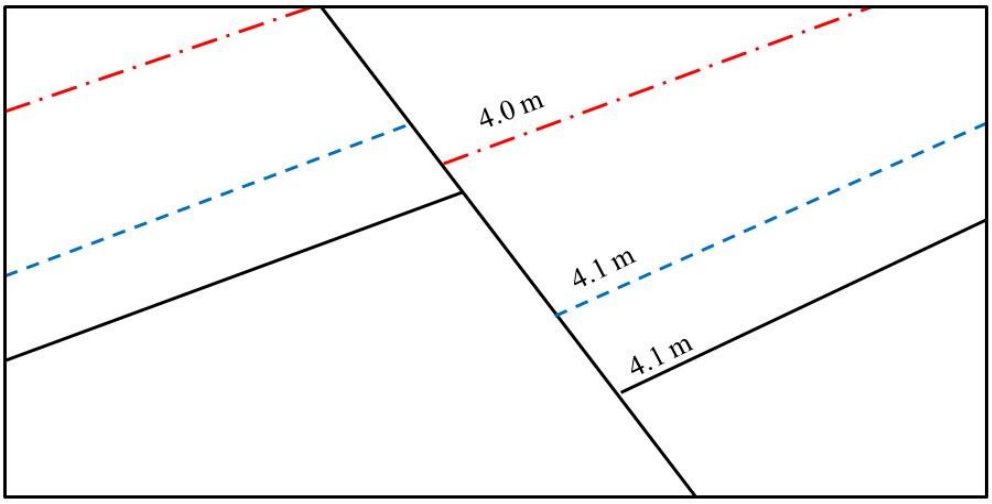

Figure 4.9 Schematic drawing of the normal displacement at the CTR side based on the photo in Figure 3.15. Looking to west.

4.5.3 Conclusion

More than 112 ka ago the layers at site CTR were tilted and subsequently dipping south. After that, there was at least one earthquake event indicated by the presence of a fault, which might have approximately a NE–SW strike direction. This event occurred between 112 and 34.3 ka before present and had magnitude Mw of minimal 7.3.

4.6 Paleoseismology of the Khlong Marui Fault Zone

As the paleoseismological study by DMR (2007) focused on the western part of the Khlong Marui Fault Zone and this study mainly on the eastern part, the age data of both studies are discussed in the following. Several TL ages in the DMR (2007) report were not used by the authors as they might have assumed they were erroneous. The age data, TL, ESR, and C–14, related to the geological descriptions in the DMR (2007) study were also reinterpreted here. All age data were summarized in Figure 4.10 and separated regarding KMFZ and RFZ, as well as site and data source.

Many study locations both for the DMR (2007) report and for this study have dominantly less than 10 ka ages (Figure 4.10) and data are in the age range from 33 to 112 ka. From the overview of the data it can be assumed that there has

been at least three periods of paleoearthquakes: 12–33 ka, 2.5–10 ka, and younger than 2.5 ka. From both studies it could be concluded that the KMFZ is still active.

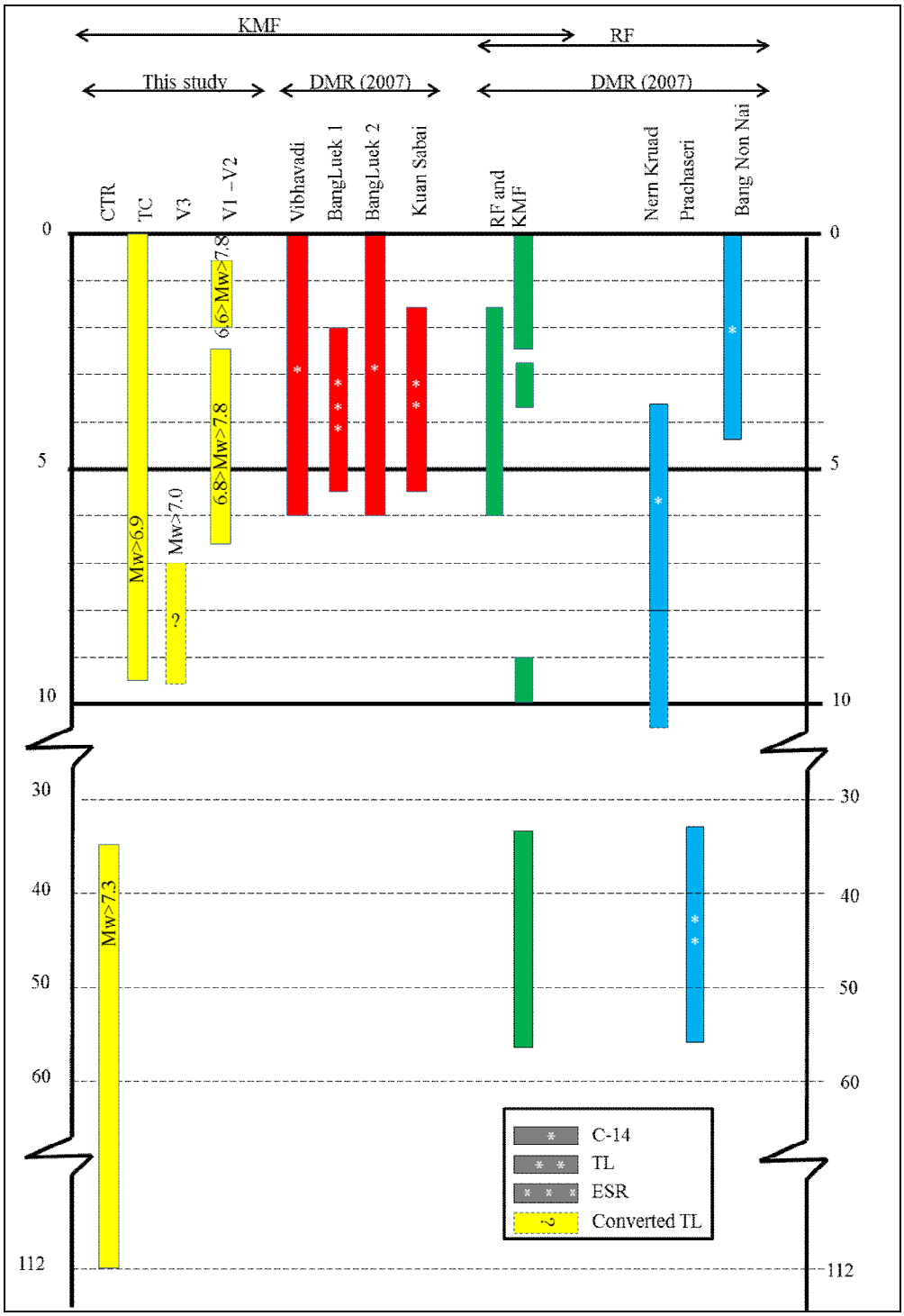

Figure 4.10 Earthquake events at KMFZ and RFZ from this study and DMR (2007), location are presented from East to West, ages presented in ka. Note that red and blue bars are re-interpreted data from DMR (2007) results and green bars are results concluded by DMR (2007).

DMR (2007) is using the surface rupture length to evaluate the paleo-magnitude along the KMF. They present magnitude values between Mw 6.4 to 7.2. In this study, the displacement of faults was used for the determination of the paleo-magnitudes, which range from Mw 6.6 to 7.8. The magnitude in this study could be less than 7.8, but there is no confirmed evidence how much is the actual displacement in horizontal direction. Moreover, all the young faults found in KMF were left lateral strike slip faults, whereas in this study there were mainly normal faults where a strike–slip component could be assumed at some sites related to the geological observations.

According to the definition of an active fault by the DMR, the KMFZ is currently active with the latest movement less than 2.17 ka ago. More evidence indicates that the fault this area moved at around 10 ka before present.

4.7 Implications for seismic hazard analysis

This study and the work from DMR (2007) have shown that earthquakes occurred along the KMFZ in the last 10 ka and therefore can be categorized as an active fault zone. The paleomagnitudes give values of Mw between 6.6 and 7.8. Such magnitude values have not been reported since instrumental data in this area are available. The three most significant instrumental earthquakes reported by TMD along the RFZ and KMFZ were on 16 May 1933 at RFZ with M 6.5, on 27 September 2006 at RFZ with M 4.7, and on 23 December 2008 at the KMFZ with M 4.1. Although two of the events occurred after 2004 when the Mw 9.1 Sumatra Andaman Earthquake occurred there is seemingly a relatively smaller effect from this mega event on the earthquake magnitudes along the fault zones. This might be related to the fact that the 2004 earthquake resulted in a relaxation state of the lithosphere (see Dürrast et al 2007). But the paleoseismological investigations show that both fault zones can generate higher magnitude earthquakes and by this indicate that these magnitudes can be expected for the future. Any seismic hazard analysis for this area has to take this into account.

4.8 Conclusion

The paleoseismological investigations in the eastern part of the Khlong Marui Fault Zone have revealed that it has to be classified as an active fault in terms of seismic hazard analysis. Although the investigated outcrops show mainly secondary faults they can be seen as conjugated fault to the main fault line (see Figure 4.11). A recent stuffy by GRC (2013) has shown that the main fault line of the KMFZ is about 20 km further south of than previously assumed in the study of DMR (2007) based on clear geological and geophysical evidence (see Figure 4.11). The paleoseismological investigations also have shown that the KMFZ can generate higher magnitude earthquakes than any seismogram has ever recorded for this area (Mw 6.6 to 7.8) and by this indicate that these magnitudes can be also expected for the future. This is important and essential for any seismic hazard analysis for this area.

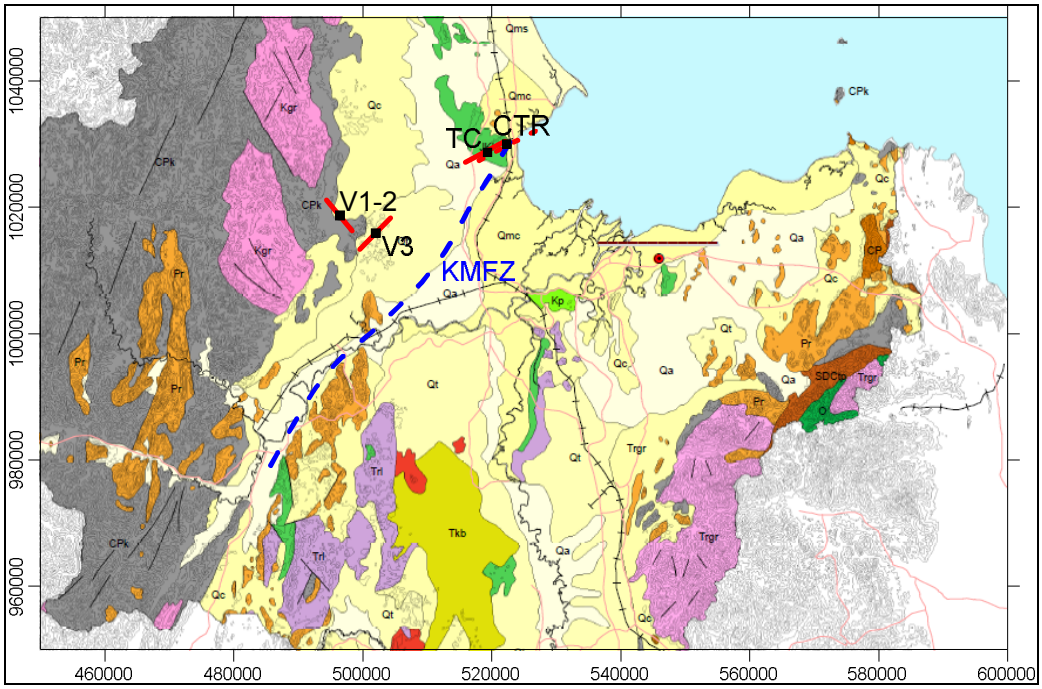

Figure 4.11 Geological map (from Bureau of Geological Survey 2007) with the locations in this study (red lines are strike directions of faults found in the outcrops) and the main fault line of the KMFZ (blue line, after GRC 2013).

An essential part for the conclusions is coming from the OSL dating of the sediments found in the outcrops. TL measurements were also carried out in this

study but the ages show much older values than the OSL data. Although the reason or reasons for these discrepancies are not fully understood yet there are several good indications that the OSL data are more reliable and therefore used in the conclusions.

4.9 Outlook on future work

All data from TL dating in this study show higher values than other methods, especially C-14 and OSL. Other studies seemingly had a similar problem (e.g. DMR, 2007). This problem could come from the luminescence properties of the quartz minerals collected in the study area. Therefore the thermoluminescence properties of quartz could be studied further in order to get some answer to this unsolved issue.

Further, more paleoseismological studies should be carried out based on more supporting data including 3D trenching or geophysical surveys. This might help to narrow down an actual displacement value and therefore a better magnitude value. This will be not an easy task as in the eastern part of the KMFZ as it is under a thicker layer of younger unconsolidated sediments.

REFERENCES

Aboelkhair, H. and Zaaeimah, M. (2012). Potential of natural gamma-ray spectrometry for mapping and environmental monitoring of black-sand beach deposits on the northern coast of Sinai, Egypt. Radiation Protection Dosimetry, 136, 1-14.

Aitken, M.J. (1985). Thermoluminescence dating. Academic Press Inc., London.

Aitken, M.J. (1998). An Introduction to Optical Dating. Oxford University Press, Oxford.

ASTM International. (2006). Standard test methods for determining the biobased content of natural range materials using radiocarbon and isotope ratio mass spectrometry analysis. Designation D 6866-06a.

BBC. (2013). Uses of radioactivity. <http://www.bbc.co.uk/schools/gcsebitesize/science/add_edexcel/radioactive_materials/radioactiveusesrev4.shtml>(Apr. 15, 2013).

Chotikasathien, W. and Kohpina, P. (1993). Quaternary geology of coastal area, Surat Thani and vicinity, southern Thailand. Journal of Southeast Asian Earth Science, 8, 313–320.

Bureau of Geological Survey (2007). Geological map of Surat Thani province. <http://www.dmr.go.th/download/pdf/South/Surat.pdf> (Apr. 15, 2013).

DMR. (2007). Investigation on Recurrence Interval in Areas Showing Trace of Movement along the Faults in Prachuab Khirikhan, Chumporn, Ranong, Surat Thani, Krabi, Phang Nga and Phuket Provinces (Ranong and Khlong Marui Faults). Department of Mineral Resources, Bangkok.

DMR. (2013). Earthquake in Thailand. <http://www.dmr.go.th/main.php?filename=Thaifelt> (July 12, 2013).

DMR and KU. (2011). Investigation on Recurrence Interval in Areas Showing Trace of Movement along the Faults in Utaradit, Nan, Pitsanulok and Sukhothai Provinces (Utaradit and Pua Faults).

Dürrast, H., Dangmuan, S. and Lohawijarn, W. (2007). Khlong Marui and Ranong Fault Zones in Southern Thailand re-activated by the 26 December 2004 Mw 9.3 Sumatra-Andaman Earthquake? Proceedings of the GEOTHAI'07 International Conference, 21-22 Dec 2007, Bangkok.

Fattahi, M. (2009). Dating past earthquakes and related sediments by thermoluminescence methods: A review. Quaternary International, 199, 104–146.

Fleming, S.J. (1979). Thermoluminescence techniques in archaeology. Clarendon Press, Oxford.

Fuchs, M. and Lang, A. (2009). Luminescence dating of hillslope deposits – A review. Geomorphology, 109, 17–26.

Galbraith, R.F. and Roberts, R.G. (2012). Statistical aspects of equivalent dose and error calculation and display in OSL dating: An overview and some recommendations. Quaternary Geochronology, 11, 1–27.

GRC (2013). Integrated geophysical studies of the fault zones in Southern Thailand. Geophysics Research Center, Prince of Songkla University, HatYai, Thailand (unpublished).

Guérin, G., Mercier, N. and Adamiec, G. (2011). Dose-rate conversion factors: update. Ancient TL, 29, 5-8.

Huntley, D.J., Godfrey-Smith, D.I. and Haskell, E.H. (1991). Light-induced emission spectra from some quartz and felspars. Nuclear Tracks and Radiation Measurements, 18, 127–131.

IAEA (2003). Guidelines for radioelement mapping using gamma ray spectrometry data. The International Atomic Energy Agency. Austria

Kitis, G., Hasan, F., Tsakiri, M. and Charalambous, S. (1982). Implication of regenerated thermoluminescence on low dose measurements. Nuclear Tracks and Radiation Measurements, 10, 571–574.

Kosuwan, S., Takashima, I. and Charusiri, P. (2004). Active fault zone in Thailand. <http://www.dmr.go.th/ewtadmin/ewt/dmr_web/main.php?filename=fault_En> (Mar. 4, 2013).

Kreutzer, S., Schmidt, C., Fuchs, M., Dietze, M. and Fischer, M. (2012). Introducing an R package for luminescence dating analysis. Ancient TL, 30(1), 1–8.

Kurniawan, A., Jasmine, A.P. and McKenzie, J. (2009). General Dictionary of Geology. Environmental Geographic Student Association, Indonesia.

Lian, O.B. and Huntley, D.J. (2002). Luminescence Dating. In Tracking Environmental Change Using Lake Sediments Basin Analysis, Coring, and Chronological Techniques, W. M. Last and H. P. Smol, eds., Kluwer Academic Publishers, Dordrecht, 182–261.

McCalpin, J.P. (2008). Paleoseismology. Academic Press, MA.

Michael, C.T. and Zacharias, N. (2000). A new technique for thick source alpha counting. Nuclear Instruments and Methods in Physics Research A, 439, 167–177.

Nichols, G. (2009). Sedimentology and stratigraphy. John Wiley & Sons, Ltd., United Kingdom.

Nutalaya, P., Sodsri, S. and Arnold, E.P. (1985). Southeast Asia Association of Seismology and Earthquake Engineering: Volume II.

Prescott, J.R., and Hutton, J.T. (1994). Cosmic ray contribution to dose rate for luminescence and ESR dating: long-term time variation. Radiation measurements, 23, 497–500.

Preusser, F., Götte, T., Martini, M., Ramseyer, K., Sendezera, E.J., Susino, G.J. and Wintle, A.G. (2009). Quartz as a natural luminescence dosimeter. Earth-Science Reviews, 97, 184–2214.

Preusser, F., Spencer, J.Q.G., Degering, D., Fuchs, M., Hilgers, A., Kadereit, A., Klasen, N., Krbetschek, M. and Richter, D. (2008). Luminescence dating: basics, methods and applications. Eiszeitalter und Gegenwart Quaternary Science Journal, 57, 95–149.

Puchalska, M. and Bilski, P. (2006). GlowFit—a new tool for thermoluminescence glow-curve deconvolution. Radiation Measurements, 41, 659–664.

Rodríguez-Pascua, M.A., Bischoff, J., Garduño-Monroy, V.H., Pérez-López, R., Giner-Robles, J.L., Israde-Alcántara, I., Calvo, J.P. and Williams, R.W. (2009). Estimation of the tectonic slip-rate from Quaternary lacustrine facies within the intraplate Albacete province (SE of Spain). Sedimentary Geology, 222, 89–97.

RTSD. (2003a). Topographic Map of Ban Yang Phrong, Scale 1:50,000, WGS-84, Series L7018, Sheet 4727 I. (Royal Thai Survey Department).

RTSD. (2003b). Topographic Map of Amphoe Khiri Ratthanikhom, Scale 1:50,000, WGS-84, Series L7018, Sheet 4727 II. (Royal Thai Survey Department).

RTSD. (2004). Topographic Map of Amphoe Phunphin, Scale 1:50,000, WGS-84, Series L7018, Sheet 4827 III. (Royal Thai Survey Department).

RTSD. (2005). Topographic Map of Amphoe Chaiya, Scale 1:50,000, WGS-84, Series L7018, Sheet 4827 IV. (Royal Thai Survey Department).

Scholefield, R.B., Prescott, J.R., Franklin, A.D. and Fox, P.J. (1994). Observation on some thermoluminescence emission certer in geological quartz. Radiation measurements, (23), 409–412.

Soumana, S., Fain, J., Miallier, D., Montret, M., Pilleyre, T.H. and Sanzelle, S. (1997). Alpha counting using scintillation techniques: Observation on TSAC calibration and gas cell use. Radiation Measurements, 27, 365–372.

Stokes, S. (1999). Luminescence dating applications in geomorphological research. Geomorphology, 29, 153–171.

Sutiwanich, C., Hanpatanapanich, T., Charusiri, P. and Trinetra, K. (2008). Seismic Hazard Analysis of the Khlong Tham Dam Project in Thailand. the International Symposia on Geoscience Resources and Environments of Asian Terranes (GREAT 2008) and 5th APSEG, Bangkok, Thailand, 416–420.

TMD. (2007). Climate of Thailand. <http://www.tmd.go.th/info/info.php?FileID=22> (Apr. 10, 2013).

TMD. (2013a). Earthquake Statistic of Thailand. <http://www.seismology.tmd.go.th/en/file/stat.pdf> (Jun. 25, 2013).

TMD. (2013b). Earthquake. <http://www.tmd.go.th/info/info.php?FileID=77> (Jul. 12, 2013).

Watkinson, I., Elders, C. and Hall, R. (2008). The kinematic history of the Khlong Marui and Ranong Faults. Journal of Structural Geology, 30, 1471–1554.

Wells, D.L. and Coppersmith, K.J. (1994). New Empirical Relationships among Magnitude, Rupture Length, Rupture Width, Rupture Area, and Surface Displacement. Bulletin of the Seismological Society of America, 84, 974–1002.

Wintle, A.G. (1997). Luminescence dating: laboratory procedures and protocols. Radiation Measurements, 27, 769–817.

Wolf, R.E. (2005). What is ICP-MS and more importantly, what can it do? <http://crustal.usgs.gov/laboratories/icpms/What_is_ICPMS.pdf> (Apr. 12, 2013).

APPENDICES

APENDIX A

TL CURVE

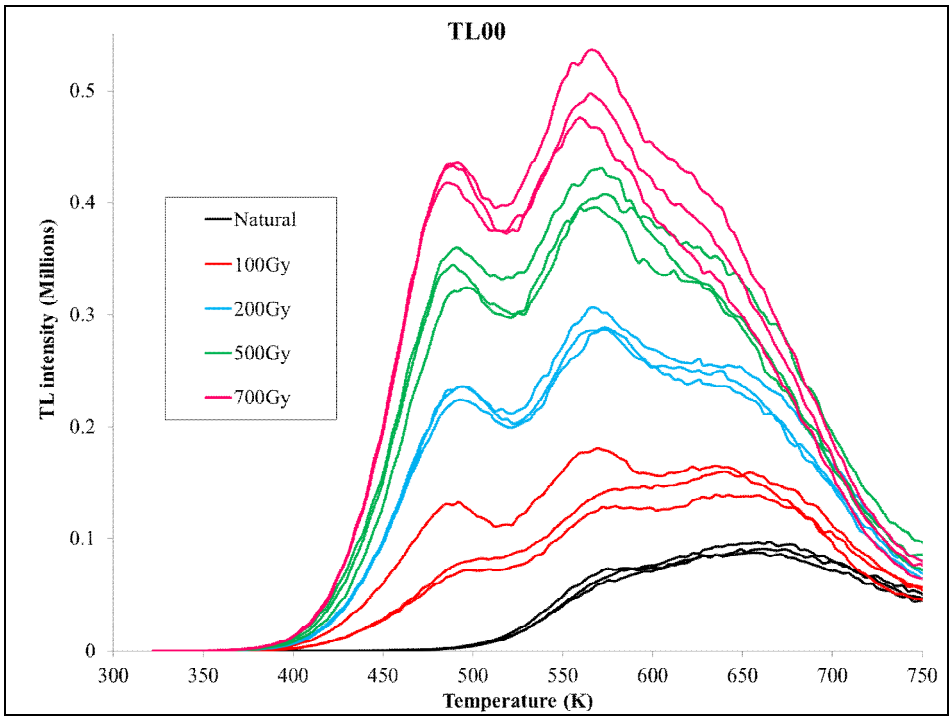

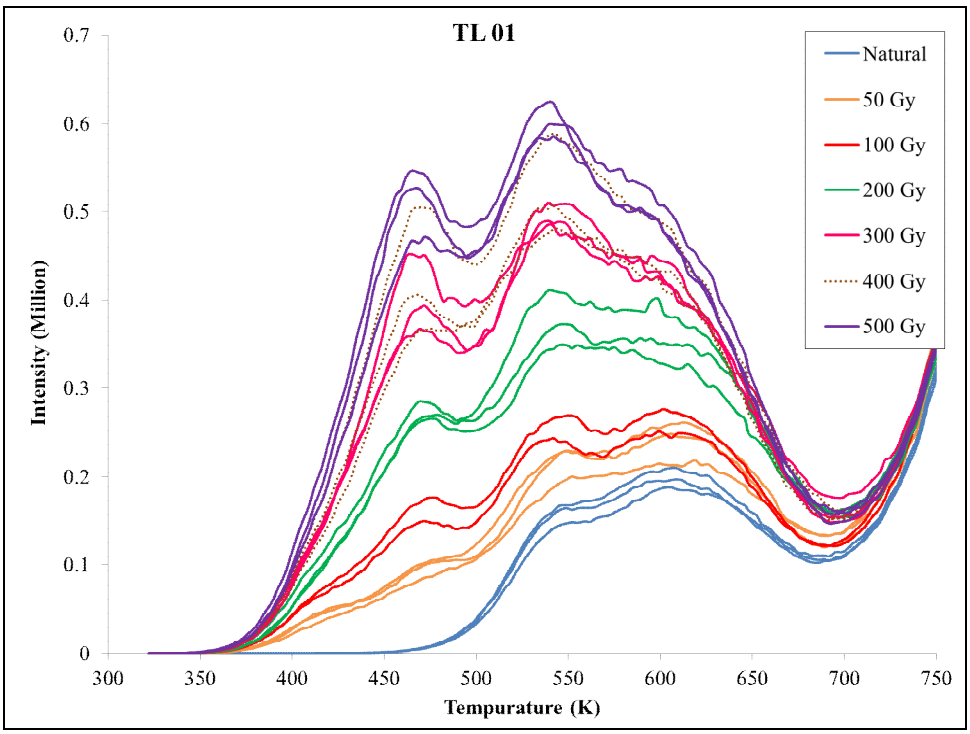
TL 01
Natural
50 Gy
100 Gy
200 Gy
300 Gy
400 Gy
500 Gy
Intensity (Million)
Tempurature (K)
0.7
0.6
0.5
0.4
0.3
0.2
0.1
0
300
350
400
450
500
550
600
650
700
750

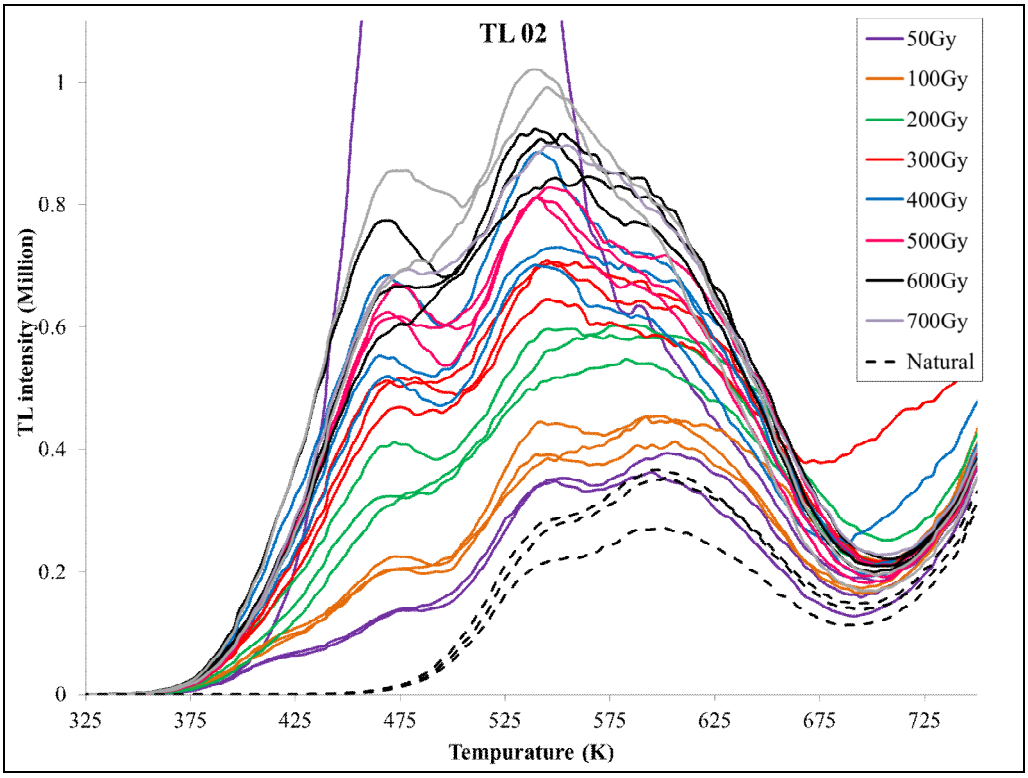
TL 02
50Gy
100Gy
200Gy
300Gy
400Gy
500Gy
600Gy
700Gy
Natural
TL intensity (Million)
Tempurature (K)
1
0.8
0.6
0.4
0.2
0
325
375
425
475
525
575
625
675
725

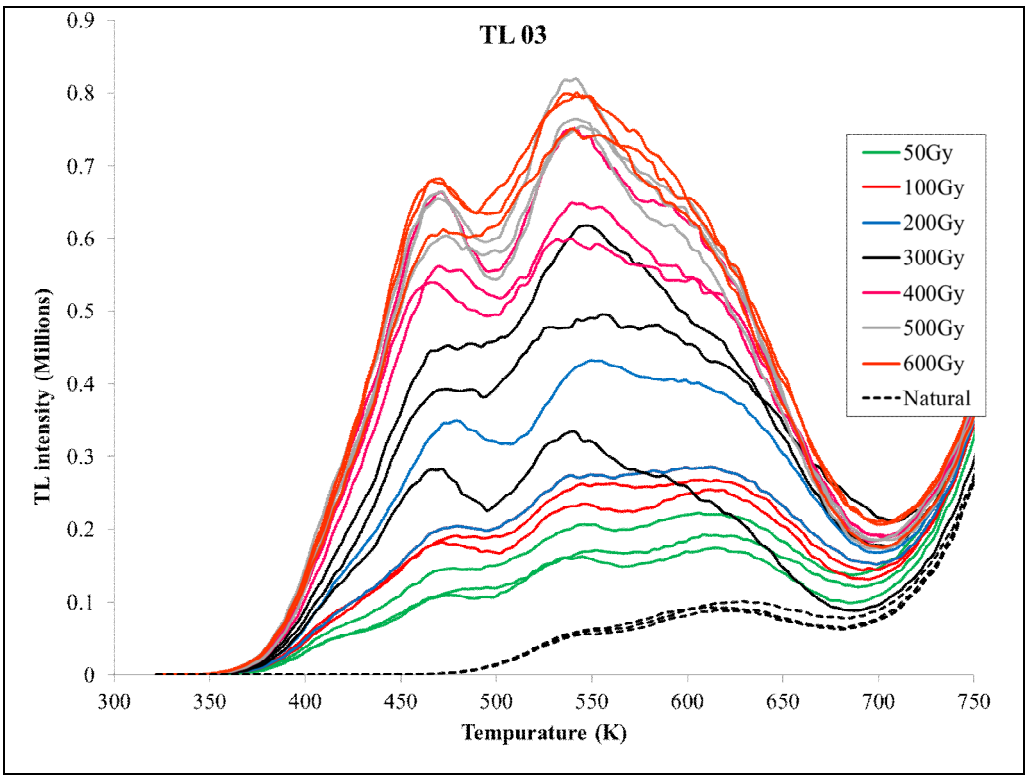
TL 03
TL intensity (Millions)
Tempurature (K)
0.9
0.8
0.7
0.6
0.5
0.4
0.3
0.2
0.1
0
300
350
400
450
500
550
600
650
700
750
50Gy
100Gy
200Gy
300Gy
400Gy
500Gy
600Gy
Natural

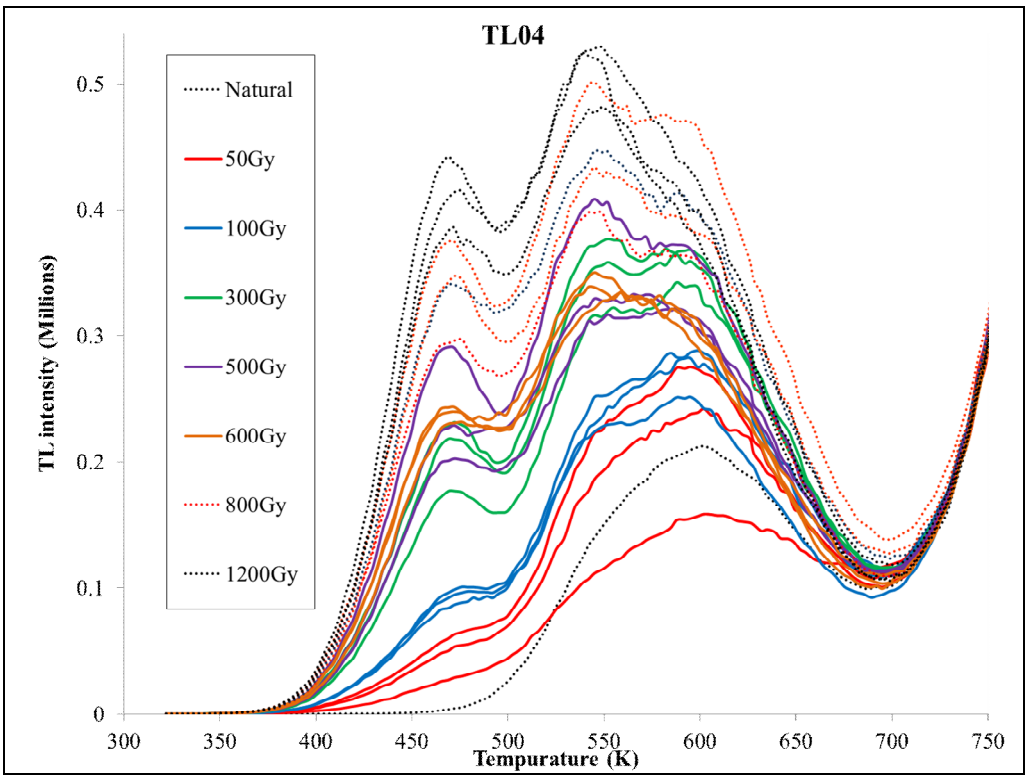
TL04
TL intensity (Millions)
Tempurature (K)
0.5
0.4
0.3
0.2
0.1
0
300
350
400
450
500
550
600
650
700
750
Natural
50Gy
100Gy
300Gy
500Gy
600Gy
800Gy
1200Gy

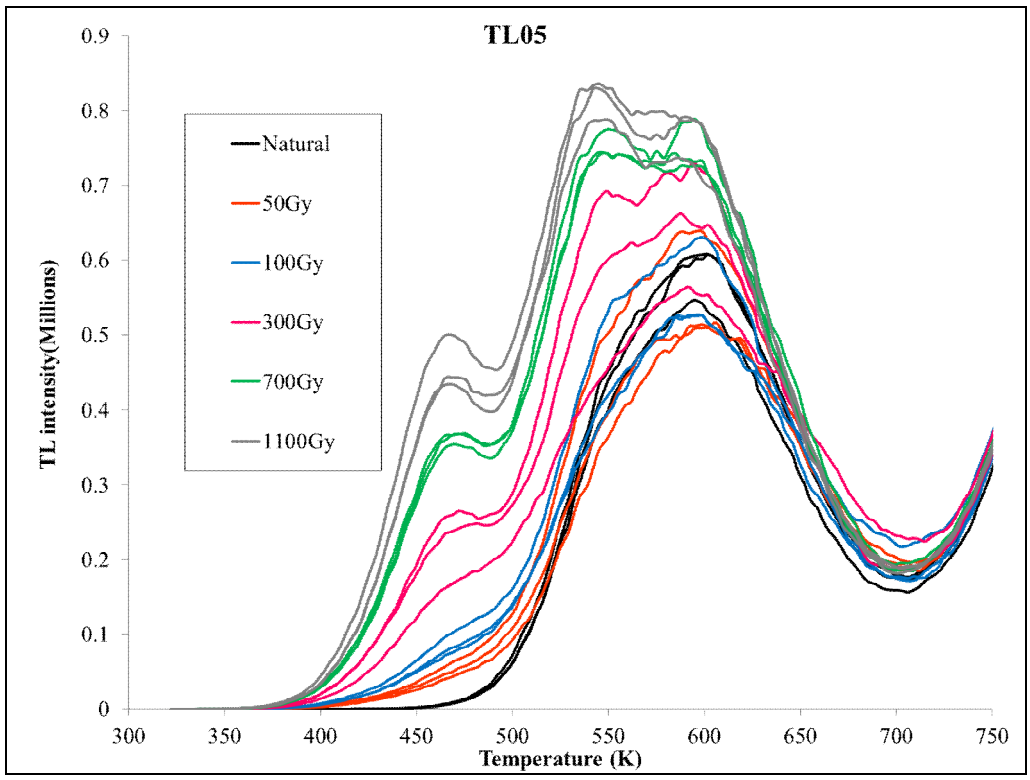
TL05
TL intensity(Millions)
Temperature (K)
Natural
50Gy
100Gy
300Gy
700Gy
1100Gy
0.9
0.8
0.7
0.6
0.5
0.4
0.3
0.2
0.1
0
300
350
400
450
500
550
600
650
700
750

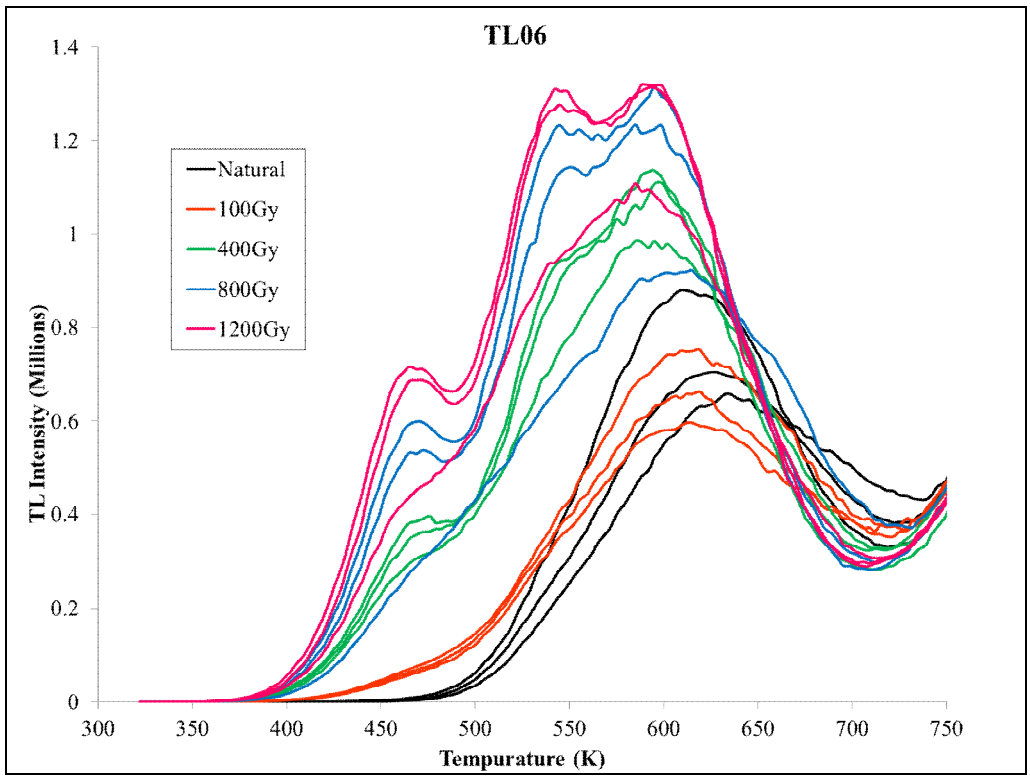
TL06
TL Intensity (Millions)
Tempurature (K)
Natural
100Gy
400Gy
800Gy
1200Gy
1.4
1.2
1
0.8
0.6
0.4
0.2
0
300
350
400
450
500
550
600
650
700
750

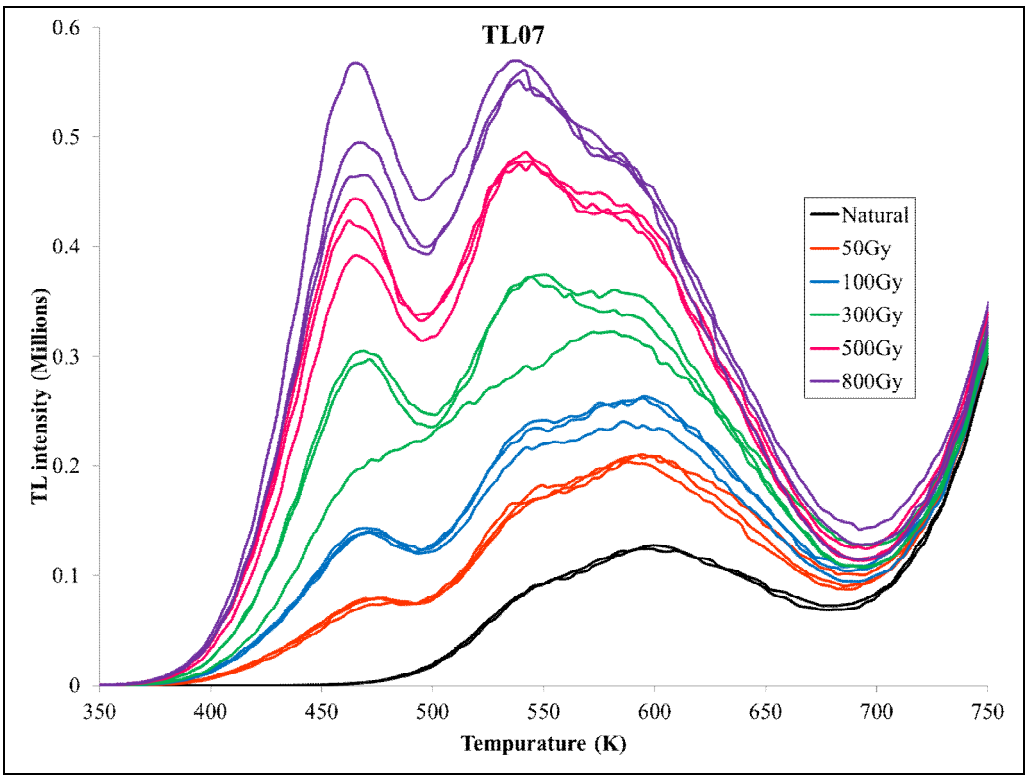
TL07
TL intensity (Millions)
Tempurature (K)
Natural
50Gy
100Gy
300Gy
500Gy
800Gy
0
0.1
0.2
0.3
0.4
0.5
0.6
350
400
450
500
550
600
650
700
750

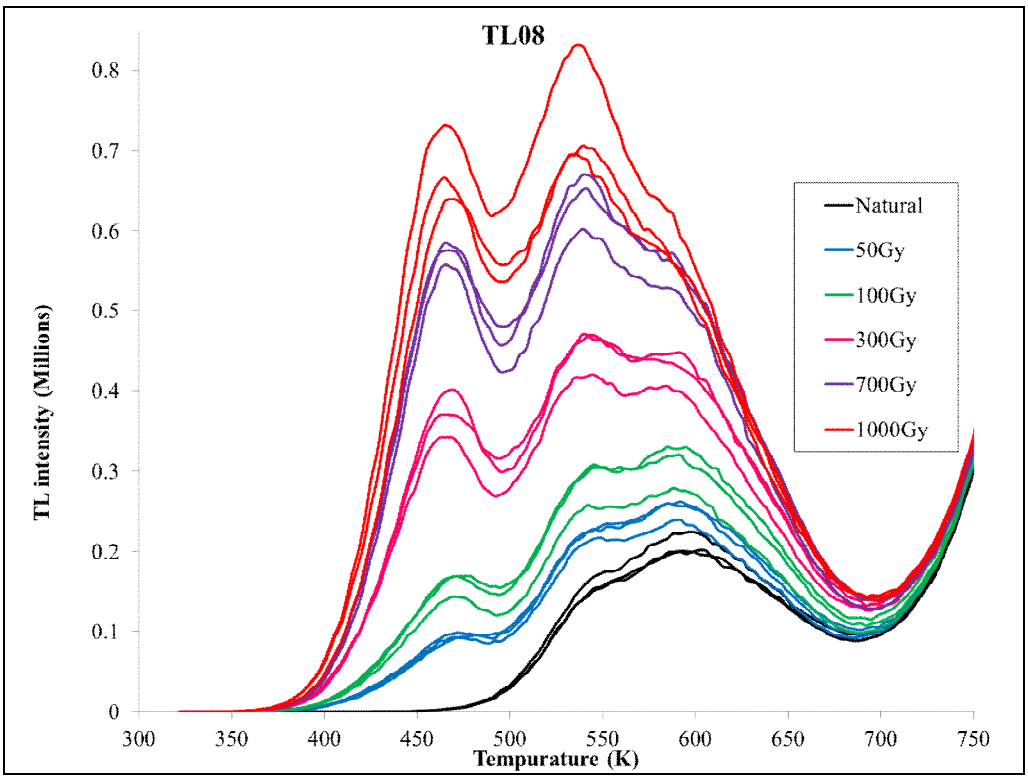
TL08
TL intensity (Millions)
Tempurature (K)
Natural
50Gy
100Gy
300Gy
700Gy
1000Gy
0
0.1
0.2
0.3
0.4
0.5
0.6
0.7
0.8
300
350
400
450
500
550
600
650
700
750

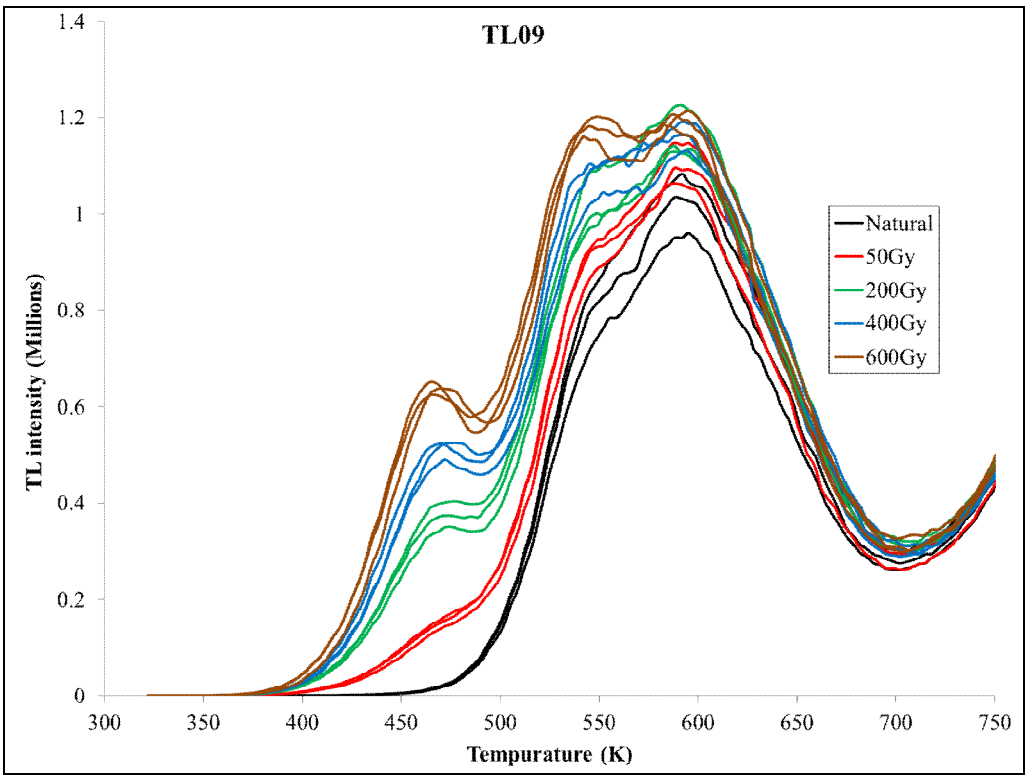
TL09
TL intensity (Millions)
Tempurature (K)
Natural
50Gy
200Gy
400Gy
600Gy
0
0.2
0.4
0.6
0.8
1
1.2
1.4
300
350
400
450
500
550
600
650
700
750

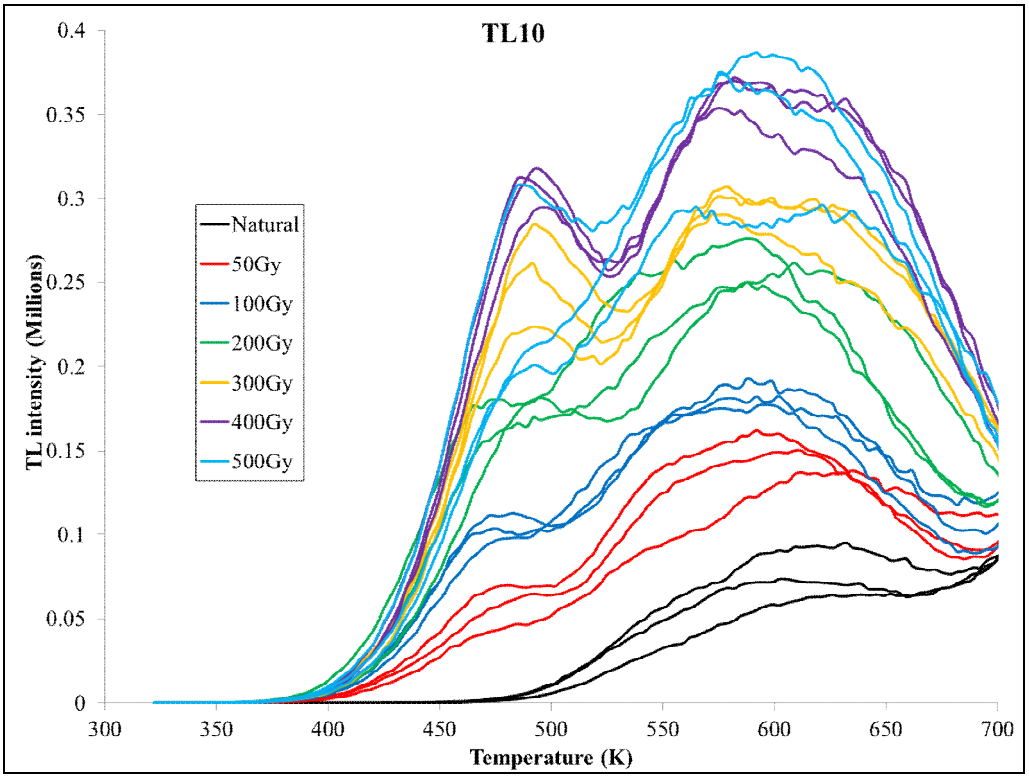
TL10
TL intensity (Millions)
Temperature (K)
Natural
50Gy
100Gy
200Gy
300Gy
400Gy
500Gy
0
0.05
0.1
0.15
0.2
0.25
0.3
0.35
0.4
300
350
400
450
500
550
600
650
700

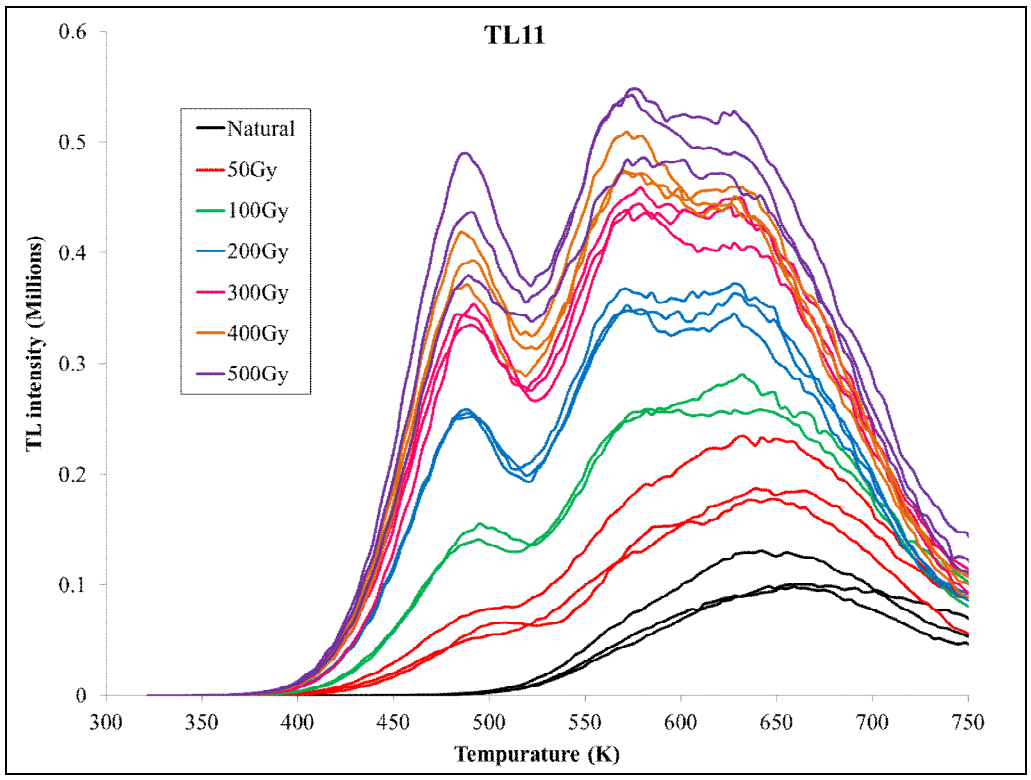
TL11
TL intensity (Millions)
Tempurature (K)
Natural
50Gy
100Gy
200Gy
300Gy
400Gy
500Gy
0.6
0.5
0.4
0.3
0.2
0.1
0
300
350
400
450
500
550
600
650
700
750

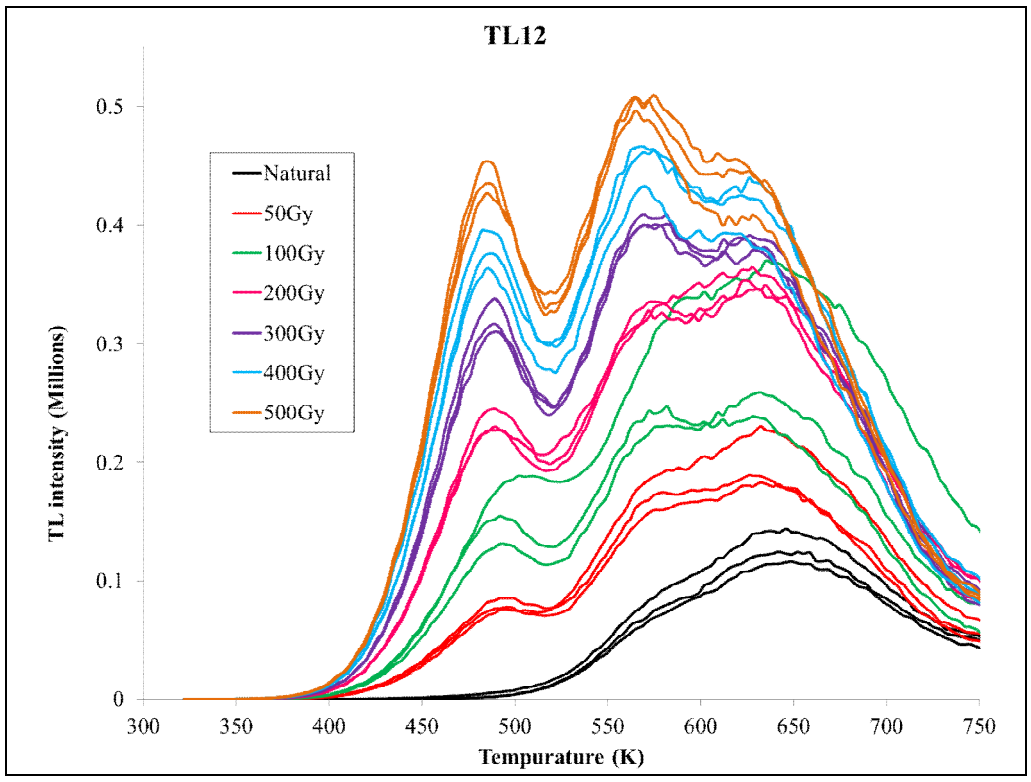
TL12
TL intensity (Millions)
Tempurature (K)
Natural
50Gy
100Gy
200Gy
300Gy
400Gy
500Gy
0.5
0.4
0.3
0.2
0.1
0
300
350
400
450
500
550
600
650
700
750

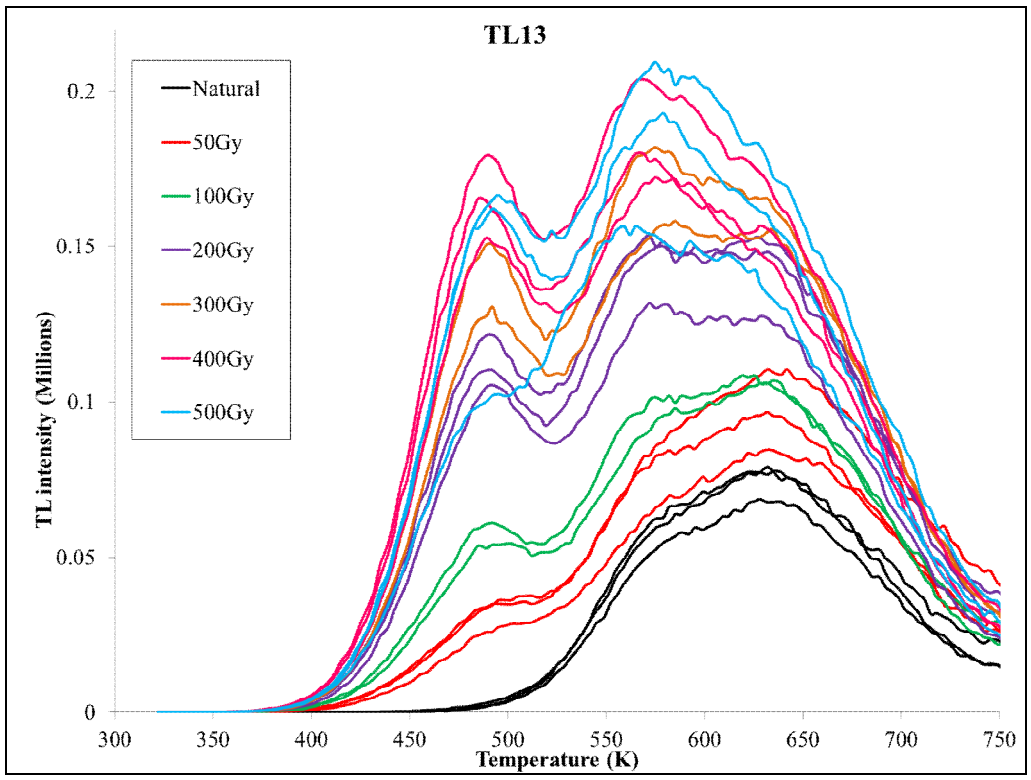
TL13
Natural
50Gy
100Gy
200Gy
300Gy
400Gy
500Gy
TL intensity (Millions)
0.2
0.15
0.1
0.05
0
300
350
400
450
500
550
600
650
700
750
Temperature (K)

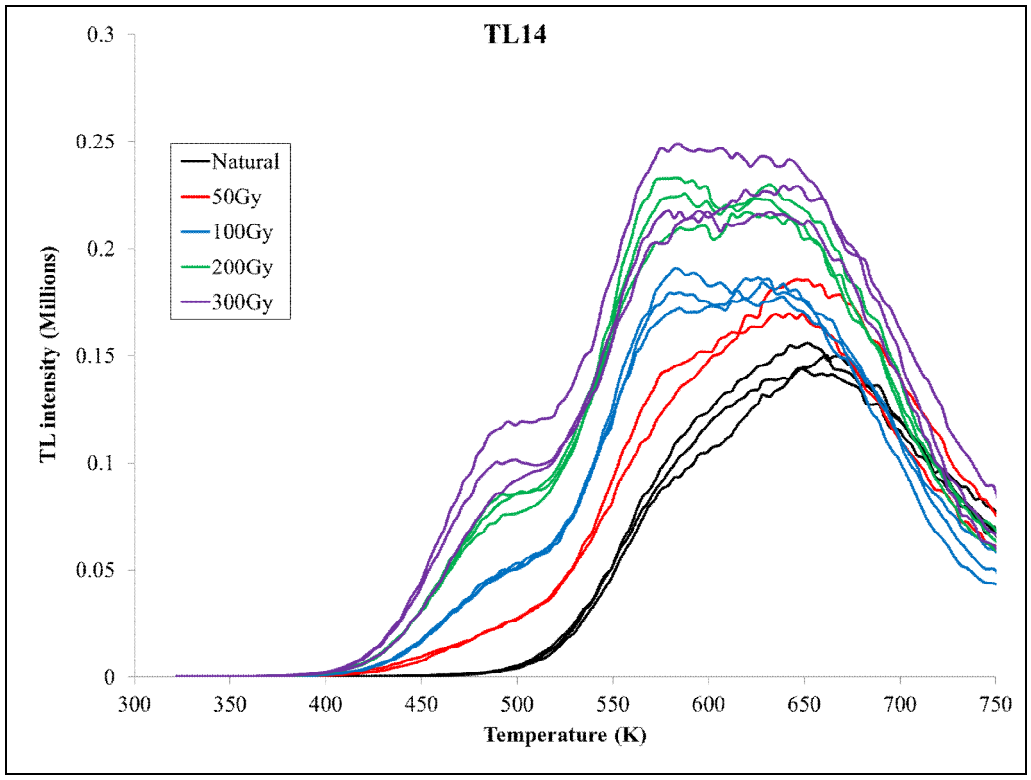
TL14
Natural
50Gy
100Gy
200Gy
300Gy
TL intensity (Millions)
0.3
0.25
0.2
0.15
0.1
0.05
0
300
350
400
450
500
550
600
650
700
750
Temperature (K)

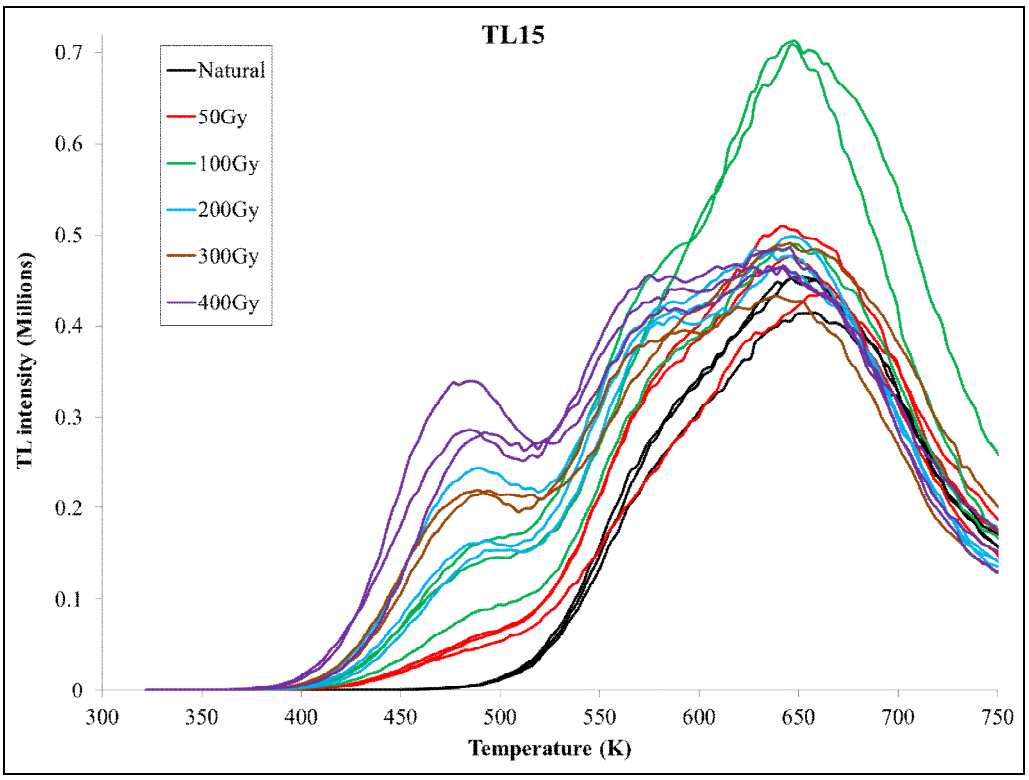
TL15
Natural
50Gy
100Gy
200Gy
300Gy
400Gy
TL intensity (Millions)
Temperature (K)
0
0.1
0.2
0.3
0.4
0.5
0.6
0.7
300
350
400
450
500
550
600
650
700
750

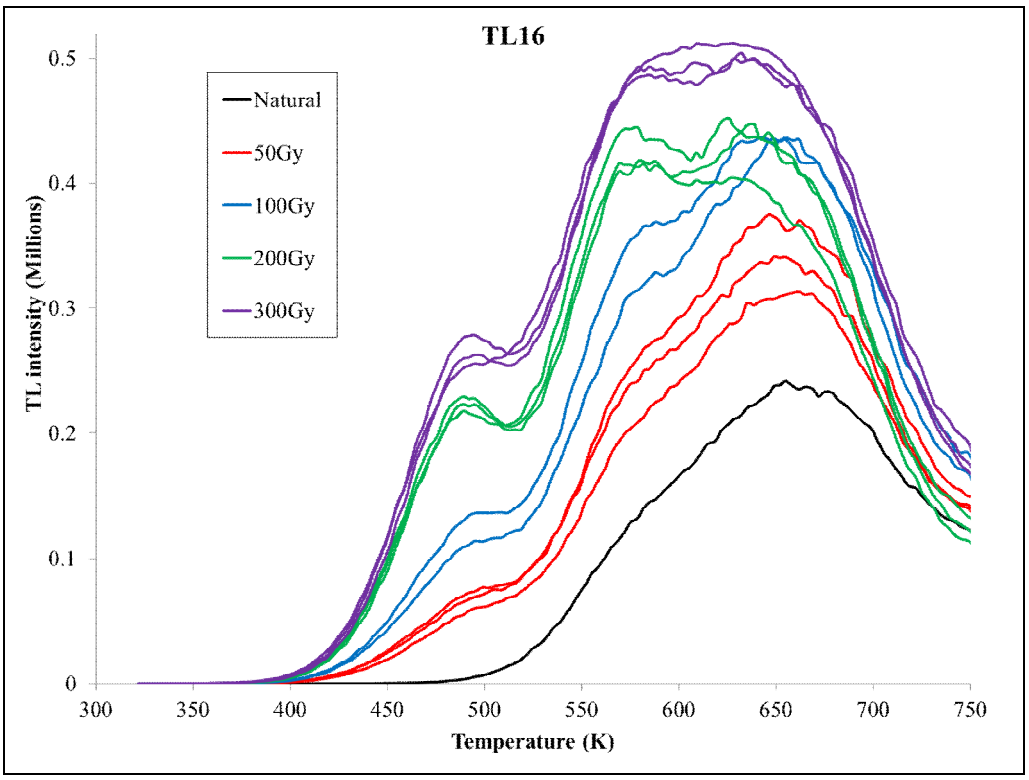
TL16
Natural
50Gy
100Gy
200Gy
300Gy
TL intensity (Millions)
Temperature (K)
0
0.1
0.2
0.3
0.4
0.5
300
350
400
450
500
550
600
650
700
750

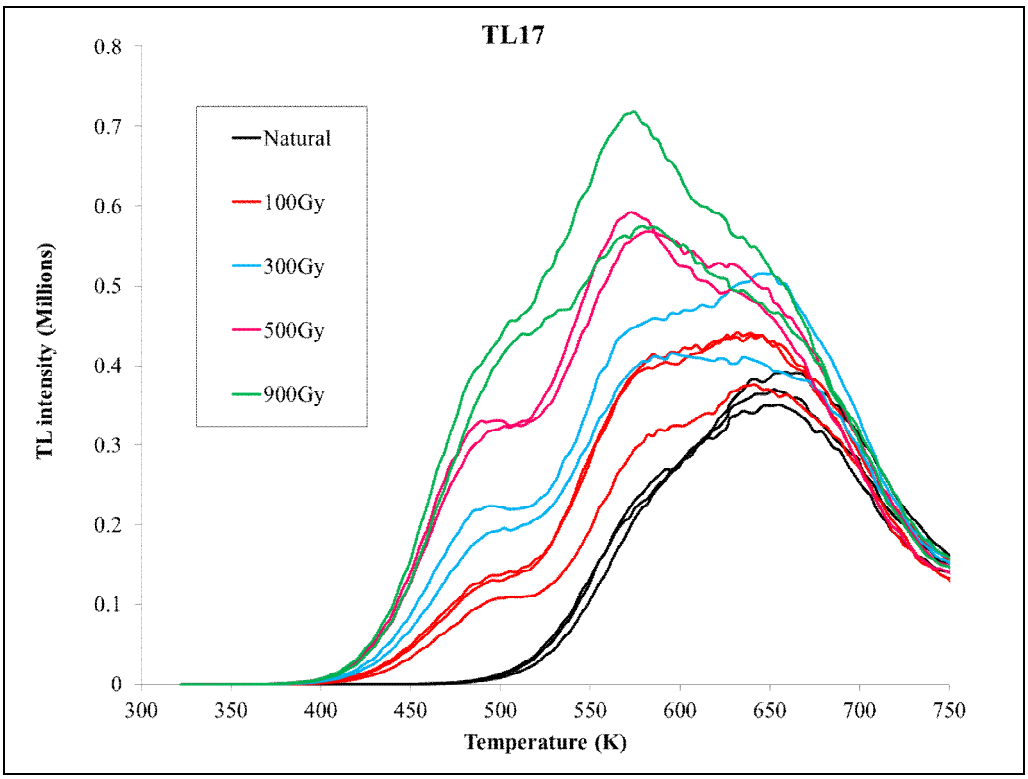
TL17
TL intensity (Millions)
Temperature (K)
Natural
100Gy
300Gy
500Gy
900Gy
0.8
0.7
0.6
0.5
0.4
0.3
0.2
0.1
0
300
350
400
450
500
550
600
650
700
750

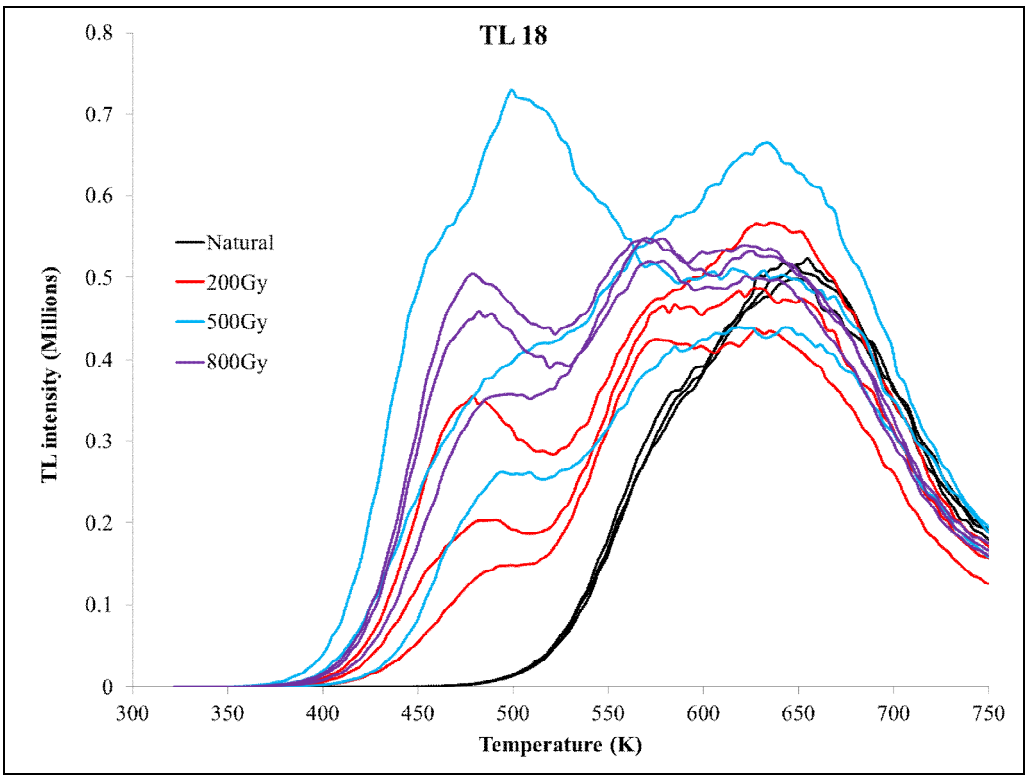
TL 18
TL intensity (Millions)
Temperature (K)
Natural
200Gy
500Gy
800Gy
0.8
0.7
0.6
0.5
0.4
0.3
0.2
0.1
0
300
350
400
450
500
550
600
650
700
750

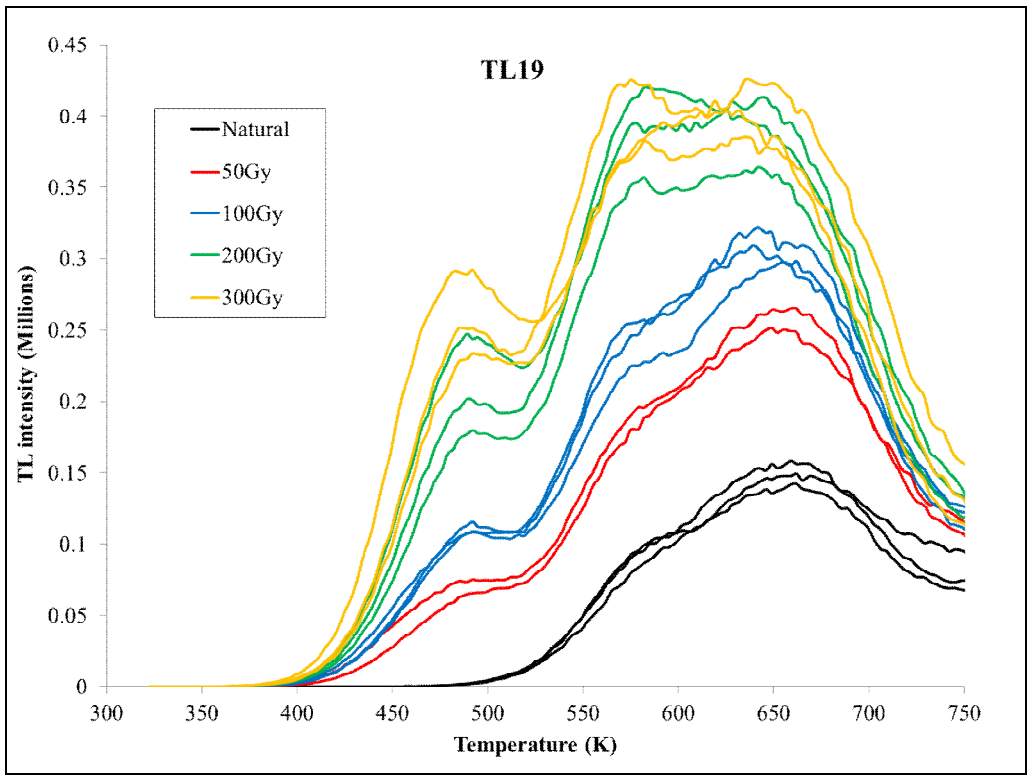
TL19
Natural
50Gy
100Gy
200Gy
300Gy
TL intensity (Millions)
Temperature (K)
0.45
0.4
0.35
0.3
0.25
0.2
0.15
0.1
0.05
0
300
350
400
450
500
550
600
650
700
750

APENDIX B

TL GROWTH CURVE

TL growth curves are presented here. Note that only data points are plotted here that contributed to the trend line. The horizontal line is the bleached quartz TL signal. Y-axis is TL deconvoluted signal in million, X-axis is artificial dose level. Equation were fitted with an exponential rise to maximum following equation:

$$y = y0 + a(1-\exp(-bx)).$$

TL00

y0	4.15E+06
a	1.36E+07
b	2.71E-03

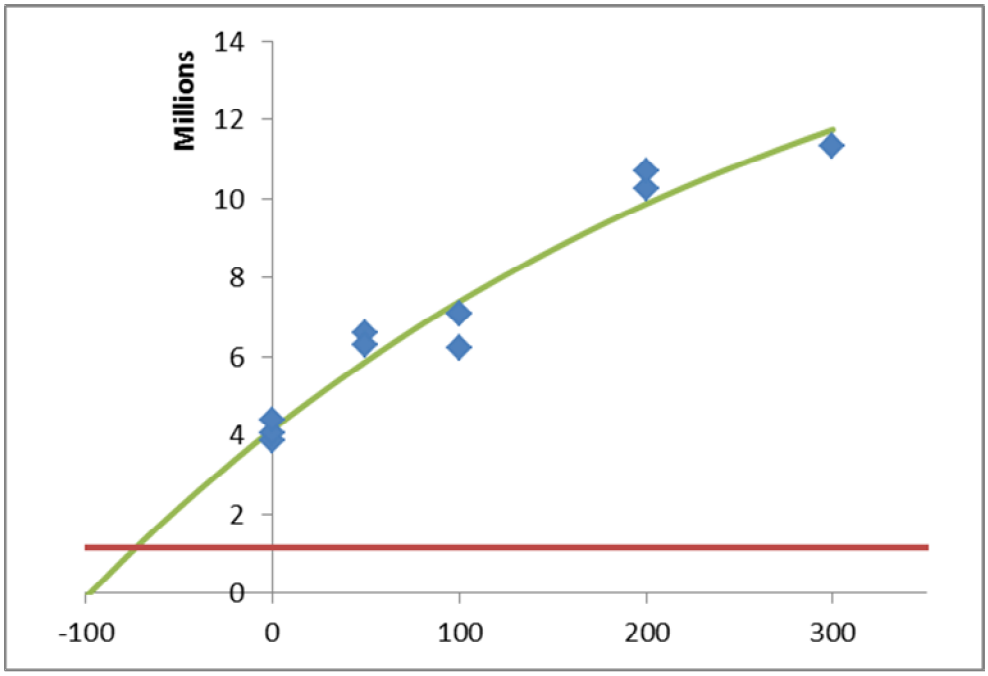

TL01

y0	9.43E+06
a	1.77E+07
b	4.66E-03

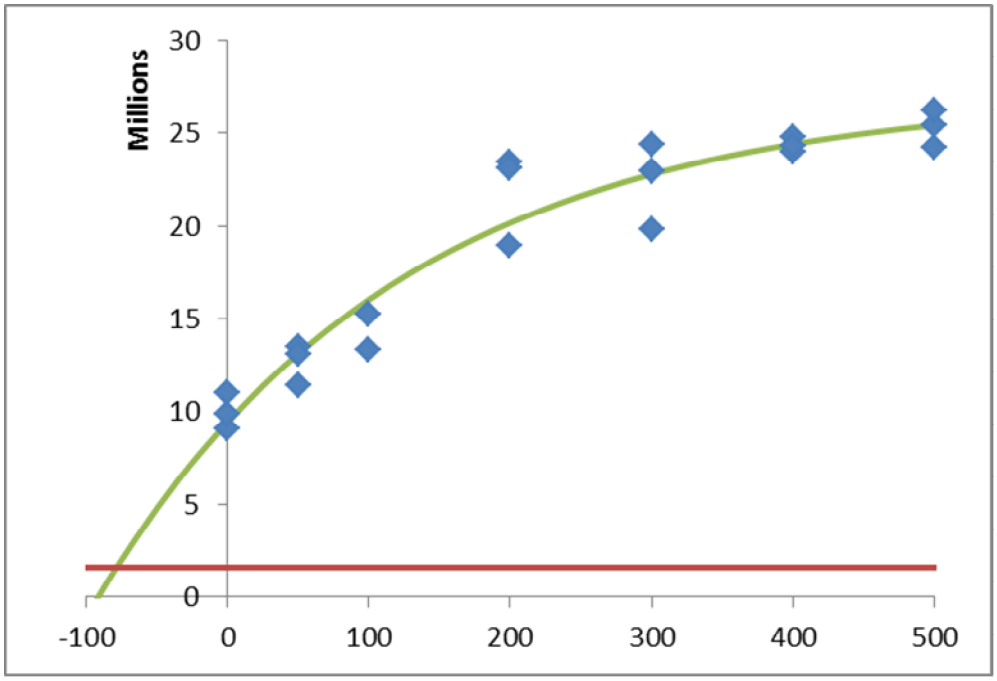

TL02

y0	1.46E+07
a	2.20E+07
b	2.87E-03

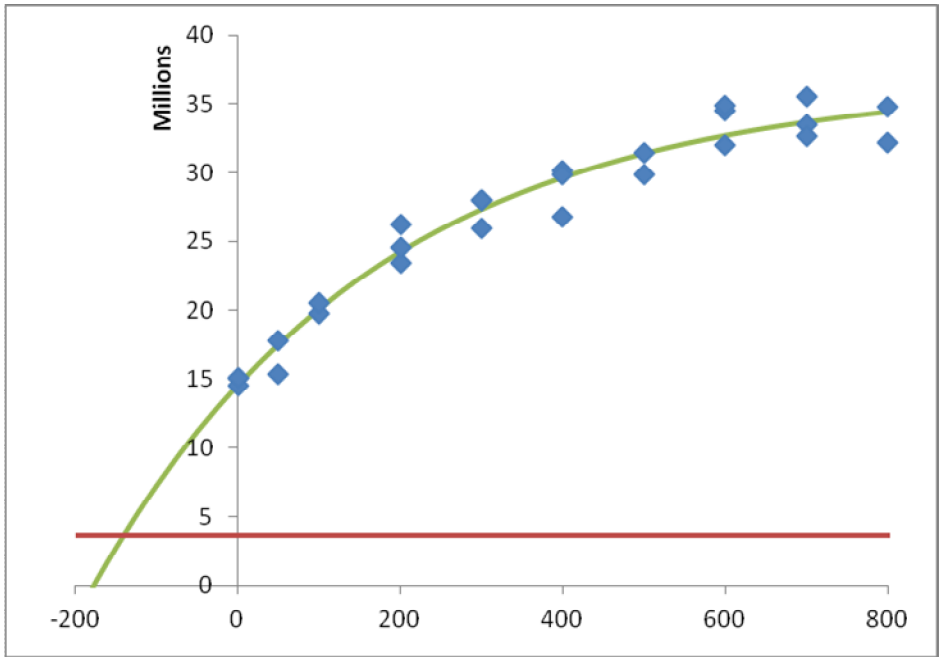

TL03

y0	4.22E+06
a	2.65E+07
b	3.55E-03

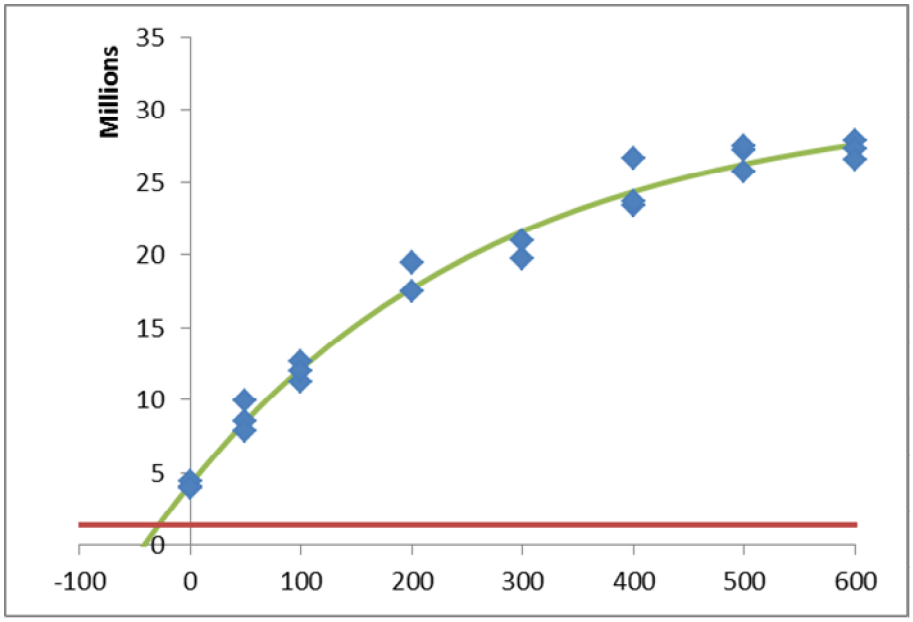

TL04

y0	1.06E+07
a	6.38E+06
b	7.57E-03

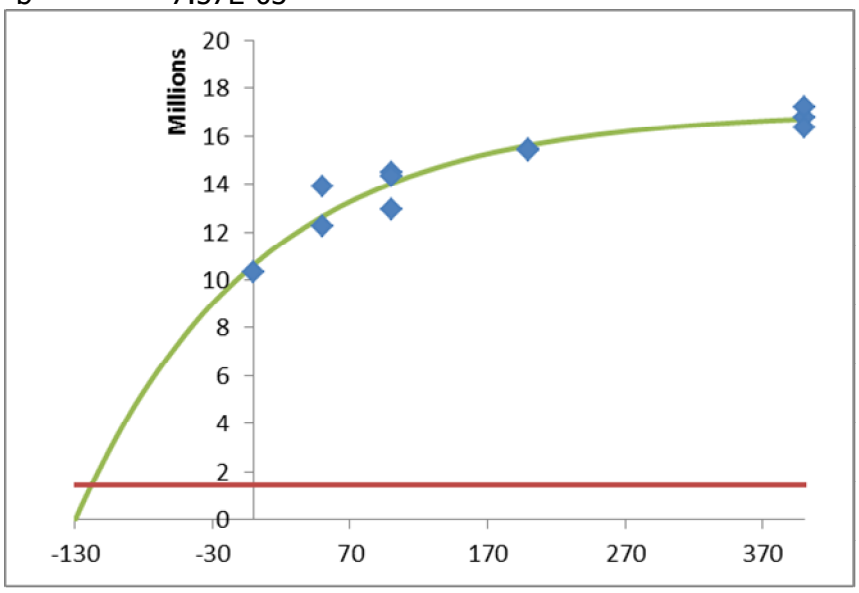

TL05

y0	2.07E+07
a	1.25E+07
b	2.15E-03

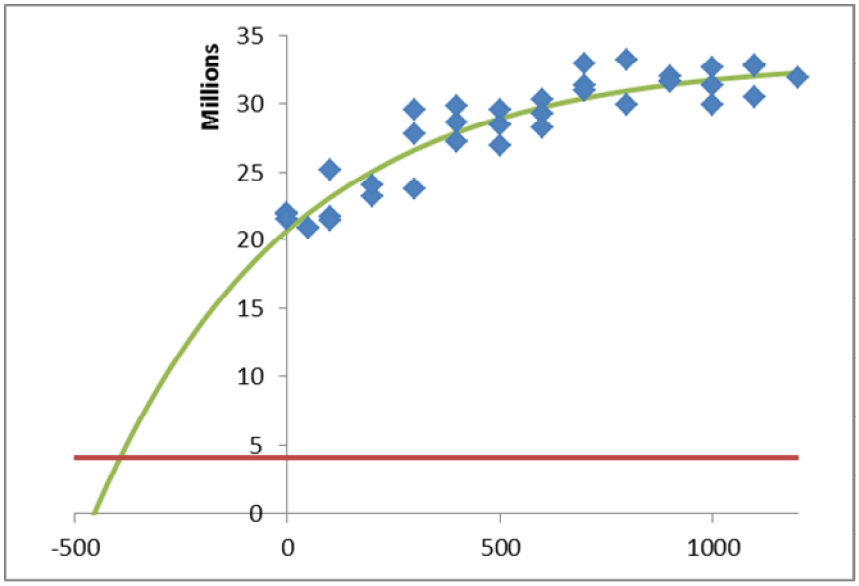

TL06

y0	3.11E+07
a	2.52E+07
b	2.30E-03

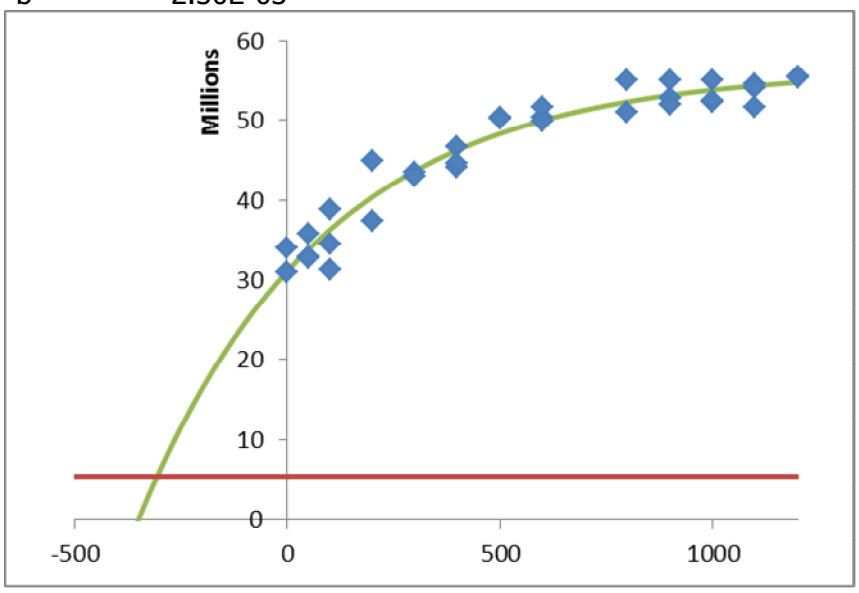

TL07

y0	5.66E+06
a	1.12E+07
b	2.97E-03

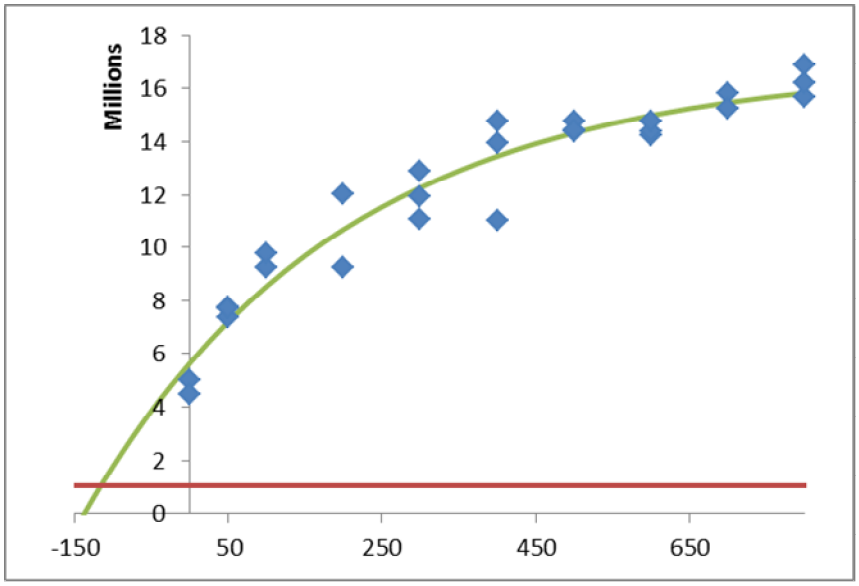

TL08

y0	8.59E+06
a	1.62E+07
b	2.84E-03

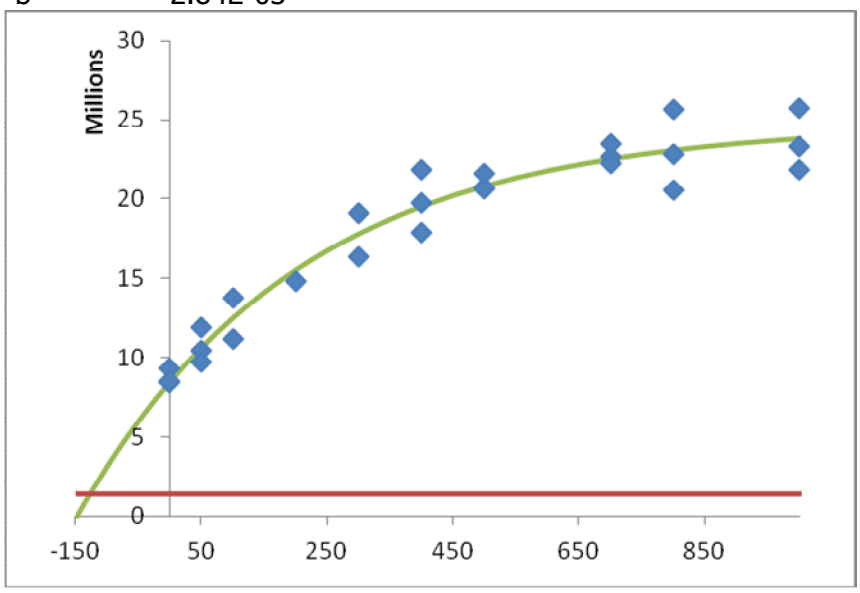

TL09

y0	4.29E+07
a	1.01E+07
b	1.66E-02

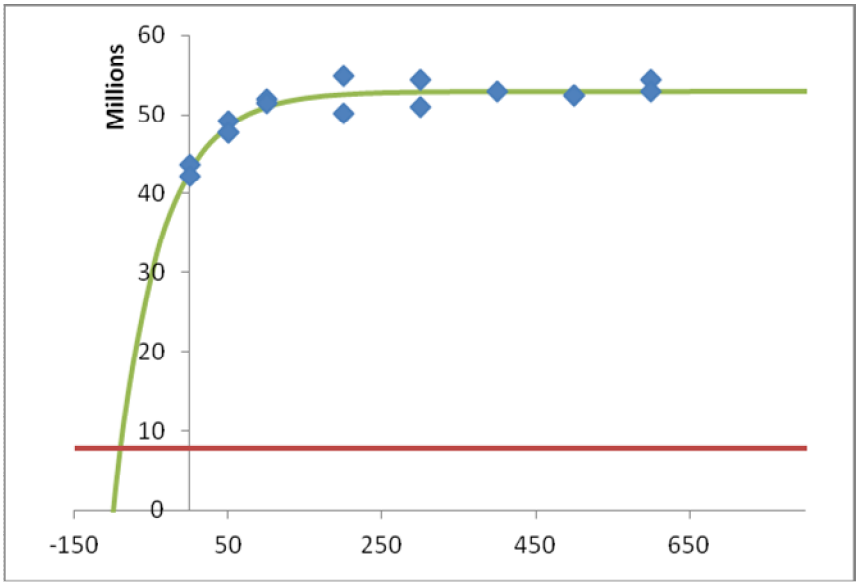

TL10

y0	3.14E+06
a	1.57E+07
b	4.89E-03

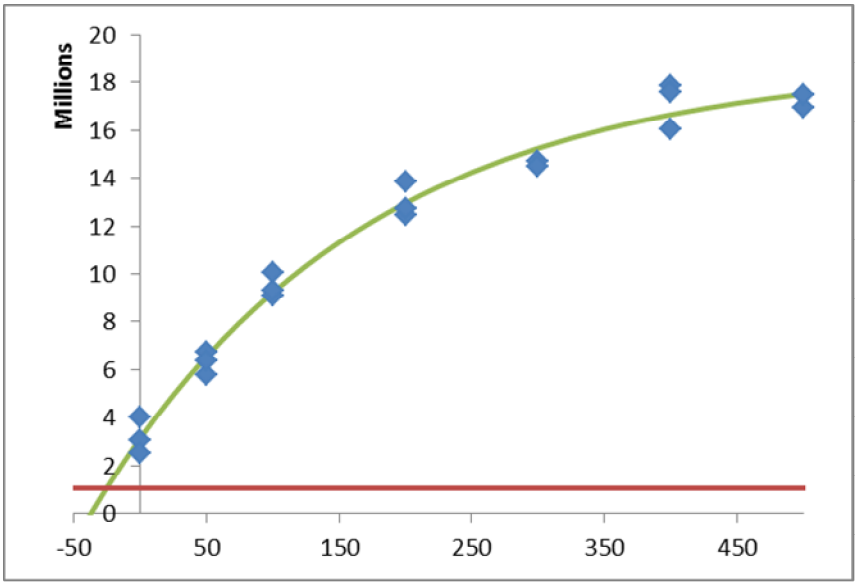

TL11

y0	6.16E+06
a	1.97E+07
b	4.80E-03

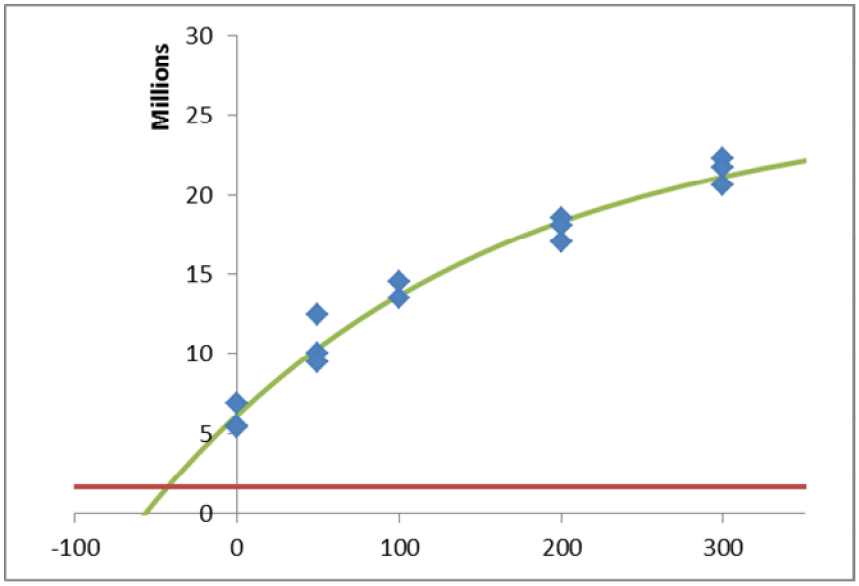

TL12

y0	5.84E+06
a	1.72E+07
b	4.97E-03

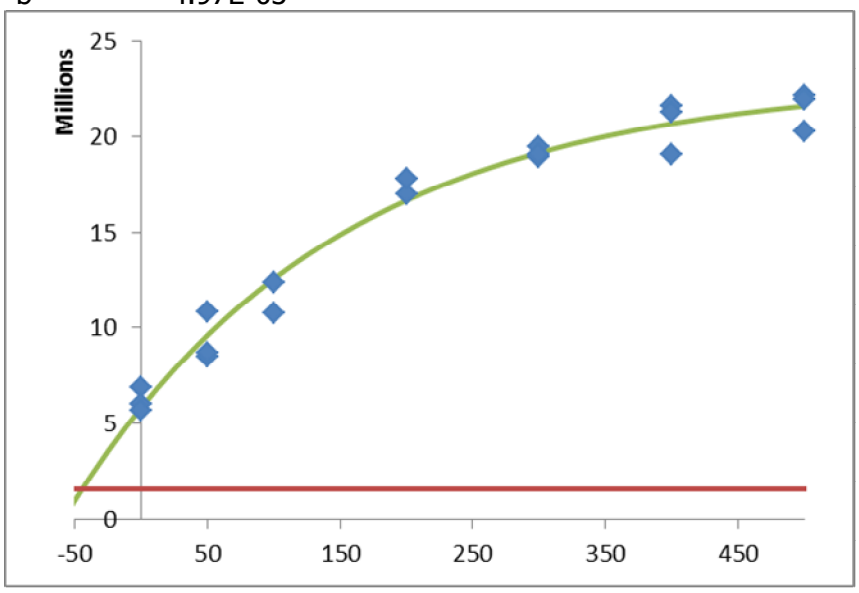

TL13

y0	3.76E+06
a	5.47E+06
b	4.76E-03

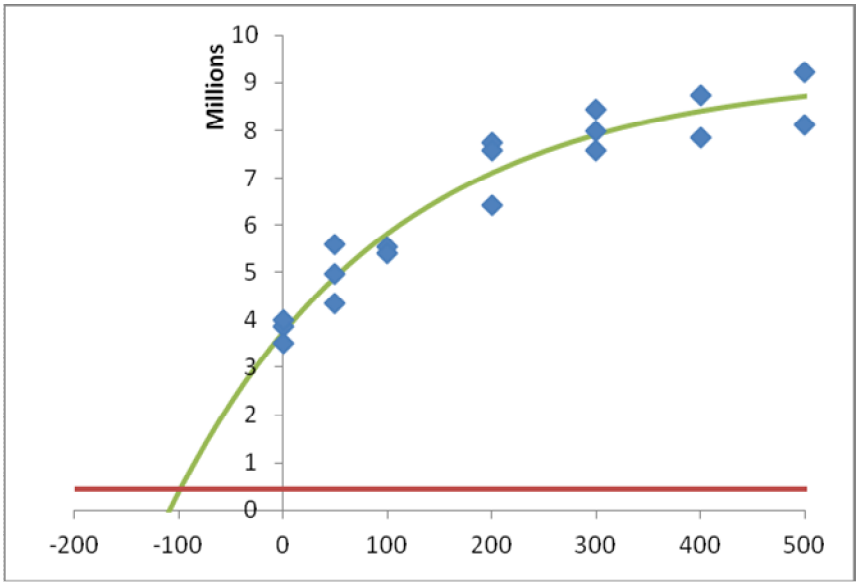

TL14

y0	7.23E+06
a	7.70E+06
b	3.51E-03

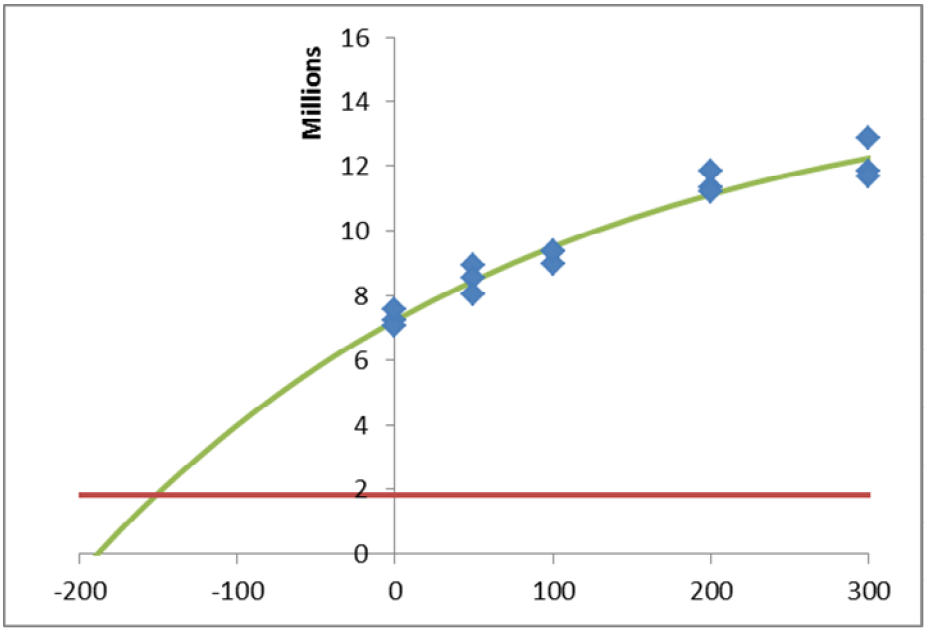

TL15

y0	1.91E+07
a	7.08E+06
b	8.80E-03

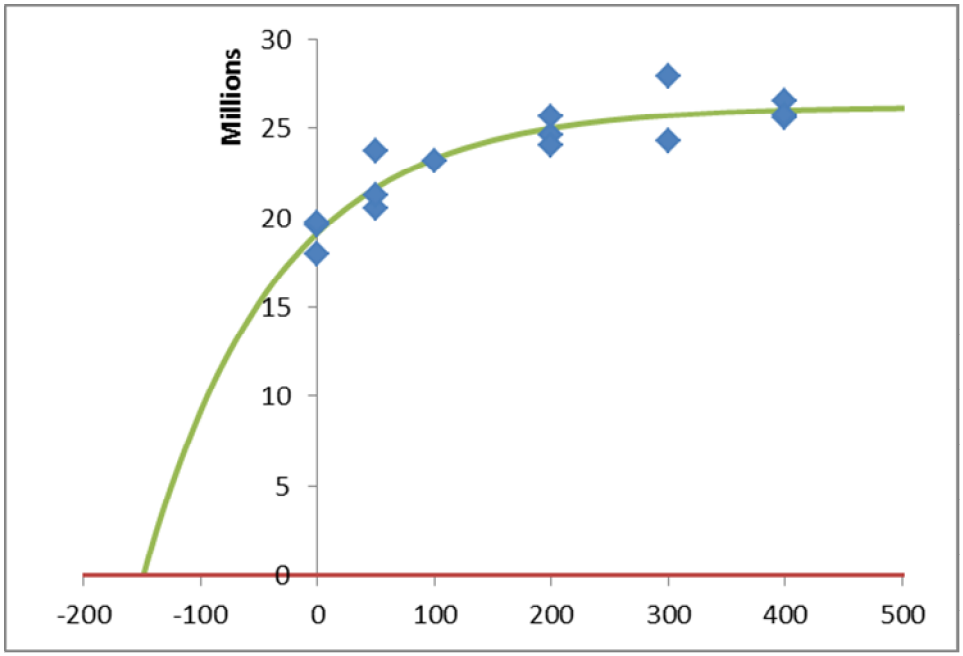

TL16

y0	9.96E+06
a	9.61E+06
b	1.46E-02

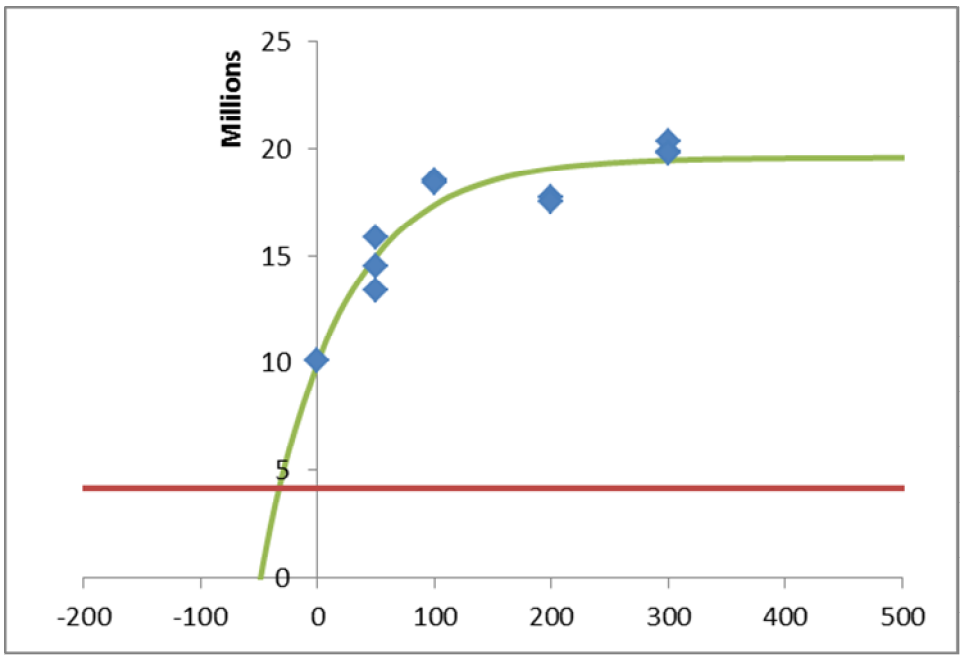

TL17

y0	1.57E+07
a	1.03E+07
b	2.73E-03

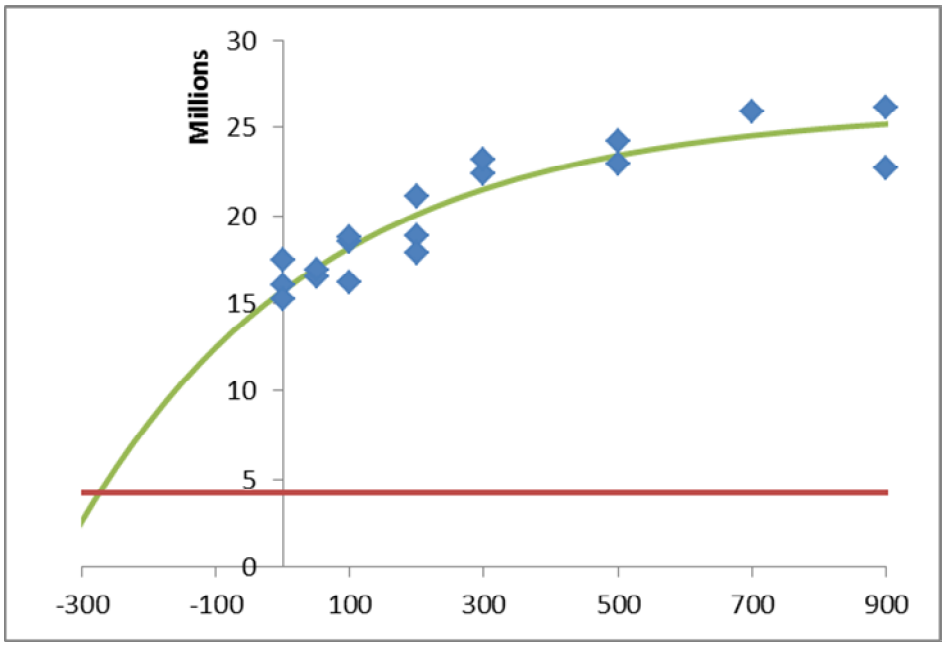

TL18

y0	2.17E+07
a	3.96E+06
b	3.46E-03

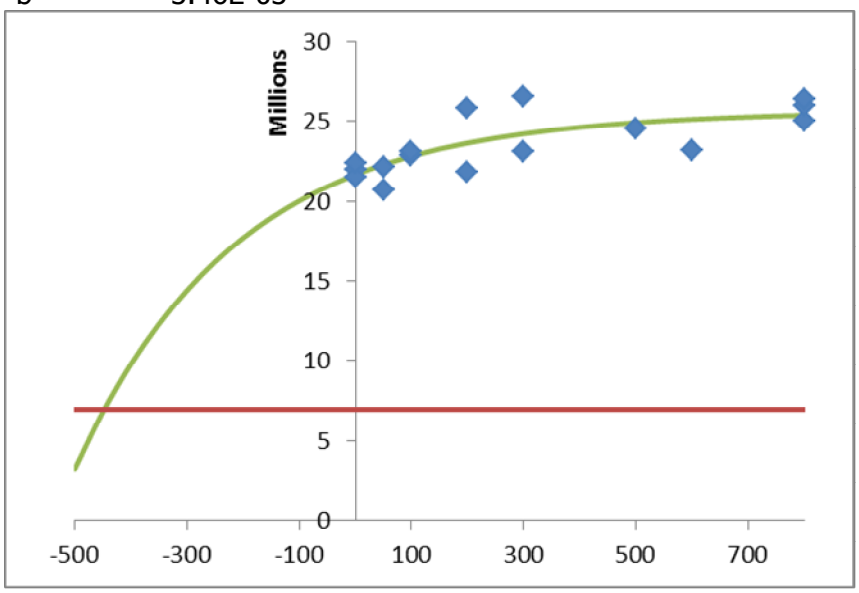

TL19

y0	6.48E+06
a	1.08E+07
b	1.05E-02

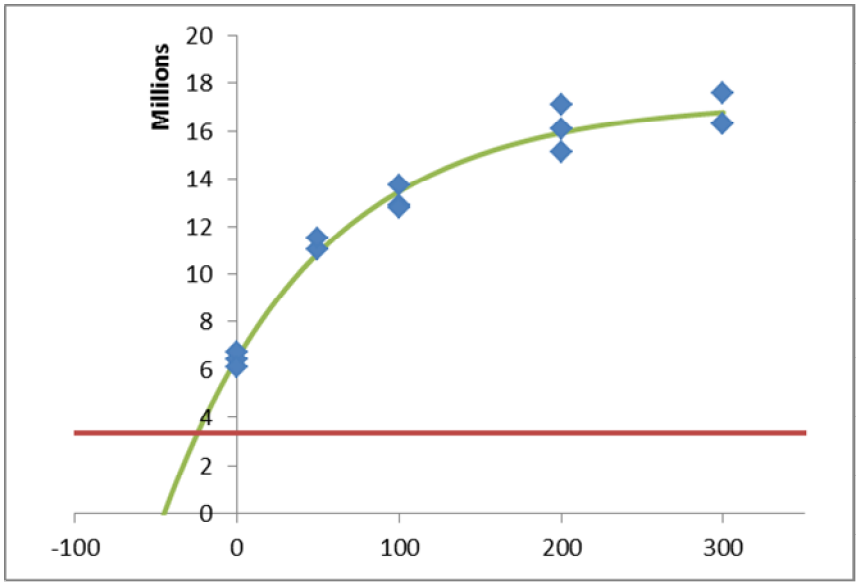

APENDIX C

OSL ED HISTOGRAM

Equivalent dose (De) presented here is shown in the x-axis in unit of seconds.

BT1168

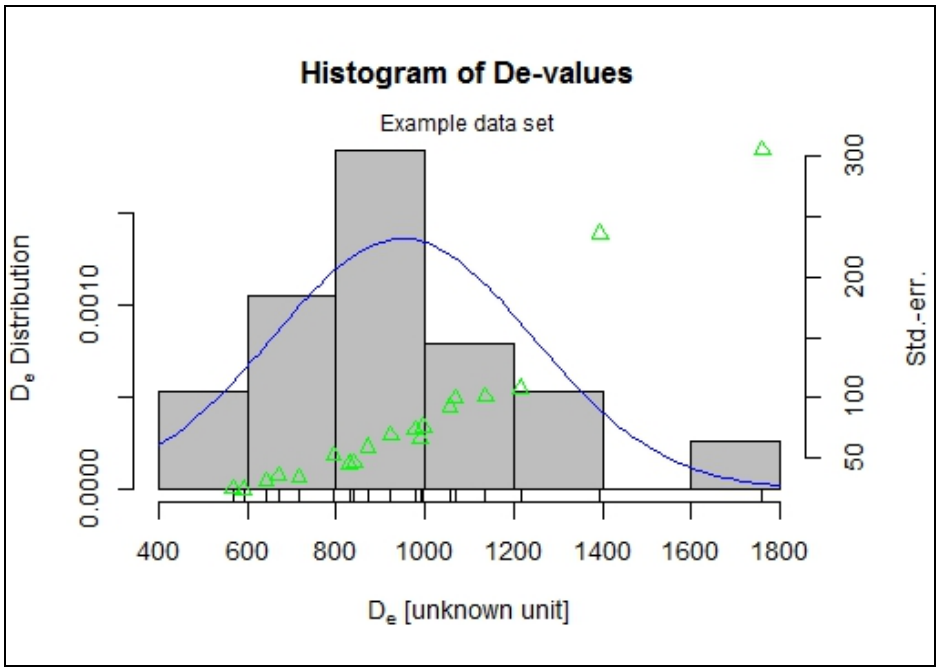

BT1169

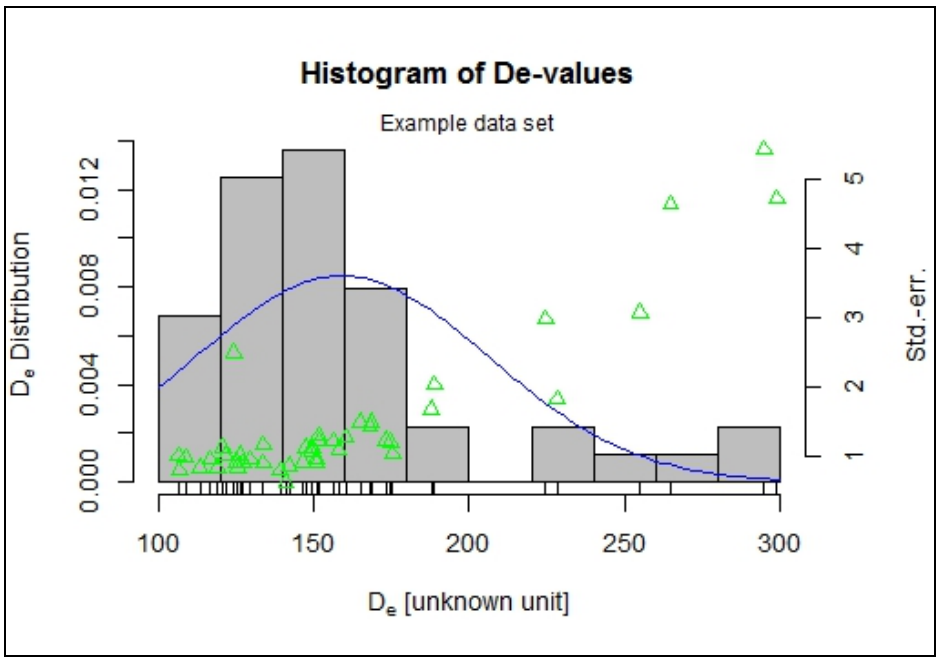

BT1170

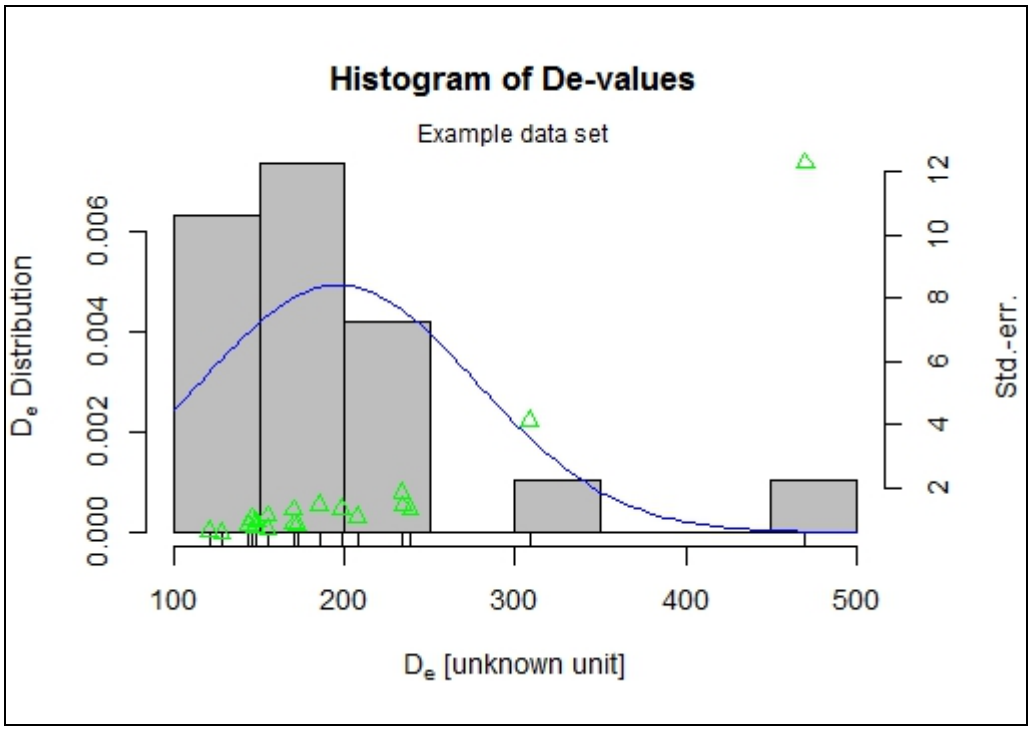

BT1171

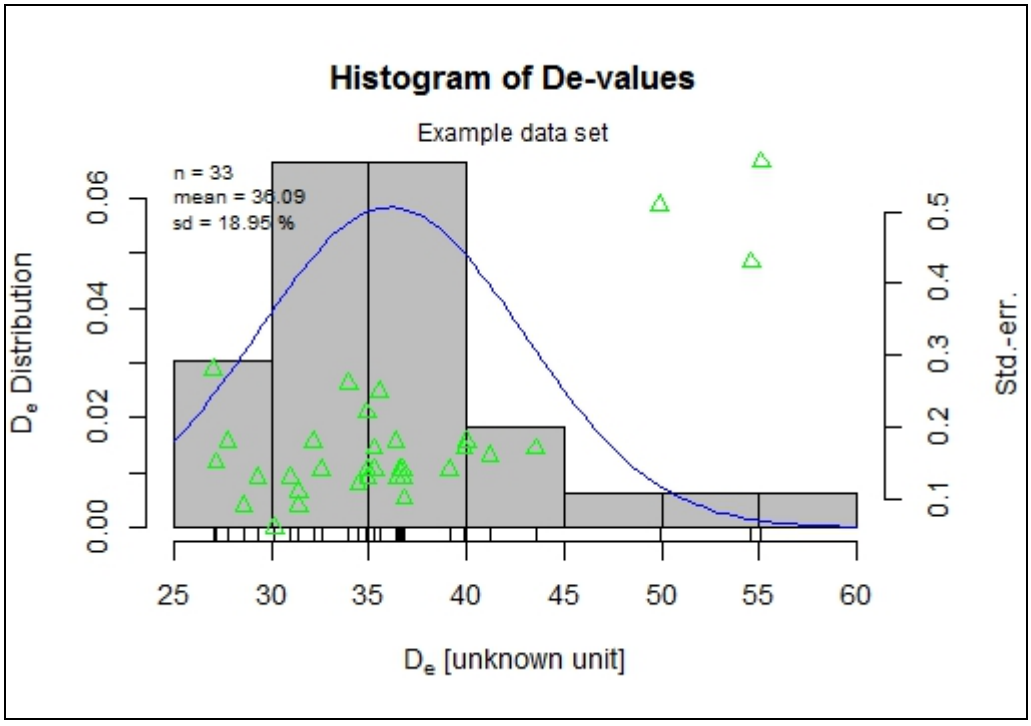

BT1172

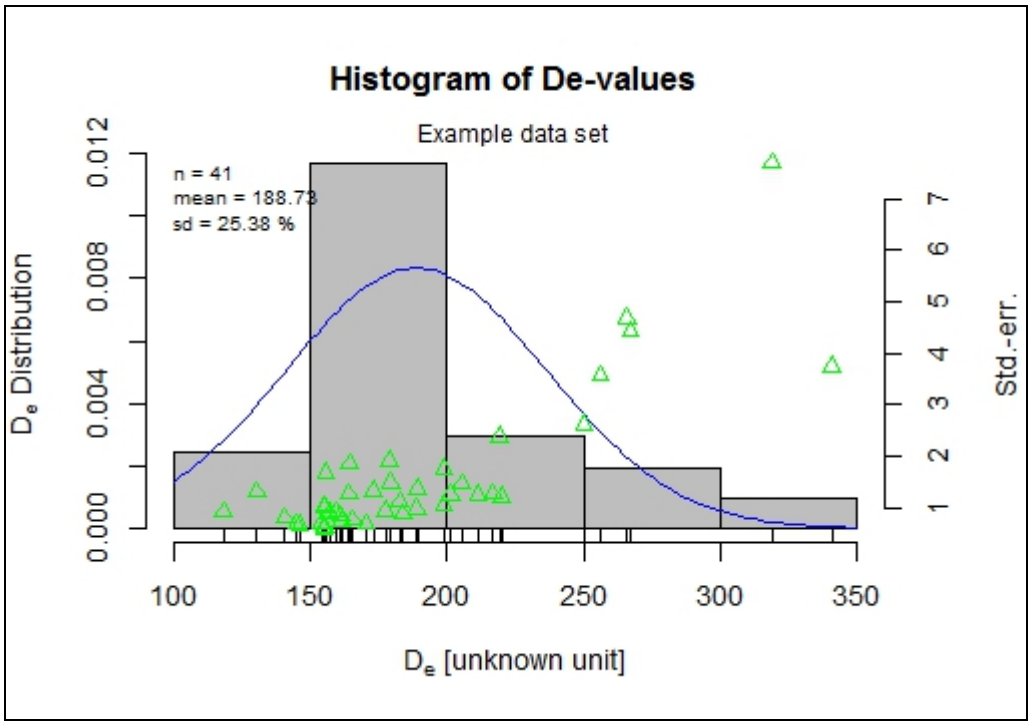

BT1173

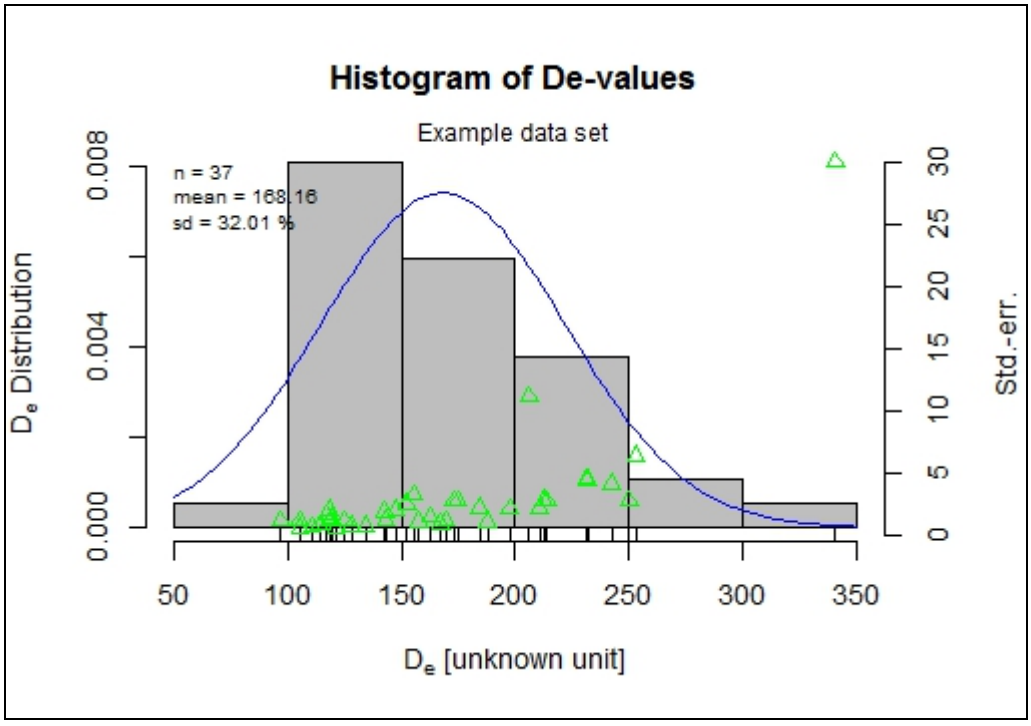

BT1174

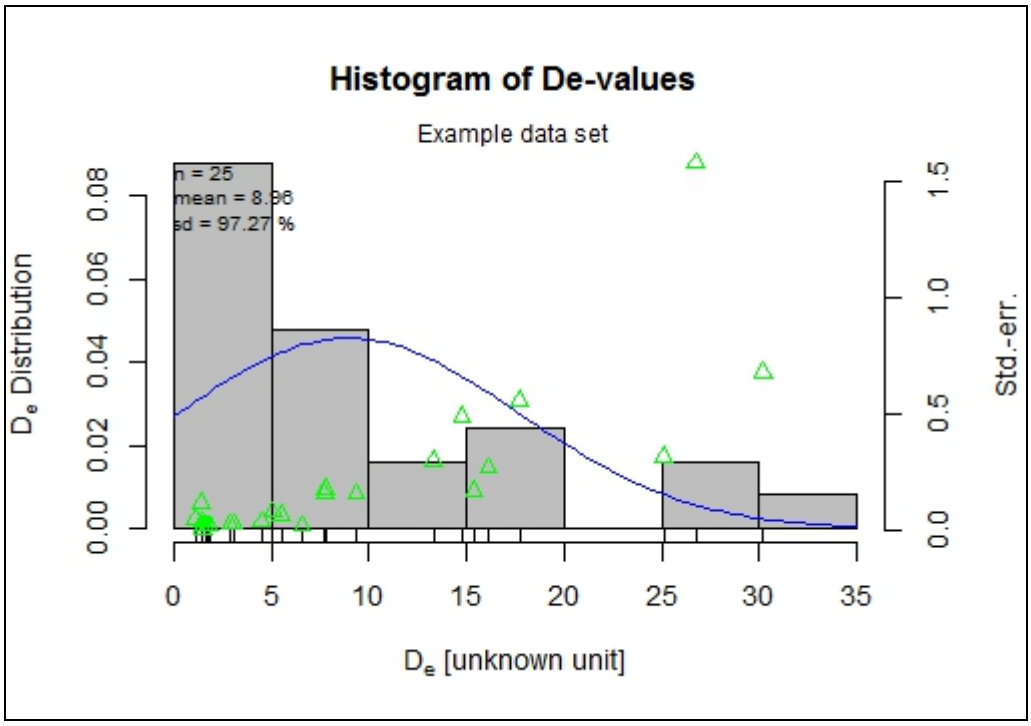

BT1175

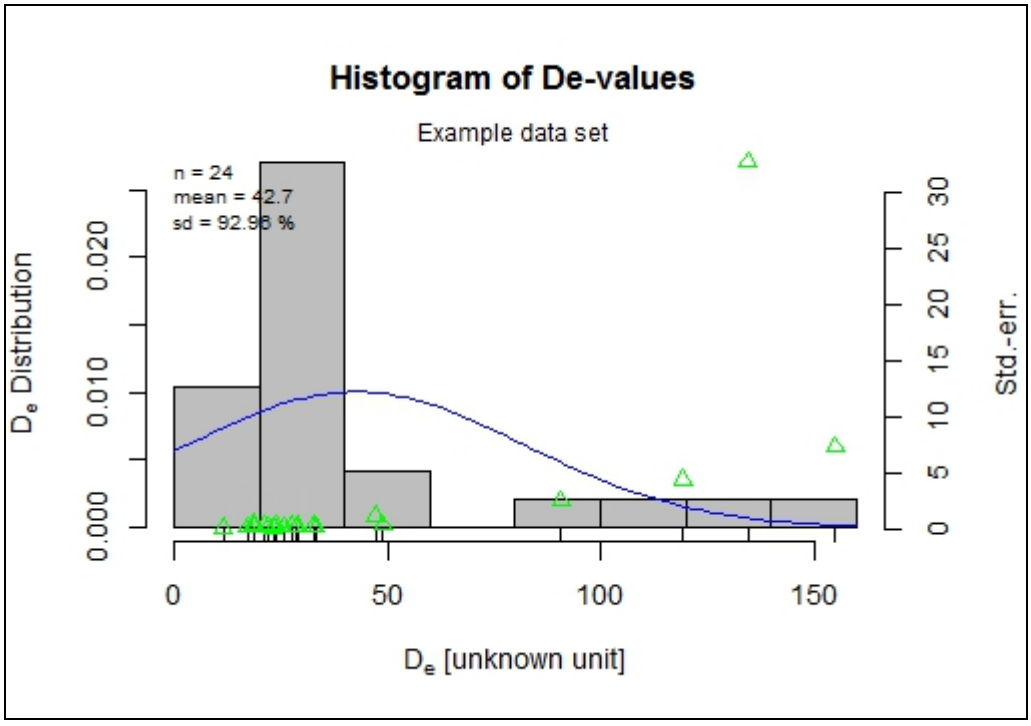

BT1176

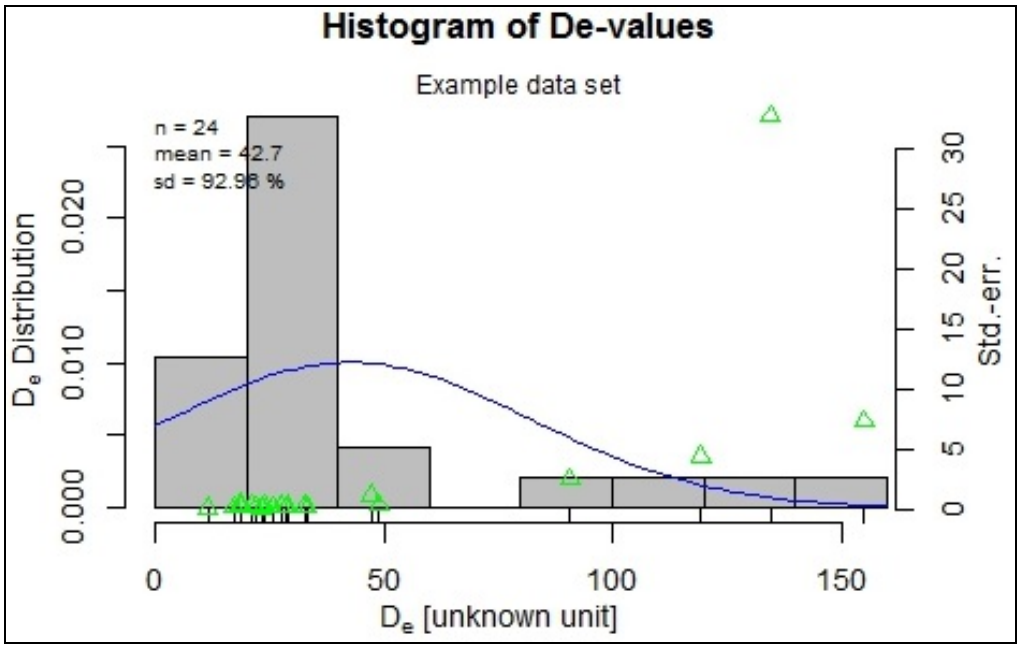

BT1177

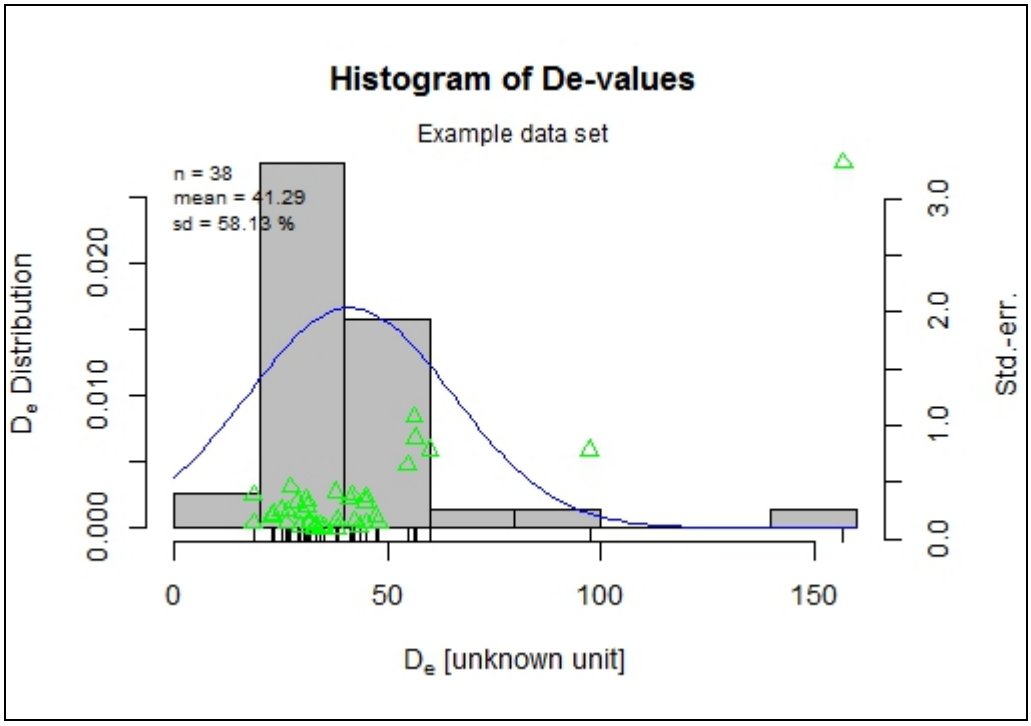

PUBLICATIONS

THE 6th

INTERNATIONAL CONFERENCE ON APPLIED GEOPHYSICS

NOV 15-17, 2012, KANCHANABURI, THAILAND

Extended Abstracts

GEOPHYSICS RESEARCH GROUP, MAHIDOL UNIVERSITY
THAILAND SOCIETY OF EXPLORATION GEOPHYSICISTS

Dating Geological Events using Thermoluminescence Technique

Prakrit Noppradit[a,b,*], **Sommai Changkian**[a,c], **Helmut Durrast**[a,b]

[a] Geophysics Research Center, Prince of Songkla University, HatYai, Songkhla, 90112, THAILAND
[b] Department of Physics, Faculty of Science, Prince of Songkla University, HatYai, Songkhla, 90112, THAILAND
[c] Department of Science, Faculty of Science and Technology, Prince of Songkla University, Pattani, 94000, THAILAND

[*], E-mail: prakrit.nop@gmail.com

ABSTRACT

Thermoluminescence (TL) dating is a suitable approach for dating geological events by sampling quartz or feldspar rich sediments. Generally, when minerals in sediments are irradiated by natural-ionizing radiation (from radioactive elements in its surrounding environment), electrons are continuously accumulated in traps. However, these accumulated electrons can be bleached and reset by sunlight. Therefore, the calculated age is the last time the sampled sediment was bleached by sunlight (not precisely the event time). Many minerals in sediments are widely applied as a dosimeter to determine its signal, for example, quartz, which is used in this study. Sediment samples were collected in Surat Thani Province, where different geological events were identified, for example, alluvial sedimentation processes or fault movements. The accumulated dose (AD) was determined by the additive dose method where the dose from an artificial source is added to the natural dose in quartz. The environmental ionizing radiation rate, or the dose rate (D), was determined from the activities of natural radioactive elements using gamma ray spectrometry. The age of the event is calculated by AD proportional to D. In this study, the calculated TL ages of alluvial sediment sequences were 122-1,900 ka. The upper sediment layer was formed about 122-225 ka ago. The lower sediment layer was formed around 1,336-1,900 ka ago shown the evidence of moving of the subsurface because of the discontinuity of a layer.

KEYWORDS: Thermoluminescence dating, Geological events, Sediments

INTRODUCTION

When studying geological events, it is necessary to carefully analyze the events, for example, by mapping the detailed structures. However, often it is also important to know the timing of the geological event and by this to answer questions, like, when did this happened or when was the fault movement?

There are many dating techniques available; both relative dating (compared with known ages) and absolute dating methods. The thermoluminescence (TL) dating is a type of absolute dating the commonly applied to date minerals in the interesting material such as archeological materials or sediments. Quartz and feldspar are often used in TL dating, because both minerals have a high abundance in sediments and can resist weathering better when compared with other minerals, such as carbonate minerals (Preusser et al., 2008). The TL dating has been widely applied in many studies, such as landscape evolution, palaeoclimate, geohazards, paleoseismology and many others (Preusser et al., 2008; Fattahi, 2009).

TL is a technique, which is using the accumulated signals, TL light, in a mineral. The intensity of the TL signal depends on the environmental ionizing-radiation and the duration the mineral has received that radiation.

Natural ionizing radiation

Preusser et al. (2008) described that the ionizing radiation naturally occurs in form of alpha, beta and gamma radiation and cosmic rays. Moreover, it can be separated into three types of ionizing radiation; cosmic radiation, external radiation, and internal radiation. The cosmic radiation is radiated from space that decreased with depth from surface. The external radiation is radiated from neighboring grains that are naturally containing radioactive elements, like potassium, uranium, and thorium. For the internal radiation, it can be mainly related to beta radiation in potassium feldspar from potassium-40.

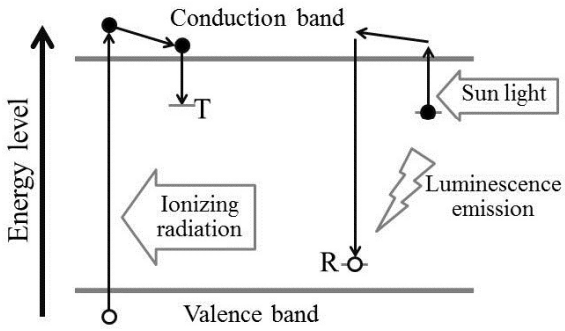

Figure 1 Thermoluminescence processes: (a) mineral received ionizing radiation and electrons are trapped and accumulated, (b) after the crystal is exposed to sunlight or heat it released luminescence light called thermoluminescence.

Physical background of TL

Preusser et al. (2008) and Fattahi (2009) described the physical background in detail. Minerals and their valence band electrons are exposed to ionizing radiation. These electrons are exited until they contain sufficient energy to reach the conduction band. Some electrons may become detached from their parent nuclei in the crystal lattice and diffuse in the vicinity of defects in the conduction band and become trapped at the trap (T) level located below the conduction band. The duration and the intensity of the radiation increase are proportional to the number of trapped electrons.

In case the accumulated electrons in the minerals are exposed to sunlight or heat, they will receive enough energy to change to the conduction band level again before suddenly decreasing their energy level to the recombination center (R), where the energy level is between T and the valence band. When particles, electrons, decrease their energy, light is released, which is the thermoluminescence (TL).

In practice, minerals, which are widely used as dosimeters and for the dating, are quartz and feldspar. Quartz, which is commonly found in sediments, can resist weathering and its properties are relatively good investigated (Preusser et al., 2009), and therefore is a preferred mineral in TL dating. However, in some environments, quartz cannot be found. Then feldspar is chosen to be the dosimeter, because feldspar can accumulate electrons in a larger amount than quartz. Feldspar can also be used to date older ages than using quartz.

Age calculation

The TL dating uses the duration and the level of the natural radiation to date the age of sediment, respectively, geological event. The accumulated electrons in the minerals, called accumulated dose (AD), and the rate of the ionizing radiation exposed to the minerals, called dose rate (D), are needed for the calculation as following

$$Age = \frac{AD}{D}.$$

The age calculated from this equation can be interpreted that the last time minerals in sediments were exposed to sunlight. The sunlight exposure or the end of it can provide evidence of a geological event occurred in the past.

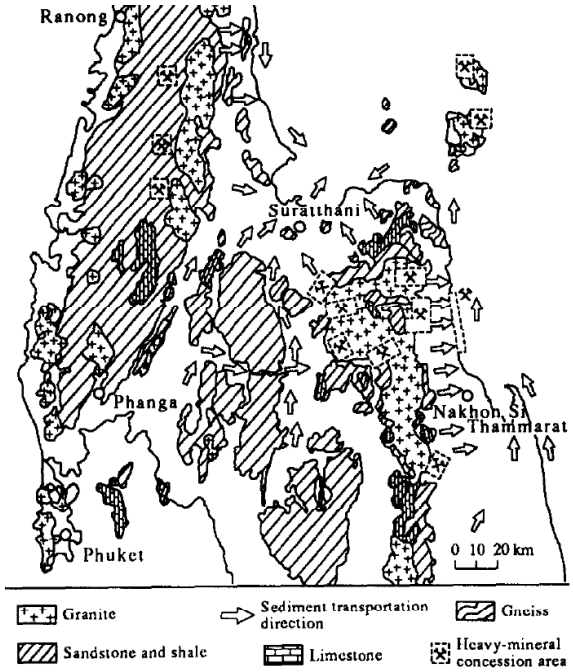

Figure 2 Geology of Surat Thani Province (Chotikasathien & Kohpina, 1993).

STUDY AREA

Surat Thani Province in the southern part of Thailand was selected as the study area. Chotikasathien & Kohpina (1993) described that the youngest sediments are generally unconsolidated and were formed in the Quaternary. The geological map (Figure 2) indicates various rock types exposed in the area as possible sources of the sediments in Surat Thani. Their ages range from Precambrian to Tertiary.

Quaternary sediments in Surat Thani Province are classified by Chotikasathien & Kohpina (1993), based on environment of deposition, into 1. non-marine lithofacies, and 2. coastal lithofacies. These two lithofacies can be further classified as following. Non-marine lithofacies: 1. Regolith: Layer of loose, hetero-geneous material covering solid rock. 2. Colluvium: Loose deposits of rock debris accumulated through the action of gravity at the base of a cliff or slope. 3. Allu-vium: Loose, unconsolidated (not cemented together into a solid rock) soil or sediments, which has been eroded,

Figure 3 TL sampling with a steel pipe in a trench (photo here taken at day light).

reshaped by water in some form, and redeposited in a non-marine setting. Coastal lithofacies: 1. Deltaic sediments: Sediments that were formed at the mouth of a river, where the river flows into an ocean, sea, estuary, lake, or reservoir. 2. Estuarine and intertidal mud flat: Coastal wetlands that were formed when mud is deposited by tides, rivers, or estuarine activities. 3. Coastal-barrier sand.

Further, the Khlong Marui Fault Zone (KMFZ) is likely to be crossing Surat Thani Province in the northern part. The KMFZ is known in Phang Nga, Krabi, and Phuket Province. Watkinson et al. (2008) studied the history of KMFZ further in the west; it shows a strike-slip environment with a mainly NNE-trending.

METHODOLOGY

Sampling

In this study, trenches and outcrops were used to collect samples for TL dating. 50 centimeter long cylindrical steel pipes were used to collect the samples perpendicular to the trench or outcrop wall at the interesting points during night time to avoid any light contamination of the samples (Figure 3). Samples were separated into two parts. The first part was processed in a dark room for measuring the thermoluminescence signals and the second one can be processed at normal light for measuring the dose rate.

TL dating procedure

Mineral separation

In this study quartz was used to date the geological events. The first part of the sample (under light protection) was then cleaned with water and washed with 15% HCl for 40 minutes. After that, 48% HF was used for 40 minutes for removing the sample skin and other contaminated minerals. Then fluoride ions were removed from the sample using 15% HCl for 15 minutes. Finally, the sample was cleaned again with distilled water and then dried.

Accumulated dose determination

A heavy liquid with 2.62 g/cm^3 density was prepared using tetrabromoethane and dipropylene glycol. Then the dry-clean sample was put into the heavy liquid and centrifuged at 2,000 rpm for 1 hour. Quartz that has a mineral density of 2.65 g/cm^3 is separated. The sample with quartz only was cleaned with distilled water and acetone and kept in small light-protection bags. Then the sample was irradiated with gamma rays using a Co-60 source at different doses from 0 to 1,400 Gy at the Office of Atom for Peace in Bangkok. For the measurement of the thermoluminescence of each irradiated sample a Harshaw 3500L reader was used. The data are shown in temperature versus TL intensity that are called glow curve, which are similar to a Gaussian peak curve (see Figure 4). The WinREMS software was used to measure and export data from the TL reader before analysis the curve by GlowFit, which was used to calculate an area under the curve. GlowFit is a freeware developed by the Institute of Nuclear Physics, Krakow, Poland (Puchalska & Bilski, 2006). The area under the peak calculated gives the total intensity. Plotting this with the irradiation dose a linear equation can be drawn. The x-axis interception (at the total intensity = 0) is called equivalent dose or accumulated dose (AD). This technique can be also called additive dose, see Figure 5.

Dose rate determination

For the determination of the dose rate the non-light protection part of the sample is used. First, the sample is crushed. After that it is kept in a sealed container for protecting against radon leakage for a period of one month. Then a gamma ray spectroscopy is carried out to determine the amount of U-238, Th-232, and K-40 by using a high-purity germanium (HPGe) detector at 1.460 MeV for K-40, 1.760MeV for Bi-214 (U-238) and 2.615 MeV for Tl-208 (Th-232). The three elements are used for calculating the dose rate (D).

The specific activity of the sample (concentration of nuclide) are calculated as following

$$a(\mathrm{Bq/kg}) = kCn$$

where $k = 1/\epsilon P \gamma M s$, a is the specific activity of the sample

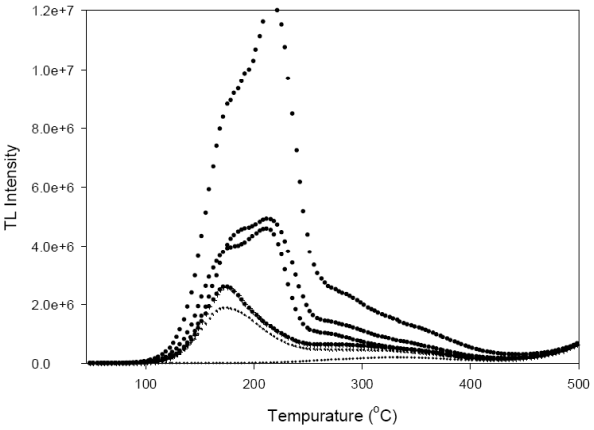

Figure 4 Example of a glow curve (Sample TL08) from the TL reader with temperature versus TL intensity for doses of 0, 200, 400, 800, 1,200, and 1,400 Gy from below to top.

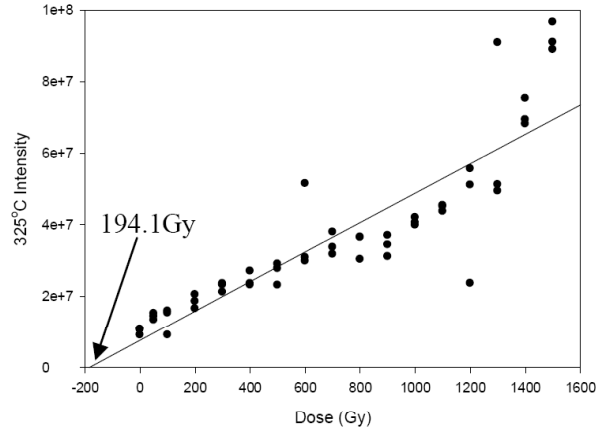

Figure 5 Dose (Gy) versus TL intensity at 325 °C of Sample TL08. Accumulated dose determination using the additive dose method gives AD=194.1 Gy.

in Bq/kg, Cn is the count rate at a certain peak, ϵ is a detector efficiency, $P\gamma$ is a number of gammas per disintegration of this nuclide for a transition at energy E, and Ms is the mass in kg of the measured sample. The emission of gamma ray, which is the ionizing radiation of the surrounding earth material, affects directly the thermoluminescence dosimeter (quartz or feldspar) over time. The dose rate is the ratio of an increment dose in a time interval. The dose rate (D) can be calculated as following:

$$D(\mathrm{nGy/h}) = a(\mathrm{Bq/kg}) \times CF(\mathrm{nGy/h\ per\ Bq/kg}),$$

where a is the concentration of nuclide, and CF is the conversion factor that 0.429 for U, 0.666 for Th and 0.042 for K (Tsertos & Tzortzis, 2003).

Table 1 Dose rate, accumulated dose, and calculated ages.

Sample (no)	Dose rate (Gy/ka)	Accumulated dose (Gy)	Age (ka)
TL08	0.864	194.1	225
TL09	0.863	1,074.1	1,240
TL10	0.763	1,445.3	1,900
TL11	0.450	55.0	122
TL12	0.437	583.3	1,336

RESULTS

The collected samples are alluvial sediments that have a sand and clay composition (Figure 6). Several samples were taken and the age based on the TL method determined. Five of the samples, their location in a trench and their age are shown in Figure 5. The TL peaks from the quartz samples mainly appeared at 153 °C, 210 °C, 275 °C, and 325 °C. The 325 °C peak is the suitable one for dating quartz minerals (Wintle, 1997); therefore this temperature peak was selected.

The measurement results of Sample TL08 are shown as an example, with the TL intensity measured and analyzed intensity for each temperature (see Figure 4 and 5). The 325 °C intensity peak was selected to find the relationship between its intensity and dose. The x-axis-interception was determined as its accumulated dose (194.1 Gy). Its dose rate then can be calculated from the gamma ray spectrometry, which is 0.864 Gy/ka. The age can be calculated to 194.1/0.864=225 ka. For the other samples the results with dose rate, accumulated dose, and age are shown in Table 1

DISCUSSION

From Figure 6 it can be seen that the L6 layer was formed about 1,336-1,900 ka ago. The L1 sediment layer on top was deposited about 122-225 ka ago. The TL09 sample with an age of 1,240 ka seemingly does not fit in the other ages related to layer L1. This difference might be related to various reasons. The sample, for example, might represent a mixed layer and as a result the TL age might also show a mixed age. Moreover, high age values often have high uncertainty, which is related to the saturation of the trapped electrons. However in this study, the graphs fitted to determine the AD are looking linear for all samples (not shown here). Further interpretations of the sedimentological implications of the TL ages are currently being done.

ACKNOWLEDGMENTS

The authors would like to thank the Development and Promotion of Science and Technology (DPST) Talent Project, Thailand, and the Electricity Generating Authority of Thailand (EGAT) for financial support. Further thanks go to the people and local government officers in the study area for supporting this work.

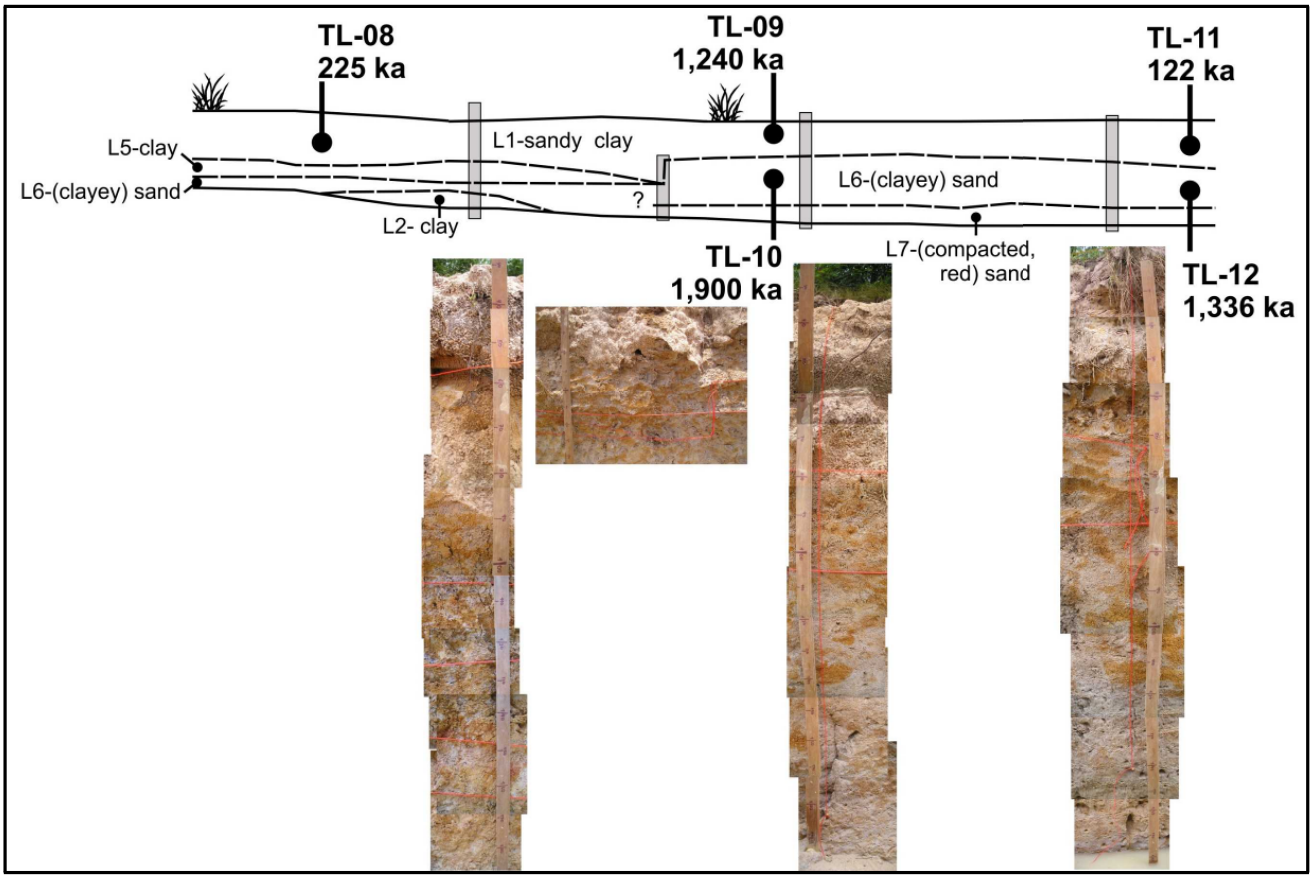

Figure 6 Location of samples in a trench, general lithology, and TL dating results.

REFERENCES

Chotikasathien, W. & Kohpina, P., 1993. Quaternary geology of coastal area, Surat Thani and vicinity, southern Thailand, *Journal of Southeast Asian Earth Sciences*, **8**, 313–320.

Fattahi, M., 2009. Dating past earthquakes and related sedimants by thermoluminescence methods: A review, *Quaternary International*, **199**, 104–146.

McKeever, S. & Chen, R., 1997. Luminescence models, *Radiation Measurements*, **27**, 625–661.

Preusser, F., Degering, D., Fuchs, M., Hilgers, A., Kadereit, A., Klasen, M., Krbetschek, M., Richter, D., & Spencer, J. Q. G., 2008. Luminescence dating: basics, methods and applications, *Eiszeitalter und Gegenwart Quaternary Science Journal*, **57**, 95–149.

Puchalska, M. & Bilski, P., 2006. GlowFit-a newtool for thermoluminescence glow-curve deconvolution, *Radiation Measurements*, **41**, 659–664.

Tsertos, H. & Tzortzis, M., 2003. Gamma-ray measurements of naturally occurring radioactive samples from Cyprus characteristic geological rocks, *Radiation Measurements*, **37**, 221–229.

Watkinson, I., Elders, C., & Hall, R., 2008. The kinematic history of the Khlong Marui and Ranong Faults, southern Thailand, *Journal of Structural Geology*, **30**, 1554–1571.

Wintle, A. G., 1997. Luminescence dating: laboratory procedures and protocols, *Radiation Measurements*, **27**, 769–817.

4th International INQUA Meeting on Paleoseismology, Active Tectonics and Archeoseismology (PATA), 9-14 October 2013, Aachen, Germany

INQUA Focus Group on Paleoseismology and Active Tectonics

Paleoseismological investigations of the eastern part of the Khlong Marui Fault Zone in Surat Thani Province, Southern Thailand

Dürrast, Helmut (1), Prakrit Noppradit (2), Ludwig Zöller (3)

(1). Geophysics Research Center, Prince of Songkla University, HatYai 90112, Thailand. Email: helmut.j@psu.ac.th
(2). Department of Physics, Faculty of Science, Prince of Songkla University, HatYai 90112, Thailand.
(3). Chair in Geomorphology, Universität Bayreuth, 95440 Bayreuth, Germany.

Abstract: *In Southern Thailand two major strike–slip faults cross the Malay Peninsula from SW to NE, the Ranong (RFZ) and Khlong Marui Fault Zone (KMFZ). Before the 2004 Sumatra Andaman Earthquake, these faults believed to be inactive. Paleoseismological investigations of the clearly exposed western part of the KMFZ have already shown that paleoearthquakes occurred in the last few thousands of years. For the eastern part, where the fault is less exposed, this study could identify at least two events between 2.53±0.19 and 6.89±0.38 ka and between 0.59±0.13 and 2.17±0.31 ka, based on field studies and optical dating, with paleoearthquake magnitudes of maximum 7.8.*

Key words*: Paleoseismology, OSL dating, Khlong Marui Fault Zone, active fault, Thailand*

On the 26 December 2004 the Mw 9.1 Sumatra-Andaman Earthquake occurred off the west coast of Northern Sumatra, Indonesia; resulting in a 1,600 km rupture along the fault boundary between the Indian-Australian Plate and the south-eastern part of the Eurasian Plate with fault slip of up to 15 m near Banda Aceh (Lay et al., 2004). The massive earthquake triggered a series of devastating tsunamis along the coastline of the Indian Ocean, killing a large number of people and inundating coastal communities around.

In southern Thailand, there are a series of faults, mainly the Ranong (RFZ) and Khlong Marui Fault Zones (KMFZ), as shown in Figure 1, which were identified as inactive before 2004 by the Department of Mineral Resources, Thailand (DMR), however no seismicity studies have been carried out. Watkinson et al. (2008) described the KMFZ and RFZ as major NNE-SSW trending strike-slip faults, diachronous reversal in shear sense, originated before but activated during the India–Eurasia plate collision. Seismological observations by Dürrast et al. (2007) in early 2005 have confirmed seismicity with low magnitudes (M<4.5) along the faults and in southern Thailand.

In 2006/07 the Department of Mineral Resources carried out a preliminarily study on the recurrence interval of the RFZ and the south-western and middle part of the KMFZ (DMR, 2007a). The exact location of the eastern part of the KMFZ is still unclear. Remote sensing, topographic surveys, and geophysical investigations were applied to study tectonic geomorphology and locate trenches and sampling locations. Thermoluminescence (TL), C-14, and electron spin resonance (ESR) dating were applied to determine the last fault movement. Trenching and outcrops were used to define sediment stratigraphy related to paleoearthquake.

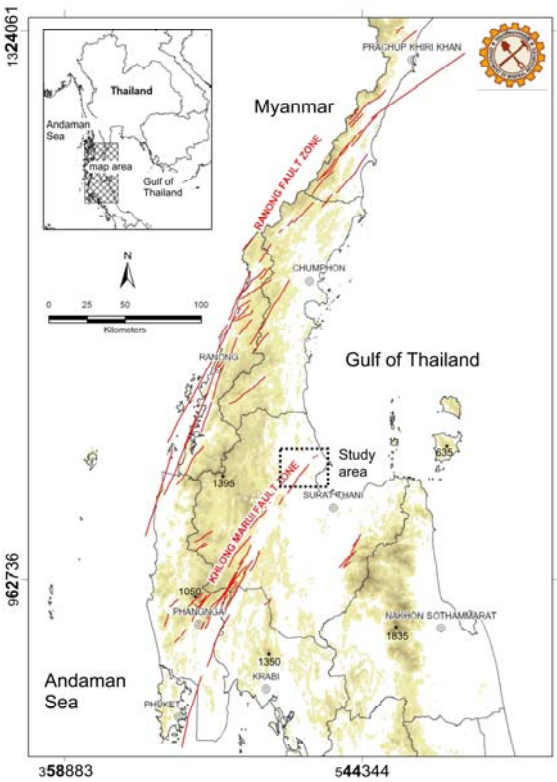

Fig. 1: Topographic map of southern Thailand with the major fault zones (after DMR, 2007a) and study area; base map in UTM WGS-84, numbers are elevations in meters.

Their study concluded that the last movement of the KMFZ was 1,200 years and that of the RFZ 2,000 years ago. Moreover, the recurrence interval of the KMFZ and RFZ is 1,000 years and 2,000 years.

In 2010/11 extensive geological and geophysical field work was carried out as part of a larger study with the objective (1) to locate the KMFZ in the western part - mainly in Surat Thani Province, north of the city of Surat Thani (see Figure 1), (2) to identify locations with evidence for paleoearthquakes, and finally (3) dating sediments related to these events, here using optically stimulated luminescence method (OSL).
Several locations in the area showed paleo-seismological events, with five sites chosen for dating (see Figure 2): V1, V2, V3 are in Vibhavadi District, TC in Tha Chang District, and CTR at the road between Chaiya and Tha Chang.

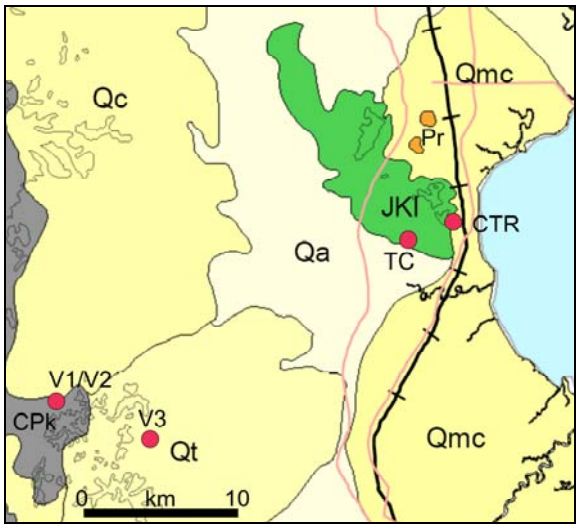

Fig. 2: Geological map of the eastern part of Surat Thani Province, Southern Thailand, showing the locations of paleoseismological events used for dating (V1/V1, V3, TC, CTR). CPk: Carboniferous, mainly shale with sandstone and siltstone, Pr: Permian Ratburi Group, mainly limestone; Oc: Quaternary colluvial deposits; Qt: Quaternary terrace deposits, Qa: Quaternary fluvial deposits; Qms: Coastal wave–dominated deposits. Red lines – main roads, black line – railway; blue - Gulf of Thailand, to the East (after DMR, 2007b).

Altogether ten samples were successfully collected from four sites (excluding V3) by using a cylindrical steel sample holder (10 cm in diameter and 50 cm long) during night time for protecting the sediments from light exposure. Samples were taken from different layers exposed in the outcrop mainly in horizontal direction. Both sides of the sample holders were sealed for transport until further processing in the laboratory. The OSL measurements were carried out at the University Bayreuth, Germany. Details about the sample preparation and measurement technique are described elsewhere (e.g. Fuchs et al., 2005; Lai et al. 2007).

Vibhavadi site V1 and V2 are approximately 36 m NNE of site V1 exposing the same face of the old pit. At site V1 three (see Figure 3 and 4) and at site V2 one OSL sample were taken (in Layer C, not shown here).

Fig. 3: Site Vibhavadi V1. Almost vertical face at a former sand pit. Photo to direction 160 (SSE). Scale (left side) 2 m.

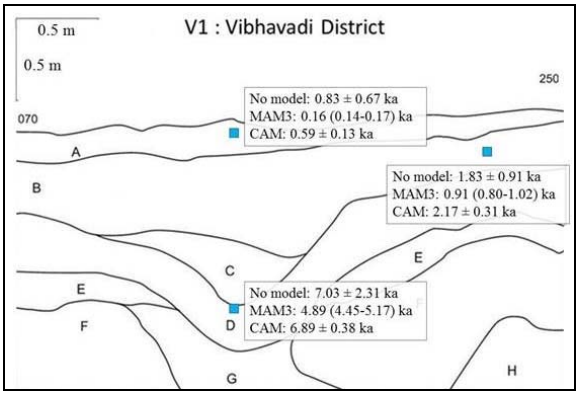

Fig. 4: Site of Vibhavadi V1. Lithological boundaries, location of OSL samples with the ages related to different age model. A: Black top soil, B: Light brown clayey sand, C: Brown-grey coloured and medium plastic clay, with black grains and black plant material, D: Dark-grey, slightly orange gravel with a few black grains and black plant material, E: Red to ochre coloured medium plastic clay, F: Fractured white-yellow sandstone. G: Yellow-white sandy clay, H: Medium plastic white-grey-yellow silty clay. MAM3 - minimum age model, CAM - central age model.

The OSL ages were determined using different age models described by Galbraith & Roberts (2012) with MAM3 the minimum age model and CAM the central age model, as shown in Figure 4. At Site V2 the ages are: no model: 2.48±0.09 ka, MAM3: 1.47 (1.37-159) ka, and CAM: 2.53±0.19 ka. From the ages a sedimentation and tectonic scenario can be drawn (see Figure 5).
Before 6.89 ka a fault has already existed there indicated by the clay (G) between the sandstone layer (F). Layer (E) was deposited above (Figure 5a and b). An earthquake event, assuming a strike slip movement, but with extensional character, occurred between 2.53 and 6.89 ka (Figure 5c), with a minimum displacement in vertical direction about one meter. An estimation of the paleoearthquake magnitude gives an Mw value of 6.8 for a maximum displacement (MD) and Mw of 7.0 for an average displacement (AD). These calculations are based on regression lines from Wells & Coppersmith (1994).

Then in the sequence, layer C and later layer B was deposited (Figure 5d). After that a second event occurred, between 0.59 and 2.17 ka, assumed a strike slip movement, but with extensional character (Figure 5e). A minimum displacement took place in vertical direction of approximately 0.5 m. Also here the estimation of the paleoearthquake magnitude gives Mw of 6.6 for a maximum displacement (MD) and Mw of 6.7 for average displacement (AD). After this second event the uppermost layer A was deposited (Figure 5f).

Faults found at Vibhavadi site, with a strike of 145-325° (NNW-SSE), are likely conjugated faults of the main KMFZ. Geological and geophysical results from the study area have shown that the actual main fault is about 20 km south of the location assumed before and shown in Figure 1 (data not shown here).

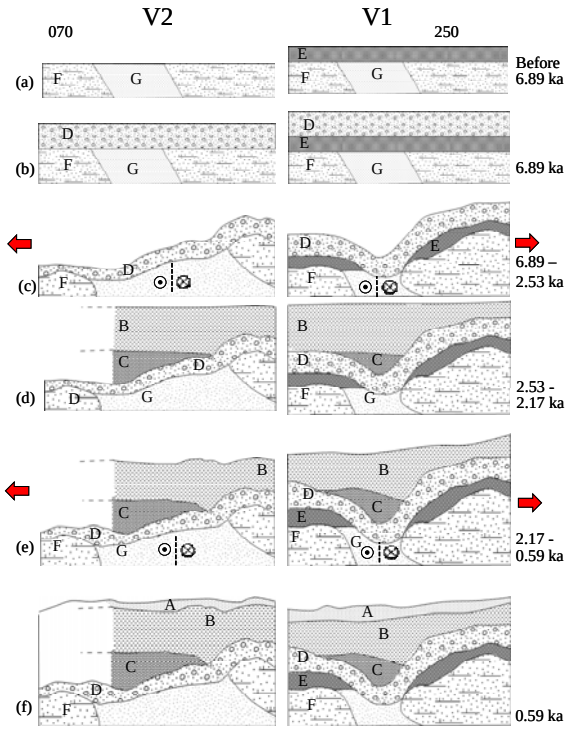

Fig. 5: Schematic geological scenarios for Vibhavadi site V1 (left) and V2 (right) from older (a) to younger (f). Two paleo-earthquakes could be identified at (c) and (e). See also Figure 4 for the abbreviations of the layers (A-G).

The faults in Vibhavadi clearly have an extensional character and are much older then the dating here. A river displacement in the vicinity of site V1 and V2 gives a horizontal displacement of about 18 m, likely the result of several events. However, if using MD and one event then the max. Mw is 7.8. The existence and strike direction of these faults in the subsurface have been confirmed by seismic investigations (not shown here).

The result from the paleoseismological investigations in this area have shown that conjugated faults related to the main Khlong Marui Fault Zone were active in the last 10,000 years with at least two identifiable events: between 2.53 and 6.89 ka and between 0.59 and 2.17 ka, and with a paleoearthquake magnitude of maximum 7.8.

Therefore, it can be concluded that the Khlong Marui Fault Zone was not inactive before 2004 as already shown by DMR (2007a) for the western part and that higher magnitude earthquakes can be expected along this fault. This might also the case for the Ranong Fault Zone further north (see Figure 1).

The clear categorization of the KMFZ as an active fault has further implications for the seismic hazard assessment and related mitigation efforts, e.g. engineering requirements for buildings and infrastructures.

Acknowledgements: The authors acknowledge support from the Electricity Generating Authority of Thailand (EGAT) and Geophysics Research Center (GRC) as well as their team members. PN was supported by Graduate School, PSU, and the Development and Promotion of Science and Technology (DPST) talent project (Thailand).

References

DMR, (2007a). Investigation on Recurrence Interval in Areas Showing Trace of Movement along the Faults in Prachuab Khirikhan, Chumporn, Ranong, Surat Thani, Krabi, Phang Nga and Phuket Provinces (Ranong and Khlong Marui Faults). Report, Department of Mineral Recourses, Bangkok, Thailand.

DMR, (2007b). Geological map of Surat Thani Province. Department of Mineral Recourses, Bangkok, Thailand. http://www.dmr.go.th/download/pdf/South/Surat.pdf.

Dürrast, H., S. Dangmuan, & W. Lohawijarn, (2007). Khlong Marui and Ranong Fault Zones in Southern Thailand re-activated by the 26 December 2004 Mw 9.3 Sumatra-Andaman Earthquake? *Proceedings of the GEOTHAI'07 International Conference*, Dec. 21-22, 2007, Bangkok, 141–144.

Fuchs, M., J. Staub, & L. Zöller, (2005) Residual Luminescence Signals of recent river flood sediments: A Comparison between Quartz and Feldspar of fine- and coarse-grain Sediments. *Ancient TL* 23, 25-30.

Galbraith, R.F. & R.G. Roberts, (2012). Statistical aspects of equivalent dose and error calculation and display in OSL dating: An overview and some recommendations. *Quaternary Geochronology* 11, 1–27.

Lai, Z.P., H. Brückner, A. Fülling & L. Zöller, (2007) Existence of a common growth curve for silt-sized quartz OSL of loess from different continents. Radiation Measurements 42 (9), 1432-1440.

Lay, T., H. Kanamori, C.J. Ammon, M. Nettles, S.N. Ward, R.C. Aster, S.L. Beck, M.R. Brudzinski, R. Butler, H.R. Deshon, G. Ekström, K. Satake, & S. Sipkin, (2004) The great Sumatra-Andaman Earthquake of 26 December 2004. *Science* 308, 1127-1133.

Watkinson, I., C. Elders & R. Hall, (2008). The kinematic history of the Khlong Marui and Ranong Faults. *Journal of Structural Geology* 30, 1471–1554.

Wells, D.L. & K.J. Coppersmith, (1994). New Empirical Relationships among Magnitude, Rupture Length, Rupture Width, Rupture Area, and Surface Displacement. *Bulletin of the Seismological Society of America* 84, 974–1002.

VITAE

Name Mr.Prakrit Noppradit

Student ID 5410220032

Education

Degree	Name of Institution	Year of Graduation
B.Sc. in Physics	Prince of Songkla University	2011

Scholarship Awards during Enrolment

- Development and Promotion of Science and Technology (DPST) talent project master program scholarship, Institute for the Promotion of Teaching Science and Technology (IPST) (2011-2013)
- Development and Promotion of Science and Technology (DPST) talent project research abroad grant at Department of Geomorphology, University of Bayreuth, Germany, Institute for the Promotion of Teaching Science and Technology (IPST) (January – May 2013)
- Teaching Assistant of the Faculty of Science, Prince of Songkla University (2011-2012)

List of Publication and Proceedings

Dürrast, H., Noppradit, P. and Zöller, L., 2013. Paleoseismological investigations of the eastern part of the Khlong Marui Fault Zone in Surat Thani Province, Southern Thailand. Proceedings of the 4th International INQUA Meeting on Paleoseismology, Active Tectonics and Archeoseismology (PATA), 9-14 October 2013, Aachen, Germany.

Noppradit, P., Dürrast, H. and Changkian, S., 2012. Dating geological event using thermoluminescence technique. Proceedings of the 6th International Conference on Applied Geophysics (Mahidol University), 15-17 Nov 2012, Kanjanaburi, Thailand, 123-130.